ABSTRACT

Title of Document: CHARACTERIZATION OF THE TWO VACCINIA VIRUS MATURE VIRION-SPECIFIC PROTEINS, A26P AND A25P

Amanda Rachel Howard, Ph.D., 2010

Directed By: Dr. Bernard Moss, Adjunct Professor, and Dr. Jonathan Dinman, Professor, Department of Cell Biology and Molecular Genetics

Poxviruses produce two morphologically distinct infectious particles, mature virions (MVs) and extracellular virions (EVs). During replication, some MVs differentiate and become wrapped with cellular membranes, transported to the periphery, and exported as EVs. Some orthopoxviruses, e.g., cowpox virus (CPXV), form large, discrete cytoplasmic inclusions called A-type inclusion bodies (ATIs) within which MVs are embedded by a process called occlusion. ATIs are composed of aggregates of the A-type inclusion protein (ATIp), which is truncated in orthopoxviruses such as vaccinia virus (VACV) that fail to form ATIs. VACV does encode a functional A26p, which along with the ATIp is required for occlusion. A26 lacks a transmembrane domain, and nothing is known regarding how it associates with the MV and regulates occlusion. Additionally, little is known about the formation of ATIs and how MVs become embedded within them. Here, experiments show that A26p is incorporated into MVs by the A27p-A17p complex and interacts

with A25p, a truncated form of the CPXV ATIp. Restoration of the full-length ATI gene is sufficient for VACV ATI formation and the occlusion of MVs. A26p directly interacts with ATIp, and this interaction, as well as the A26p-A27p interaction, are required for occlusion. The data demonstrates that ATI mRNAs are transported out of viral factories (VFs) and translated in the cytoplasm. ATIs enlarge both by new protein synthesis and by coalescence, which requires microtubules. ATIs do not nucleate around MVs but rather MVs move along microtubules to embed within ATIs. Taken together, the data suggest a model for occlusion in which MVs move along microtubules to ATIs that are translated from mRNAs in the cytoplasm. At the ATIs, A26p has a bridging role between ATIp and A27p, and A27p provides a link to the MV membrane. Although the specificity of A26p for MVs suggested A26p might regulate wrapping, I did not detect an effect of either the deletion of A26 or occlusion on the production of EVs.

CHARACTERIZATION OF THE TWO VACCINIA VIRUS MATURE VIRION- SPECIFIC PROTEINS, A26P AND A25P

By

Amanda Rachel Howard

Dissertation submitted to the Faculty of the Graduate School of the
University of Maryland, College Park, in partial fulfillment
of the requirements for the degree of
Doctor of Philosophy
2010

Advisory Committee:
Dr. Jonathan Dinman, Chair
Dr. Bernard Moss, Co-Chair
Dr. Alison McBride
Dr. James Culver
Dr. Siba Samal

Dedication

For my brother, co-captain of garden explorations and collector of rocks.

Acknowledgements

I would like to acknowledge my mentor, Dr. Bernard Moss, for his inspiring brilliance and unwavering patience. I thank Dr. Jeanmarie Verchot-Lubicz who showed me GFP under a microscope for the first time. Thanks to my committee members for their input and advice. I am grateful to my co-workers for sharing their ideas and climbing canyons with me. And finally, I would like to thank my family, especially my grandfather, Charles Howard, for his mantra "be good and work hard." Finally, thanks to my mother, Eileen Mustain, who has always let me be whoever I wanted to be, even a unicorn.

Table of Contents

List of Tables

List of Figures

List of Abbreviations

A	Adenine
Ab	Antibody
ATI	A-type inclusion body
ATIp	A-type inclusion body protein
bps	Base pairs
C	Cytosine
˚C	Degrees Celsius
CFP	Cyan fluorescent protein
CPXV	Cowpox virus
DAPI	4',6-diamidino-2-phenylindole
DMEM	Dulbecco's modified Eagle medium
DNA	Deoxyribonucleic Acid
dsDNA	Double-stranded DNA
DsRed	*Discosoma sp.* red fluorescent protein
ECTV	Ectromelia virus
EFC	Entry-fusion complex
EM	Electron microscopy
EMEM	Earle's modified Eagle medium
EV	Extracellular virus
FBS	Fetal bovine serum
g	Gravity
G	Guanine

GAGs	Glycosoaminoglycans
GAPDH	Glyceradldehyde-3-phosphate dehydrogenase
GFP	Green fluorescent protein
h	Hours
hpi	Hours post infection
HRP	Horseradish peroxidase
IPTG	Isopropyl-ß-D-thiogalactopyranoside
ITR	Inverted terminal repeat
IV	Immature virion
kbps	Kilobase pairs
kDa	Kilodalton
LDS	Lithium dodecyl-sulfate
MAb	Monoclonal antibody
min	Minutes
mg	Milligram
ml	Milliliters
mM	Millimolar
MOI	Multiplicity of infection
MPXV	Monkeypox virus
mRNA	Messenger RNA
MTOC	Microtubule organizing center
MV	Mature virion
nm	Nanometer

nt	Nucleotide
ORF	Open reading frame
PAb	Polyclonal antibody
PEG	Polyethylene glycol
PBS	Phosphate-buffered saline
PFU	Plague forming units
RNA	Ribonucleic acid
RT	Room temperature
SDS-PAGE	Sodium dodecyl sulfate-polyacrylamide gel electrophoresis
T	Thymidine
U	Uracil
µg	Microgram
µl	Microliter
µm	Micrometer
U	Uracil
UTR	Untranslated region
VACV	Vaccinia virus
VARV	Variola virus
WR	Western Reserve
WV	Wrapped virus
WHO	World Health Organization
YFP	Yellow fluorescent protein

Chapter 1: Review of literature

1.1 The *Poxviridae*

1.1.1 Classification

The family *Poxviridae* has large double-stranded DNA genomes and is distinguished by a replication cycle that occurs entirely in the cytoplasm of infected cells and an unique, complex virion architecture. Poxviruses have been grouped with other large eukaryotic DNA viruses (genomes > 100 kbp) that replicate exclusively or partially in the cytoplasm called the Nucleo-Cytoplasmic Large DNA Viruses (NCLDV). The NCLDVs are comprised of diverse families including poxviruses, asfarviruses, iridoviruses, phycodnaviruses [1], mimiviruses [2], and marseillevirus [3] that likely share a common viral ancestor [1]. The family *Poxviridae* can be divided taxonomically into two subfamilies, the *Entomopoxvirinae* and the *Chordopoxvirinae*. The *Entomopoxvirinae* infect insects and are subdivided into the genera Alphaentomopoxviruses, Betaentomopoxviruses, and Gammaentomo-poxviruses [4]. The *Chordopoxvirinae* infect diverse vertebrate species including mammals, birds, and reptiles and are comprised of eight genera: *Suipoxvirus*, *Avipoxvirus, Capripoxvirus, Leporipoxvirus, Molluscipoxvirus, Orthopoxvirus, Parapoxvirus,* and *Yatapoxvirus.* Classification of poxvirus species within genera is based on criteria such as particle morphology, antigenic relatedness, genetic similarity, and host range [4, 5].

1.1.2 Orthopoxviruses

The *Orthopoxvirus* genus has a broad tropism and includes important causes of disease in humans [5]. Species in the *Orthopoxvirus* genus include the camelpox, cowpox, ectomelia, monkeypox, taterapox, vaccinia, and variola viruses. The most significant members of the Orthopoxvirus genus in human disease include variola virus (VARV), monkeypox virus (MPXV), and vaccinia virus (VACV). VARV is the most prominent of the orthopoxviruses as it is the causative agent of smallpox, a historically devastating disease. Smallpox was eradicated in 1977 through worldwide vaccination effort using a strain of another important orthopoxvirus, VACV. Despite eradication, VARV is rated as one of the top bioterrorism threats by the US Centers for Disease Control and Prevention (CDC) and efforts continue to develop a more efficacious vaccine and new antivirals. MPXV is an emerging important zoonotic disease because there is no proven treatment for the disease in human infections, and human-to-human transmission of MPXV has occurred [6]. In addition to serving as the vaccine against VARV, VACV has become extremely useful as a potential tool for the development of recombinant vaccines, and advancements in molecular biology have been made through genetic and biochemical studies of aspects of the VACV life cycle. VACV is the most characterized of the poxviruses and most of our understanding of poxvirus biology comes from studies on VACV [5].

1.1.3 Virion structure

Poxvirus virions have a complex morphology that lacks both symmetry and

defined structures such as glycoprotein spikes that characterize other types of viruses. Instead, poxvirus virions are highly asymmetric, brick-shaped particles and are one of the largest viruses at about 360 X 270 X 250 nm in size (Figure 1-1)[7-9]. Moreover, poxviruses produce three types of particles, mature virions (MV), wrapped virions (WV), and extracellular virions (EV), that differ from one another in the number of surrounding envelopes and the protein composition associated with those envelopes. The most abundant particle produced during infection, the MV, is predominantly protein by dry weight with ~3.2% DNA and ~5% lipid [10] and trace amounts of RNA, spermine, and spermidine [5]. MV particles consist of a dumbbell-shaped core surrounded by a single lipoprotein membrane [5] of about 5-6 nm in thickness [9]. Under the lipoprotein membrane, two lateral densities with an unknown function called lateral bodies are located in the concavites of the dumbbell core [5]. The core consists of two layers that together are about 18 nm in thickness surrounding an inner cavity that contains nucleoprotein [9].

1.1.4 Genome organization

Poxviruses have double-stranded linear DNA genomes that range from 143-300 kbp [5]. About 100 genes are conserved among the chordopoxviruses, and about 50 of them are also conserved in entomopoxviruses. Despite variability in genome size and nucleotide sequences, the structure of poxvirus genomes as well as the organization of ORFs within the genomes are conserved. The VACV genome is 195 kbp and contains ~200 ORFs [11]. The most variable genes are found at the ends of the genome and typically encode proteins involved in host-interactions [5]. VACV genome ends contain 10 kbps of inverted terminal repetitions (ITRs), which are

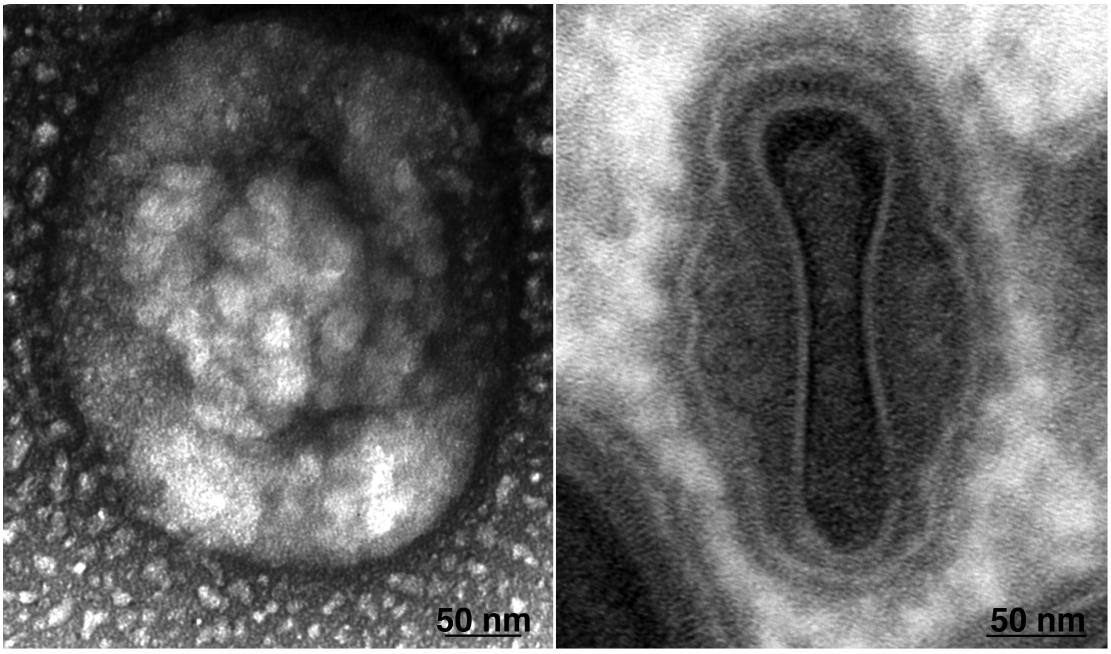

Figure 1-1. Mature virion morphology. The left panel shows a scanning electron micrograph of a mature virion. Virions lack symmetry and prominent, distinct structural features. The right panel is a transmission electron micrograph of a mature virion showing a brick-shaped particle surrounded by a single lipoprotein membrane with a condensed core structure. Scale bars, 50 nm. Images were generously provided by Andrea S. Weisberg.

identical nucleotide sequences in opposite orientations [12, 13]. The genome terminates with an A/T rich region that forms a covalently closed hairpin loop that links the two DNA strands [14]. The central region of the genome contains conserved genes that encode proteins involved in essential processes such as transciption, replication, and virus assembly [5]. Most poxvirus genes are non-overlapping, and each ORF has an upstream promoter that regulates transcription at early, intermediate, or late times during infection. The ORFs have different transcriptional orientations and are transcribed rightward (R) leftward (L) from the genome.

1.1.5 Genome nomenclature

VACV genes are named based on both their location in the genome as determined by restriction mapping using the restriction endonuclease Hind III and their transcriptional orientation [11]. Hind III-digestion of VACV strain Western reserve (WR) genome yields 15 digested products named by mobility in agarose gels. The fragments are designated A-O, with A being the largest and O the smallest [15]. The ORFs are numbered based on the positions from left to right within the digested fragments, and the transcriptional orientation from left to right (R) or right to left (L) is designated. For example, the A26L gene is the 26^{th} ORF in the A Hind III fragment and is transcribed from right to left (L). The gene and protein names are typically the same except that the protein name lacks the transcriptional orientation, and for further clarification, I have included a "p" to designate the protein product of a gene. For example, the A26L gene encodes the A26 protein, or A26p.

1.2 Virus Replication

1.2.1 Attachment and entry

VACV infects numerous cell types and several different animal species. Although both MV and EV particles are infectious, EVs must first shed the outer membrane to expose the entry-fusion complex (EFC), which is located in the MV membrane [16]. The processes leading to the release of viral cores into the cytoplasm can be delineated into two steps: attachment and entry (Figure 1-2). Four VACV proteins have been identified as important in mediating virus attachment A27p, D8p, H3p, and A26p. A27p, D8p, and H3p bind glycosoaminoglycans [17-19], while A26p binds the extracellular matrix protein laminin [20]. Attachment is generally considered important for tethering virions to the cell surface for signaling and uptake, but individual deletions of the VACV genes encoding attachment factors does not prevent cell entry [21].

VACV can enter cells by low pH induced fusion from within endosomes [22-24] or by fusion at the plasma membrane [21]. Entry requires the coordination of several MV-membrane proteins that are associated with or form a complex known as the entry-fusion complex (EFC) [25]. There are 9 integral EFC proteins (A16p [26], G9p [27], A21p [28], A28p [29], G3p [30], H2p [31], J5p [25], L5p [32], and O3p [33]) all of which are required for entry. L1p and F9p are associated with the EFC and are also required for entry [34, 35]. The I2 protein is required for entry, although it has not yet been shown to be part of the EFC [36]. The specific roles of the EFC proteins at different stages during the entry process are not known and a specific receptor(s) for VACV has not been identified [37]. Upon fusion at the

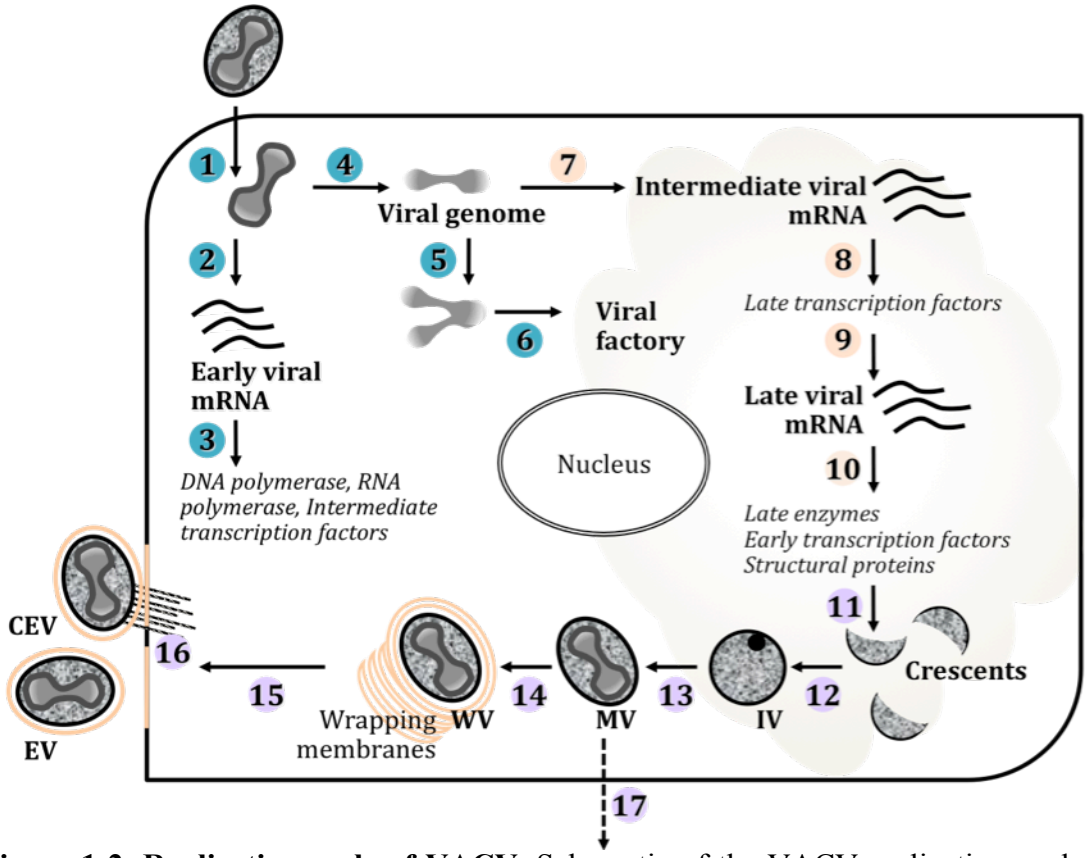

Figure 1-2. Replication cycle of VACV. Schematic of the VACV replication cycle with numbered and color-coded steps : pre-replicative (blue), post-replicative (salmon), and morphogenesis (purple). events highlighted in blue or salmon, respectively. Morphogenesis is highlighted in purple. (1) MV enter by fusion at the plasma membrane or within endosomes delivering the core into the cytoplasm. (2) Early mRNAs are synthesized within the cores and extruded into the cytoplasm. (3) Early mRNAs encode proteins required for replication of the DNA genome and the initiation of intermediate transcription. (4) The viral genome is uncoated and (5) replicates by a rolling hairpin mechanism that generates concatemers. (6) Replication occurs within viral factories, which also coordinate intermediate transcription/translation, late transcription/translation, and assembly of MVs. (7) Intermediate transcription occurs after genome replication and (8) late transcription factors are translated from intermediate mRNAs. (9) Late transcription factors regulate the transcription of late mRNA, which (10) is translated into early transcription factors and structural proteins that become packaged into virions. (11) Crescent membranes are the first morphogenesis intermediates distinguishable by electron microscopy. (12) Crescents grow and surround genomes and viral proteins forming spherical immature virions (IV). (13) IV condense and undergo complex changes to form the brick-shaped mature virion (MV). (14) A subset of MVs become doubly membrane wrapped at either the trans-Golgi network or endosomal cisternae to form wrapped virus (WV), which have three viral membranes. (15) WV traffic along microtubules to the plasma membrane where the outer membrane fuses releasing the extracellular virus (EV). (16) EV that remain on the surface of the cell are called cell-associated EV or CEV and they can polymerize actin tails to propel into adjacent cells. (17) MVs remain in the cytoplasm until lysis of the cell.

plasma membrane or from within endocytic vesicles, the MV membrane is lost and viral cores are released into the cytoplasm to initiate virus infection.

1.2.2 Virus gene expression

VACV gene expression is temporally regulated and genes can be classed as pre- and post-replicative depending on whether expression occurs before or after DNA replication, respectively (Figure 1-2)[5]. The pre-replicative class includes early genes, and the post-replicative class includes intermediate and late genes. Global analysis of the VACV transcriptome revealed the production of 118 pre-replicative ORFs and 93 post-replicative ORFs [38]. In general, early genes express proteins required for early functions such as nucleotide biosynthesis and DNA replication as well as proteins that combat host-defense mechanisms. Intermediate and late genes encode proteins required for later functions such as virion assembly and morphogenesis.

Each class of genes also has a conserved stage-specific promoter sequences that temporally regulates their expression [39-41]. All VACV genes are transcribed by a multisubunit DNA-dependent RNA polymerase (RPO) that is comprised of at least 8 core proteins. Additionally, each stage encodes accessory transcription factors required for initiation of transcription of the subsequent class of genes. Early gene products are required for the transcription of intermediate genes, the products of which are required for late gene transcription. Late genes, in turn, encode transcriptional regulatory factors necessary for early transcription, which are packaged along with the viral genome into virion cores for the initiation of early gene transcription in newly infected cells [42].

Following entry, cores associate with microtubules and move to sites within the cytoplasm where early gene transcription occurs [43, 44]. Synthesis of early mRNAs can occur within minutes of infection, and early mRNAs are extruded from pores in the core. The early transcription apparatus includes the VACV RPO, an RNA-polymerase associated protein of 94 kDa (Rap94), the VACV early transcription factor (VETF), capping and methylating enzymes, poly(A) polymerase, topoisomerase, and two nucleic acid-dependent ATPases [5]. The stage-specific transcriptional regulatory factors for early transcription include Rap94 and VETF. Rap94 interacts with the RPO and possibly prevents transcription from intermediate and late promoters. Rap94 also interacts directly with VETF [45], which is a heterodimer with ATPase and DNA-binding activities that binds early promoters. Cessation of early transcription follows dissociation of the core, which is thought to dismantle the early gene transcription apparatus [5].

Intermediate transcription requires DNA replication [46], intermediate promoter sequences, and is mediated by viral intermediate transcription factors (VITF) (VITF-1, VITF-2, VITF-3 [47]), capping enzyme, and the RPO. VITF-1 and VITF-3 are virally encoded, whereas VITF-2 is cellular [47, 48]. VITF-1 is encoded by the VACV E4L gene and also functions as an RPO subunit, and VITF-3 is a heterodimer of proteins encoded by the VACV A8R and A23R genes [47]. VITF-2 activity is complemented by the Ras-GTPase-activating protein SH3 domain-binding protein (G3BP) and/or p137, the cytoplasmic activation/proliferation-associated protein-1 [48].

Late transcription begins after intermediate transcription and continues

throughout the remainder of the virus life cycle. Initiation of transcription requires the viral RPO, three intermediate proteins, one early protein, and a cellular protein. The intermediate genes G8L, A1L, and A2L encode the VACV late transcription factors (VLTFs) VLTF-1, VLTF-2, and VLTF-3, respectively, which represent the minimal viral proteins required for late transcription [46]. Additionally, the early H5R gene product [49] and the host protein VLTF-X [50] stimulate late transcription. Purified nuclear riboproteins A2/B1 and RBM3 can complement VLTF-X function individually or together *in vitro* [51]. VLTF-X co-purifies with a late promoter DNA-binding activity, and none of the viral VLTFs bind late promoters suggesting recruitment of VLTFs and the RPO to late promoters might be mediated by a host factor [42].

VACV mRNAs have a 5' cap and are 3'polyadenylated. However, both the 5' and 3' ends of the different temporal classes have unique features. About half of the VACV genes have an early promoter [52], which consists of the consensus core sequence AAAAAATGAAAAAA/TA [40] separated by 12-17 nucleotides from a downstream initiator element, which is an A or G residue. In contrast, both intermediate and late transcripts have initiator elements that result in the production of mRNAs that have a 5'poly(A) leader sequence up to 30-40 nucleotides in length [53]. Intermediate transcription core promoters are AT rich 14 bp sequences that are 10 or 11 bp upstream from the initiator element, TAAA. Late promoters consist of a 20 bp, A-T rich core and a downstream initiator element, TAAAT that is often followed by G nucleotide, TAAATG. The ATG in the initiator element often serves as the start codon for protein synthesis. Initiation occurs within the A triplet of the

initiator elements of both intermediate and late promoters, and additional A residues are added by a slippage mechanism to form a 5' poly(A) leader [54]. Slippage is thought to occur by the stuttering of the polymerase at the A triplets found in the TAAA initiator element of intermediate promoters and the TAAAT in late promoters.

The early gene mRNAs are distinguished from the other classes by homogenous 3'ends. The 3'ends of early mRNAs are generated by regulated transcriptional termination, which occurs 20-50 nucleotides downstream of the signal sequence UUUUUNU [55, 56]. Unlike early mRNAs, both intermediate and late mRNAs lack a conserved termination signal sequence and therefore have heterogenous 3' ends [57]. Interestingly, four late mRNAs have been shown to have unique homogenous 3'ends: telomeric transcripts from vaccinia virus [58], transcripts from the gene encoding the second largest subunit of RNA polymerase (A24R) in vaccinia virus [59], transcripts from the F17R gene [60], and transcripts from the gene encoding the major protein component of the A-type inclusion (ATI) bodies [59]. The mechanism of 3′ end formation of the telomeric transcripts and the A24 transcripts has not been shown, but the ends of the F17R and ATI transcripts are generated by site-specific cleavage of a precursor RNA [60, 61].

The site-specific cleavage of the ATI mRNA is mediated by a 43-nucleotide RNA cis-acting element and the resulting ends are 3' polyadenylated. The cis-acting element is composed of at least two noncontiguous regions with a spacer region of 10 bases whose composition may be changed without interfering with RNA 3′ end formation. The sub-element containing the cleavage site is upstream of the other sub-element. Host control elements are also bipartite, the cleavage site is downstream of

the other cleavage element and they do not resemble the ATI mRNA elements in sequence. Portions of the two noncontiguous regions are complementary to each other, suggesting the possibility that the two regions form a specific structure that participates in 3′ end formation [62]. The cleavage site in the F17R transcript does not have sequence homology or predicted structural homology to the ATI cleavage sites, however, the H5 protein has been implicated as the cleavage factor for both transcripts [60].

Each RNA class exhibits rapid turnover following synthesis. Recently, it was shown that two viral de-capping enzymes, D9p and D10p, remove the 5' cap destabilizing viral transcripts [63, 64]. D9 is regulated by an early promoter and D10 is regulated by a late promoter [65, 66]. In addition to a role in the regulation of viral mRNAs, D9 and D10 de-capping and destabilization of host transcripts likely contributes to the shutdown in host protein synthesis.

1.2.3 Virus genome replication

Unlike most DNA viruses, poxviruses replicate their double stranded DNA genomes entirely in the cytoplasm of infected cells (Figure 1-2). Therefore, the majority of the proteins required for replication are virally encoded early proteins. VACV replication occurs in discrete, juxtanuclear bodies called viral factories (VF) and initiates between 1-2 h post-infection, following disassembly of the core [5]. Proteins important for VACV replication and processing of viral DNA include the following: DNA polymerase encoded by E9L, primase/NTPase encoded by D5R [67, 68], uracil DNA glycosylase encoded by D4R [69], processivity factor encoded by A20R, protein kinase encoded by B1R, and Holliday junction resolvase encoded by

A22R [70]. Poxviruses also encode enzymes involved in the synthesis of deoxyribonucleotides such as a thymidine kinase, thymidylate kinase, ribonucleotide reductase, and dUTPase. None of these precursor metabolism enzymes is essential for replication in cell culture, although deletion of the thymidine kinase and ribonucleotide reductase genes attenuates infection *in vivo* [5].

Replication is poorly understood, but is thought to proceed by a rolling hairpin, strand displacement mechanism [5]. In this model, one of the hairpin termini becomes nicked providing a primer for leading strand DNA synthesis in the 5' to 3' direction [71]. Replication results in head-to-head and tail-to-tail concatemerized genomes that get resolved following late gene synthesis of the resolvase, A22p. There are also findings that suggest lagging strand synthesis might be occurring. Small DNA fragments covalently linked to RNA have been reported suggestive of the existence of Okazaki fragments [72]. The VACV D5 protein was demonstrated to have primase activity [68, 73], and the VACV ligase encoded by the A50R gene was shown to be required for viral DNA replication in cells in which cellular ligases were knocked down [74]**.**

1.2.4 Virus factories

Poxviruses replicate their genomes, transcribe intermediate and late genes, translate intermediate and late mRNAs, and assemble progeny virions within specialized compartments called viral factories or VFs (Figure 1-2) [75-78]. Each VF arises from one infectious virion [78, 79]. After entry, cores move along microtubules and accumulate at the cytosolic side of rough-ER membranes where the genome is released for replication [44]. As DNA replication ensues, the progeny genomes

become surrounded in ER-derived cisternae [80, 81]. Cytoplasmic VFs are visible by electron microscopy as early as 3 hpi and are amorphous electron-dense regions containing nucleic acid and devoid of organelles (Figure 1-3A). Confocal microscopy of DAPI-stained VFs shows compact bodies that expand in size during the course of infection presumably due to an increase in the amount of genomic DNA (Figure 1-3B) [79, 80, 82]. During expansion, VFs migrate to juxtanuclear locations along microtubules, and VFs can collide and fuse together during this migration [82]. By 5 hpi, at the onset of virion assembly, the ER envelope begins to disassemble. DAPI staining reveals that VFs lose their compact appearance and begin to dissipate during the course of infection presumably because genomic DNA is being packaged into virions.

A recent study showed that VFs coordinate genome replication with transcription and translation as well as virus assembly [79]. In contrast to early mRNA transcription,which takes place inside cores, intermediate and late mRNAs are transcribed and translated within VFs [44, 79]. DAPI staining revealed VFs are not uniform masses but instead have tunnel-like cavities giving them a ‘sponge’-like appearance. The cavities appear to connect with the cytoplasm resulting in the increase of the cytoplasm-factory interface area. The viral mRNA as well as viral and host intermediate transcription factors A23p and Ras-GTPase-activating protein SH3 domain-binding protein (G3BP), respectively, localized to these tunnel-like cavities or subdomains within the VFs. It was also shown that transcription is intimately associated with translation within the VF subdomains. Confocal microscopy revealed that two cellular translation initiation factors, eIF4E and eIF4G, as well as poly(A)

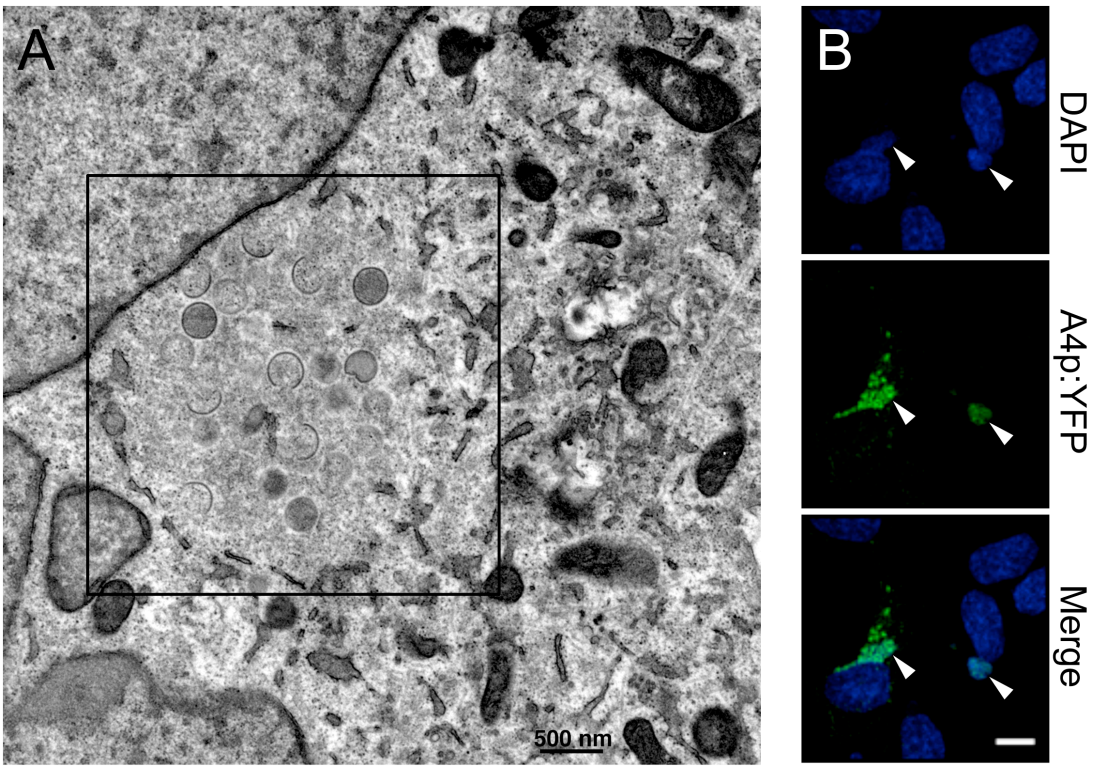

Figure 1-3. Viral factories. (A) Transmission electron micrograph of VACV viral factory (boxed) containing morphogenesis intermediates early post infection. Scale bar, 500 nm. (B) Images show two infected cells with A4p:YFP in viral factories (arrowheads). HeLa cells were infected with a recombinant VACV expressing YFP fused to a core protein, A4p. Blue, DAPI; green, A4p:YFP. Scale bar, 10 μm.

RNA were coincident with G3BP in the cavities [79]. Additionally, staining with antibodies to the P proteins of the large ribosomal subunit showed the presence of ribosomes in VFs. Finally, experiments in which cells were infected with two different recombinant VACVs, each expressing a different fluorescent protein (CFP and YFP) fused to a late viral protein, resulted in individual cyan or yellow VFs in the same cell. This showed that transcription and translation occur from the input virus genome within the boundary of the VF [79].

1.2.5 Mature virion morphogenesis

Poxviruses undergo an intricate assembly process that yields two infectious virions that are morphologically distinct, MVs and EVs (Figure 1-4)[77, 83]. Morphogenesis begins with a growing crescent-shaped membrane supported by a protein lattice. Crescents envelope the genome along with core protein precursors and seal becoming immature virions (IV), which in turn lose the support and mature into infectious, mature virions (MV). MV acquire two additional membranes forming the intracellular wrapped virus (WV) and following egress and fusion at the plasma membrane the outer membrane is lost to release the doubly wrapped EVs and CEVs (Figure 1-2).

Assembly begins in the VF roughly 4 hpi [83], and the first distinct structures visualized by electron microscopy are crescent-shaped precursors and immature virions (IVs)(Figure 1-4)[84]. The composition and origin of crescents is disputed, but they are most likely single-membrane structures. Although recent work suggests they might be derived from ER membranes [85, 86], there is no direct evidence demonstrating the presence of ER proteins on viral membranes. Crescents have a

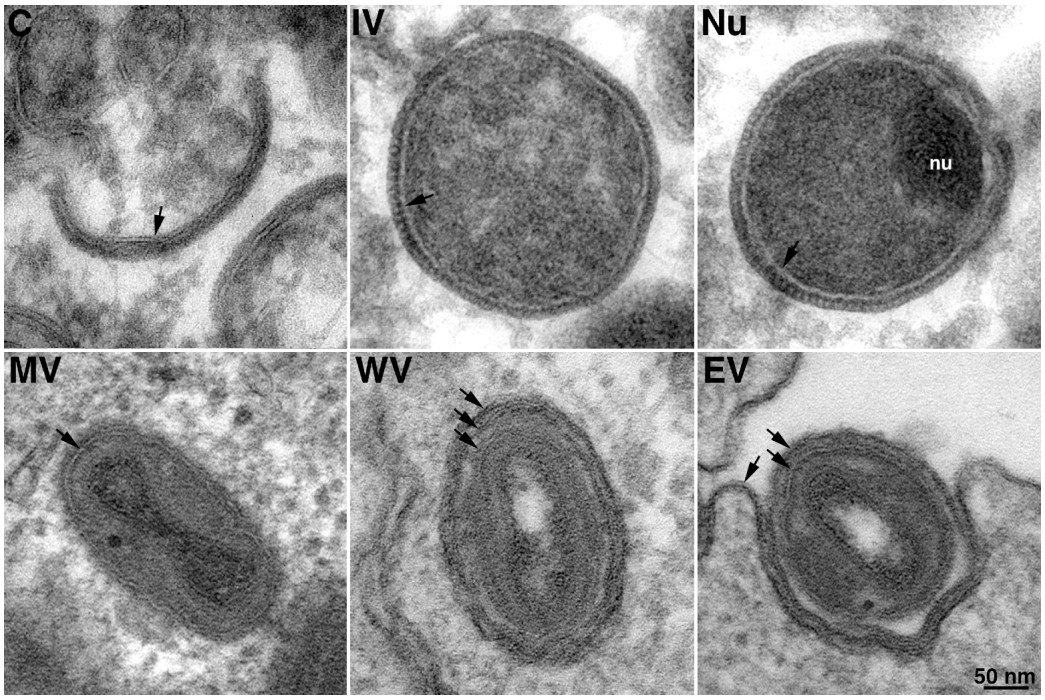

Figure 1-4. Transmission electron micrographs of different stages during VACV virion morphogenesis. (C) Crescents; (IV) immature virion; (Nu) nucleoid; (MV) mature virion; (WV) wrapped virion; (EV) extracellular virion. Arrows indicate membranes. The MV has one membrane, which is also present WVs and EVs. The WV has three membranes, and the EV has two membranes having lost the outer membrane at the plasma membrane. Images were generously provided by Andrea S. Weisberg.

lattice coat comprised of trimers of the D13 protein arranged on the membrane surface in a honeycomb lattice that appear as electron-dense 'spicules' by electron microscopy [87, 88]. Crescents envelope viroplasm forming 300 nm, spherical IVs Following loss of the supportive protein lattice, IVs condense and mature into the brick-shaped, infectious MV particles.

Electron microscropic studies of conditional lethal VACV mutants have identified several viral proteins required for crescent formation. Repression of two viral membrane proteins, A14p and A17p, demonstrated their requirement for crescent formation. A17p is a transmembrane protein that spans the viral membrane twice with both termini extending into the cytoplasmic face of the membrane and a hydrophilic loop within the lumen [89, 90]. The N-terminus of A17p binds and recruits D13p, which forms a lattice that likely confers stability and curvature [87, 88, 91]. Repression of soluble proteins H5p [92], G5p [93], A11p [94], H7p [95], and F10p [96-98] also results in an absence of crescent-shaped membranes. F10p is a dual specificity kinase associated with viral membranes and is required for phosphorylation of the A14 and A17 proteins [99], which are transmembrane proteins required for membrane biogenesis. Additionally, the F10p phosphorylates the H5p and the A30 protein. A30p, along with F10p, G7p, J1p, D2p, D3p, and A15p are core proteins that form a complex that mediates the filling of crescents with viroplasm during IV formation [100, 101]. Before the crescent membrane grows to a closed, spherical IV, the genome is acquired and condenses to a 'nucleoid' appearing as a circular, electron-dense body by electron microscopy (Figure 1-4). How the genome is packaged is not well understood, but repression of the core proteins A32p and I6p

or the A17 membrane protein blocks the incorporation of genomic DNA into IVs. Additionally, repression of the Holliday resolvase, A22p, perturbs concatemer resolution and results in the accumulation of IVs without nucleoids [84].

Maturation of IVs to infectious MVs involves several processes including the loss of the D13p honeycomb lattice, the proteolytic processing of proteins, and the formation of disulfide bonds [84]. This complex process results in brick-shaped MV particles comprised of ~80 proteins (Figure 1-4)[84]. The loss of the D13p lattice requires the proteolytic processing of A17p. After IVs are formed, the N- and C-termini of A17p are both proteolytically processed by the viral protease I7p at AG16↓A and AG185↓A motifs. This cleavage results in the loss of the D13p scaffold and the IV collapses to form the brick-shaped MV [91]. Cleavage of the core proteins A3p, A10p, A12p, L4p, and G7p at the consensus AG↓X motif is also required for maturation and is also likely mediated by the I7 protease [5]. Thus, proteolytic processing of at least one membrane protein (A17p) and five core proteins is required for the maturation of IVs to MVs.

The formation of infectious MV also requires the modification of disulfide bonds in several MV-membrane proteins. Cellular disulfide bond formation occurs within the ER lumen, but viral proteins are exposed to the reducing cytoplasm of infected cells. Therefore, VACV encodes its own redox system that shows specificity for viral proteins localized to the viral membrane [102]. Repression of any of the VACV redox proteins, the E10, A2.5, and G4 proteins, results in an arrest in morphogenesis [103-105].

1.2.6 Extracellular virion morphogenesis and egress

Most MVs remain in the cell until cellular lysis and are surrounded by a single lipid membrane [106]. Some MVs, however, acquire two additional membranes to WV (Figure 1-4). Wrapped virions, in turn, traffic to the plasma membrane and become exocytosed, losing the outermost membrane upon release to the cell surface as either CEV or extracellular virions (EV)(Figure 1-4)[107]. CEVs remain attached to the cell surface, whereas EVs are released into the extracellular millieu. CEV and EV production requires several steps (Figure 1-2): (1) wrapping of MV to form WV, (2) WV egress to the plasma membrane, (3) fusion of the outermost WV membrane with the cytoplasmic leaflet of the plasma membrane, and (4) CEV dissemination by the polymerization of actin tails.

MVs require microtubules for movement from VFs to sites of wrapping [108]. Live cell imaging of cells infected with recombinant VACV expressing the yellow fluorescent protein (YFP) fused to the core protein A4p showed that movement of MVs between VFs and sites of wrapping is bidirectional, saltatory, and disrupted by the microtubule depolymerizing drug nocodazole [108]. The viral protein(s) and molecular motor(s) involved in this MV movement are currently unknown [108, 109].

The two additional membranes acquired for WVs are derived from either the trans-Golgi network (TGN) or endosomal cisternae [110, 111]. The wrapping membranes contain six virus-encoded proteins that are not present in MVs and regulate the formation of CEV and EV: F13p, B5p, A33p, A34p, A36p, and F12p [112-117]. A27p also regulates wrapping, but is found in both MV and EV/CEV particles. Repressing the expression of any of these gene products results in a small plaque phenotype because CEV/EV particles are required for effective cell-to-cell

spread and plaque formation. Wrapping requires wrapping membrane-associated proteins F13p and B5p [115, 117, 118] and MV membrane-associated A27p [119]. F13L-, B5R-, and A27L-deletion viruses produce small plaques, and WV is not detected in infected cells by electron microscopy [115, 117, 119]. Disulfide-bonded trimers of A27p are attached to the MV membrane by protein-protein interactions with the MV transmembrane protein, A17p [120-122]. The A27-A17 interaction is mediated through C-terminus of A27p, which contains an alpha helical "anchoring domain [120, 123]." The precise role of A27p in wrapping is unknown; however, EM studies have shown that A27p is almost exclusively associated with the cytosolic face of the MV membrane [124], and it is suggested that A27p might interact with the wrapping membrane through interactions with a virus or host protein(s). It was suggested that A27p might be a movement factor, but live cell imaging showed that MV could move bidirectionally between VFs and sites of wrapping in the absence of the A27p [108].

F13p is located between the EV/CEV outer envelope and the MV membrane [107]. F13p lacks a transmembrane domain and is instead anchored to membranes through two palmitylated cysteines [125]. F13p is the target of an antiviral compound known as ST-246 [4-trifluoromethyl-N-(3,3a,4,4a,5,5a,6,6a-octahydro-1,3-di oxo-4,6-ethenocycloprop [f]isoindol-2(1 H)-yl)-benzamide] that inhibits EV production and protects mice from orthopoxvirus-induced disease [126]. The role of B5p in wrapping in not understood, but it contains a putative phospholipase motif that is essential for the production of WV and is located on the outside of the CEV/EV membrane [127]. F12p and E2p have also been implicated in wrapping. E2p is

abundant in EVs, but unlike F12p it is also present in MV [128]. A study recently showed that F12p and E2p interact in a complex [129] and the deletion of either genes causes defects in WV formation resulting in a small plaque formation [128, 129].

WVs hijack kinesin-1 motors and traffic along microtubules during egress [130, 131]. WV movement requires coordination of the F12 and A36 proteins, which are found on the outermost envelope of WV and are not present in CEV and EV [132, 133]. Conventionally, the A36p was considered the movement factor required for WV transport because A36p was shown to interact with microtubules and the deletion of the A36R gene blocked the recruitment of kinesin-1 motors to WVs [134, 135]. Subsequent studies, however, showed that A36p functions in movement by anchoring the movement protein, F12p, which lacks a transmembrane domain, to the WV particle membrane [136, 137]. F12p mimics the structure of cellular kinesin light chain (KLC) and this property was demonstrated to be required for the recruitment of the kinesin-1 motor to virions [137]. Upon reaching the cortical actin network at the cell periphery, A36p is phosphorylated causing WV to disassociate from kinesin-1 motors [138], and the outer membrane of WV fuses with the plasma membrane to present the particle on the cell surface as CEV or result in the particles release as an EV [139].

CEV can induce the formation of motile actin-containing cell projections to propel itself to neighboring cells [140]. The formation of these tails is abrogated when expression of the A36R, A33R, and A34R genes is repressed. Actin tail formation is induced by the src-kinase phosphorylation of A36p, which accumulates in the plasma

membrane under CEV [107]. Phosphorylated A36p recruits cell proteins Nck, Grb2, N-WASP and Arp2/3 to polymerize actin beneath the CEV particle [133, 138, 141, 142]. A36p is incorporated into wrapping membranes by A33p [133] via its interaction with A34p [143].

MVs are the most abundant particles produced during VACV infections, although the MV to EV ratio varies among cell types and virus strains [144]. The mechanism by which MV differentiate to become wrapped or to remain the cytoplasm until lysis is unknown [145]. The MVs of some orthopoxviruses have an alternative fate in that they are retained in the cytoplasm within proteinaceous inclusion bodies. Formation of inclusion bodies and the embedment of MVs within them are mediated by homologs of the VACV A25 and A26 proteins, respectively.

1.3 Virus Inclusion Bodies

1.3.1 A-type inclusion bodies, ATIp, and A25p

Some orthopoxviruses, including strains of cowpox (CXPV), ectromelia (ECTV), fowlpox, canarypox, and raccoonpox can embed MVs in cytoplasmic, proteinaceous matrices (Figure 1-5)[146-150]. These protein matrices were named A-type inclusion bodies (ATIs) to distinguish them from B-type inclusion bodies, or VFs, formed by poxviruses for replication and assembly. When viewed by thin section electron microscopy ATIs appear as well-defined, circular, electron-dense matrices that can be several microns in diameter (Figure 1-5). ATIs form subsequent to viral

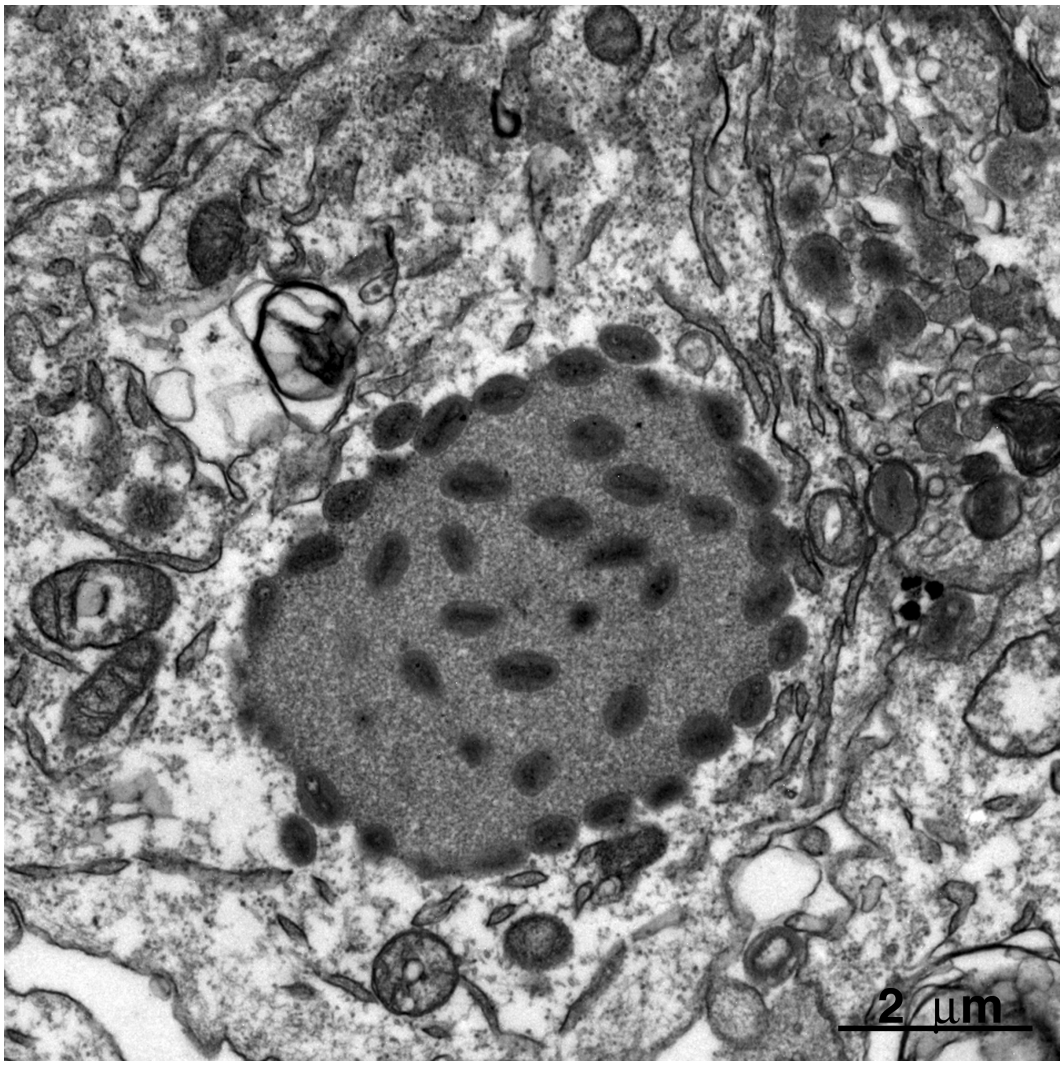

Figure 1-5. Transmission electron micrograph of an A-type inclusion body embedded with mature virions. Scale bar, 2 µm. Image was generously provided by Andrea S. Weisberg.

DNA replication throughout the cell and increase in size during infection [151]. Unlike VFs, ATIs do not contain nucleic acid and are not surrounded by membranes [152]. VFs and ATIs are similar, however, in that they both recruit ribosomes [79, 152, 153]. In electron micrographs of thin-sliced sections from cells infected with CPXV, polyribosomes and nascent protein pulse-labeled with 3H-leucine were seen at the peripheries of ATIs [152, 153]. Subsequent experiments suggested that viral RNA was associated with the polyribosomes at surface of ATIs, but the specific RNA was not identified [153].

The ATI is formed entirely by a single known viral protein, the ATIp [151]. The ATIp is a late protein and is one of the most abundantly synthesized proteins in infected cells at late stages of virus replication [151]. ATI proteins are high molecular weight (160 kDa in CPXV), hydrophobic proteins that contain 14 repeats of about 30 amino acids each called the ATIp repeats [151, 154]. Orthopoxviruses that do not form inclusion bodies encode a truncated ATI protein that lacks these repeats. An ATIp homolog encoded by the A25L gene (VACVWR148) of the Western Reserve (WR) strain of VACV contains a deletion of two adjacent adenylate residues resulting in synthesis of a C-terminally truncated, 94-kDa protein [151, 155, 156]. This A25 protein contains the N-terminal half of ATIp including the first four ATIp repeats and six amino acids of the fifth repeat. This protein is not sufficient for inclusion body formation and has no known function in VACV replication.

1.3.2 Occlusion and A26p

The embedment of MV within ATIs is a process referred to as occlusion. At late stages in the replication cycle, MVs are found closely packed throughout the

matrices and encrusting the surface of ATIs (Figure 1-5)[157]. Only MVs become embedded and crescents and IVs are not typically seen within ATIs, although some IVs can be detected within them in the presence of the drug rifampicin, which blocks IV maturation [152]. Occlusion requires full-length homologs of the VACV A26 protein and orthopoxviruses that do not embed MVs within ATIs have mutated A26 genes (27, 42). Full-length A26p is 60-kDa in size, lacks predicted functional domains, and is expressed late during infection. A26p is somehow incorporated into the MV membrane although it lacks a predicted transmembrane domain [158, 159]. A C-terminal region of A26p shares 44% amino acid identity to the C-terminal, alpha helical "anchoring domain" of the A27p. A27p also lacks a transmembrane domain. Instead, the anchoring domain of A27p mediates protein-protein interactions with the transmembrane protein A17p for incorporation into the MV membrane [123]. Although VACV does not form inclusion bodies, the VACV A26L gene (VACVWR149) is intact, and the VACV A26p can complement the defective A26p homolog in the Brighton red (BR) strain of CPXV (CPXV-BR) [160].

It is unknown how A26p mediates occlusion, but it has been suggested that A26p might function in the retrograde movement of MVs to inclusion bodies [160]. In this model, MVs that lack A26p move to sites of wrapping and MVs that have A26p move to inclusion bodies for embedment. The main observation supporting this hypothesis is the spatial separation of MV from inclusion bodies seen in cells infected with orthopoxvirus strains expressing a truncated A26p. Additionally, an ECTV strain that embeds MVs within ATIs forms smaller plaques than a strain that encodes a truncated A26p and does not embed MVs within ATIs [157]. As mentioned

previously, a small plaque phenotype is characteristic of a defect in the production of CEV/EV. Conversely, a large plaque phenotype could be indicative of a greater production CEV/EV. It was hypothesized that A26p provides an equivalent function in transporting VACV MVs away from sites of wrapping [160]. The VACV Copenhagen strain encodes a truncated A26p and was reported to produce more EV than the VACV IHD-J strain that encodes a full-length A26p [145]. The conservation of the A26L gene among orthopoxviruses irrespective of ATI formation suggests A26p has a function in addition to its role during MV occlusion.

1.3.3 Insect Virus Inclusion Bodies

Members of three diverse families of insect viruses including the *Baculoviridae* (baculoviruses) and the *Poxviridae* (entomopoxviruses) embed virions in inclusion bodies [161-163]. Members of the nucleopolyhedroviruses (NPVs), a genus in the family *Baculoviridae,* have rod-shaped, enveloped nucleocapids that house a circular, 80-180 kb dsDNA genome and, unlike poxviruses, replicate in the nuclei of infected insect cells [164]. Baculoviruses produce two types of infectious virions, the budded virus (BV) and the occlusion-derived virus (ODV). Like EVs, BVs bud from the plasma membranes of infected cells and are important for systemic spread within the insect. ODVs form later during infection in the nuclei of infected cells and become embedded in polyhedra [165]. Polyhedra containing ODVs are released from the cell by lysis. Following consumption by a susceptible host, the polyhedra are dissolved by the strong alkaline pH of the insect midgut to initiate primary infection [162].

Polyhedra are ordered crystalline structures of about 0.15-3 μm in size and are

primarily composed of a matrix protein is called polyhedrin. Polyhedrin is an abundant 30-kDa protein synthesized very late during infection that does not have homology to the ATIp [161, 166]. Another viral protein that associates with polyhedra is the polyhedron envelope protein (PE). PE forms an envelope coat around polyhedra that is thought to provide stability [167] and deletion of the PE gene results in the production of fragile polyhedra with structural defects observable by electron microscopy [162]. The genes encoding polyhedrin [168] and PE are considered non-essential because deletion does not affect BV production in tissue culture. The mechanism of ODV embedment or occlusion within polyhedra remains to be elucidated. However, the *Bombyx mori* nucleopolyhedrovirus (BmNPV) Bm56 protein was recently implicated as an occlusion factor [169]. Bm56 is a 15.8-kDa late protein that is associated with the NPV nucleocapsid. The deletion of the Bm56 gene resulted in the production of aberrant polyhedra lacking embedded ODVs [169]. Like the genes required for the formation of polyhedra, the gene encoding Bm56 is dispensable in cell culture [169].

Entomopoxviruses (EPXVs) have a linear, 225 kb dsDNA genome [170]. Similar to orthopoxviruses and baculoviruses, EPXV infections result in the production of two types of infectious virions: the extracellular virus (EV) and the occluded virus (OV). EVs bud from the plasma membrane and are important for dissemination within the insect, whereas OVs become embedded within inclusion bodies called spheroids that are released from the cell upon lysis [170]. Spheroids form in the cytoplasm post-replication and contain mature OVs arranged randomly throughout the matrix of the spheroid. Purified OVs are morphologically similar to

orthopoxvirus MVs and are large (170-250 x 300-400 nm), complex particles surrounded by a lipoprotein membrane [171]. OVs comprise at least 40 structural proteins although little is known about the location or distribution of those proteins in the virus particle [170]. EPXV infections initiate with the ingestion of OV-embedded spheroids from which the OVs are liberated in the alkaline conditions of the insect midgut.

Spheroids are ovoid, electron-dense structures consisting of a paracrystalline lattice [172] and can vary in size from 5-20 μm [173]. The primary matrix protein of spheroids is the 115-kDa late protein, spheroidin, which is the most highly expressed entomopoxvirus protein during infection [170, 174, 175]. Spheroidin homologs can contain up to 46 cysteine residues, which are thought to be important for assembly into inclusions, and the C-terminal 200 amino acids are highly hydrophobic. Spheroidin does not share amino acid homology with the ATIp of orthopoxviruses, and ATIs are not crystalline structures [175]. The gene encoding spheroidin, *sph*, was found to be dispensable in cell culture despite having high conservation among EPXVs [176].

EPXVs that infect coleopteran (beetles) and lepidopteran (moths and butterflies) insects can form another type of inclusion body called spindles, which do not contain virions [172]. Spindles are fusiform paracrystalline inclusions composed of a single protein called fusolin, which lacks sequence homology to the spheroidin and the orthopoxvirus ATIp. Spindles are found outside of spheroids, but they can become occluded in spheroids along with OVs [170, 172]. Although fusolin is dispensable in tissue culture, spindles greatly enhance infectivity *in vivo* by disrupting

the protective peritrophic membrane lining the insect gut [177].

Baculovirus polyhedra and EPXV spheroids both have fibrils associated with them in infected cells. The baculovirus P10 protein interacts with microtubules and forms filament-like fibrils early in infection [178, 179]. Later, P10 forms tubular structures that lack microtubules and that penetrate the nucleus and associate with the surface of the polyhedra. EPXV fibrils are comprised of the filament-associated late protein of entomopoxviruses (FALPE)[180]. Unlike P10, FALPE filaments do not show an association with host cell microtubules (2). P10 and FALPE share a relatively low amino acid identity, however both proteins have a proline-rich stretch of amino acids and a basic C-terminal tail [180]. The genes encoding P10 and FALPE are both dispensable in tissue culture, and the precise role of fibrils in inclusion formation, occlusion, and transmission is not well understood. P10 is thought to assist in formation of the PE-envelope [180], because deletion of the *p10* gene results in fragile polyhedra that resemble those formed in the absence of the PE protein [162]. It has been proposed that P10 tubules may confer protection to polyhedra following death and decay of the host insect [178].

Embedment of insect virions within inclusion bodies mediates efficient delivery of infectious virions to the insect midgut and is thought to protect virions from heat and UV irradiation during horizontal transmission among emergent populations of insects [162]. The biological significance of orthopoxvirus occlusion within ATIs is unknown. However, analogous to the inclusion bodies produced by insect viruses, inclusion bodies are generally thought to provide stability to MV and to protect them from the environment upon lysis of the cell.

Chapter 2: Vaccinia virus A26 and A27 proteins form a stable complex tethered to mature virions by association with the A17 transmembrane protein

2.1 Introduction

Vaccinia virus (VACV), a member of the *Poxviridae,* undergoes an elaborate assembly process involving the sequential formation of morphologically distinct infectious virus particles [181]. The mature virions (MVs) are the most abundant infectious particles and are released upon cell lysis. The MV consists of: (i) a dumbbell-shaped core containing the viral double-stranded DNA genome, structural proteins, and enzymes and factors for early gene transcription; (ii) lateral bodies of undefined nature that are nestled in the concavities of the core; and (iii) an external lipoprotein membrane. Membranes derived from either the trans-Golgi network or endosomal cisternae envelop a subset of MV particles to form doubly wrapped virions (WVs) [182-184]. WVs traffic along microtubules to the periphery of the cell, where the outer membrane fuses with the plasma membrane to release enveloped virions (EVs) [185-188]. Many EVs remain associated with the outer surface of the plasma membrane and mediate spread to neighboring cells on the tips of actin-containing microvilli [189, 190]. Some poxviruses (e.g. cowpox, ectromelia, raccoonpox, fowlpox, and canarypox but not VACV or variola virus) occlude MVs in a proteinaceous body called an A-type inclusion (ATI) that is thought to protect the virus particles in harsh environmental conditions [191].

Recent mass spectroscopy studies indicate that MVs are comprised of

approximately 80 polypeptides [192-194]. Although EVs are essentially MVs with an outer membrane, there are some differences. Thus, VACV proteins A25 (VACVWR148) and A26 (VACVWR149) are present in MVs but absent from EVs [195]. A25p has a predicted mass of 84 kDa and is a truncated, apparently non-functional homolog of the cowpox ATI matrix protein [155, 156, 196]. VACV A26 is a 58-kDa full-length homolog of the occlusion factor required for incorporating MVs into the ATI matrix [197]. Nevertheless, A26p is conserved in orthopoxviruses irrespective of their capacity to form ATIs, suggesting an additional role. Ulateo and co-workers [195] suggested that A26p acts as a switch to enhance the production of MVs at the expense of EVs. Following up on this idea, McKelvey et al. [197] suggested that A26p might enhance retrograde transport of MVs. However, the effect of deleting the A26 gene on EV production has not been reported. More recently, A26p was shown to bind laminin and to function in cell attachment [198].

In this chapter I show that A26p exists in a complex with three other viral proteins: A25p, A27p and A17p. The interaction of A26p and A27p is direct and stabilized by a disulfide bond. The interaction of A26p with the A17p transmembrane protein is mediated through A27p and this provides the anchor for localization of A26p on the surface of MVs. Since A27p is required for EV formation [199], the interaction of A26p and A27p provided a plausible mechanism for A26p to negatively regulate wrapping. However, EV formation was not enhanced by deletion of A26p in two cell types analyzed.

2.2 Materials and Methods

2.2.1 Cells and viruses.

African green monkey kidney BS-C-1, rabbit kidney epithelial RK-13, and human HeLa S3 cell cultures were maintained in minimum essential medium with Earle's salts (Quality Biological, Gaithersburg, MD) supplemented with 10% fetal bovine serum, 2 mM L-glutamine, 100 units/ml of penicillin, and 100 µg/ml of streptomycin. Infections were carried out in medium containing 2.5% fetal bovine serum and otherwise supplemented as described above. Recombinant viruses derived from the VACV Western reserve (WR) strain were propagated as described previously [200].

2.2.2 Antibodies for Western blotting.

Rabbit polyclonal antibodies against the following VACV proteins were used: A27p [201], A17p [202], and A3p (R. Doms and B. Moss, unpublished data). Anti-HA (Bethyl Laboratories, Inc., Montgomery, TX) and anti-V5 (Invitrogen, Carlsbad, CA) antibodies were conjugated to horseradish peroxidase.

2.2.3 Recombinant virus and plasmid construction.

The A27 deletion (vYFP-A4/ΔA27 denoted here as vΔA27) and revertant viruses (vYFP-A4/ΔA27-rev denoted here as vΔA27.Rev) and vA4-YFP used to generate vΔA27 were previously described [203, 204]. Both express the yellow fluorescent protein fused to the N-terminus of A4 and have A27L deleted from its native locus. vΔA27.Rev has a full-length copy of the A27L gene under its native promoter in the thymidine kinase locus [204]. The A26 deletion virus (vΔA26) was

generated from a recombinant VACV WR virus that expresses luciferase via a synthetic early-late promoter (WRvFire) [205] by replacing the A26L gene with a cassette that expresses the enhanced green fluorescent protein. vA26V5 was derived from VACV WR by homologous recombination with a PCR product containing the A26L gene with a C-terminal V5 epitope tag (GKPIPNPLLGLDST) under the control of the A26L promoter and the enhanced green fluorescent protein open reading frame (ORF) regulated by the late promoter derived from the A17R gene, and A26L downstream flanking sequences. Recombinant viruses expressing enhanced green fluorescent protein were clonally purified by four consecutive rounds of plaque isolation. Genome modifications were verified by sequencing.

pA26V5 was generated by PCR-amplification of V5-tagged A26L from vA26V5 genomic DNA using the forward primer 5'-CTTAACTCTTTTGTTAATTAAAAGTATATTCAAAAAATGAG-3' and the reverse primer 5'-CTACGTAGAATCGAGACCGAGGAGAGGGTTAGGG ATAGGCTTACC-3'. The resulting PCR product included the A26L ORF and a 48 bp upstream region containing the predicted late promoter consisting of an A/T rich region and the TAAATG initiator element at the –1 position [206]. pA26ΔCV5 contains the A26L sequence coding for amino acids 1-409 of A26 plus a C-terminally appended V5 tag under the control of the A26L promoter sequence as above. Primers 5'-CTTAACTCTTTTGTTAATTAAAAGTATATTCAAAAAATGAG-3' and 5'-<u>CTACGTAGAATCGAGACCGAGGAGAGGGTTAGGGATAGGCTTACC</u>TTCTT CTACAGGAAGAAGTTTCGGCCTC-3' (V5 sequence underlined) were used to amplify the A26 sequence coding for the N-terminal 409 amino acids from VACV

WR DNA. pA26ΔNV5 expresses the C-terminal 220 amino acids of A26 fused to a C-terminal V5 epitope tag. Forward primer 5'-GAAAAATTTAGCAATG ATGCTATACTCGTTTATATTAGAACAAAC-3' and reverse primer 5'-CTACGTAGAATCGAGACCGAGGAGAGGGTTAGGGATAGGCTTACC-3' were used to amplify the C-terminal fragment of A26 from vA26V5 DNA. To add the A26 promoter sequence, the above PCR product was used as a template in a reaction using the primers 5'-CTTAACTCTTTTGTTAATTAAAAGTATATTCAA AAAATGAGTTATATAAATGGAAAAATTTAGCAATGATGCTATACTCG-3' (A26 upstream sequence including the promoter underlined) and 5'-CTACGTAGA ATCGAGACCGAGGAGAGGGTTAGGGATAGGCTTACC-3'. A plasmid including the A27L ORF and the upstream 49 bp shown to be sufficient to drive expression of A27 [204] was also generated. All recombinant PCR products were amplified using Accuprime *Pfx* (Invitrogen), blunt-end ligated into pCR-BluntII-TOPO (Invitrogen), and verified by DNA sequencing.

The PCR product used to construct pT7.A26V5 was generated using primers 5'-GGCCG**C/TCGAG**ATGGCGAACATTATAAATTTATGGAACG GAATTGTACC-3 and 5'-GGC**G/TCGAC**CTACGTAGAATCGAGACC GAGGAGAGG-3', which introduced N-terminal *Xho*I and C-terminal *Sal*I restriction sites (bold), respectively, for directional cloning into the pTNT vector (Promega, Madison, WI) under the control of the T7 promoter. Similarly, the A27L gene was amplified with primers 5'- GCCCGG**C/TCGAG**ATGGACGGAACTCTTTT CCCCGGAGATG-3' and 5'- GGC**G/TCGAC**CTAAGCGTAGTCTGGGACGTCG

TATGGGTACTCATATGGGCGCCGTCCAGTCTG-3' thereby introducing the influenza virus hemagglutinin (HA) epitope tag (YPYDVPDYA) before the stop codon to generate pT7.A27HA.

2.2.4 Transient expression of proteins.

Six-well plates of BS-C-1 cells were infected at a multiplicity of 5 PFU per cell in Opti- MEM reduced serum media (Invitrogen) for 1 h. Following adsorption, monolayers were washed twice with Opti-MEM, and 1 μg of each plasmid in 8 μl of Lipofectamine 2000 (Invitrogen) in fresh Opti-MEM (Invitrogen) was added. Monolayers were harvested after 18-20 h.

2.2.5 Virus purification.

MVs were purified from HeLa cell extracts by sedimentation through two 36% (w/v) sucrose cushions and banding once on a 25 to 40% (w/v) sucrose gradient as described previously [207]. For CsCl gradient purification, approximately 6 X 10^7 BS-C-1 cells in two T150 flasks were infected with vΔA27 at a multiplicity of 5 PFU per cell and then transfected with pA26V5 in the presence or absence of pA27 (1 μg each plasmid per 1 X 10^6 cells). After 24 h, the cells were harvested and subjected to two 36% sucrose cushions followed by banding on a 25%-40% sucrose gradient as described above. The sucrose gradient purified virus was resuspended in 500 μl of 10 mM Tris-HCl (pH 9.0) and layered onto a preformed CsCl gradient (1.23 g/ml to 1.29 g/ml) and centrifuged at 180,000 X g for 4 h at room temperature as described [208].

2.2.6 Immunoaffinity purification and Western blot analysis.

Intact cells or sucrose gradient-purified virions were solubilized in lysis buffer

(150 mM NaCl, 50 mM Tris-HCl pH 8.0, 1% NP40) for 30 min on ice. Following brief sonication, the extracts were clarified by centrifugation and incubated with unconjugated agarose A beads (Invitrogen) for 1 h at 4°C. The extracts were then rotated 4-12 h at 4°C with antiserum prior to incubation with pre-washed agarose A beads overnight at 4°C. Anti-V5 immunoaffinity purification was carried out per the manufacturers instructions using the above lysis buffer. Bound fractions were eluted in lithium dodecyl sulfate (LDS) loading buffer (Invitrogen), resolved by sodium dodecyl sulfate-polyacrylamide gel electrophoresis (SDS-PAGE) using 4-12% NuPAGE Bis-Tris gels in NuPAGE MOPS running buffer (Invitrogen), transferred to a nitrocellulose membrane and analyzed by Western blotting using rabbit polyclonal antiserum and anti-rabbit immunoglobulin G (IgG) conjugated to horse radish peroxidase (Pierce, Rockford, IL) consecutively or with anti-V5 antibody and anti-HA-horse radish peroxidase antibodies as described above. Bound IgG was detected using the SuperSignal chemiluminescent substrates (Pierce). For analysis of whole cell lysates, cells were collected by centrifugation and resuspended in LDS sample buffer (Invitrogen) prior to SDS-PAGE. *N*-ethylmaleimide (NEM, Sigma) was added to cells prior to lysis as previously described [209].

2.2.7 Biotinylation of purified virions.

Sucrose gradient-purified virions were rotated with 1 mg/ml of sulfosuccinimidyl 2-(biotinamido)-ethyl-1,3-dithiopropionate (EZ-Link sulfo-NHS-SS-biotin, Pierce) for 30 min at 4°C. Excess biotin was quenched with 50 mM Tris-HCl, pH 8.0. Virions were pelleted by centrifugation at 20,000 x *g* for 30 min at 4°C and solubilized by the addition of SDS-PAGE sample buffer. To recover biotinylated

proteins, samples were rotated with NutrAvidin agarose beads (Pierce) for 1 h at 4°C. The supernatant fraction was removed and the beads were washed five times in cold phosphate buffered saline (Quality Biological, Inc.). Biotinylated proteins were then eluted using LDS sample buffer plus 50 mM dithiothreitol and analyzed along with the unbound fractions by SDS-PAGE and Western blot analysis.

2.2.8 EV release assay.

RK-13 and HeLa cells were infected with VACV strain WR or vΔA26 at a multiplicity of 0.1 PFU per cell. After 48 h, the supernatant, which contains the EV, was removed and clarified using low speed centrifugation. The monolayers, containing MV, were washed and lysed by freeze-thawing. Both supernatants and cell lysates were titered using BS-C-1 cells and overlaid with medium containing 2.5% fetal bovine serum plus 0.5% methylcellulose. After 48 h, plaques were stained with crystal violet and counted. To measure adherent EVs, cells were treated with varying amounts of trypsin in medium without fetal bovine serum for 45 min at 37˚C [189]. Supernatants were removed from monolayers and clarified by low speed centrifugation prior to titration as above.

2.3 Results

2.3.1 Functional interaction of A26p with A27p.

During an analysis of proteins in MVs purified from cells infected with the A27L deletion mutant vDA27, I noticed that a 60-kDa polypeptide was missing (Figure 2-1). The band from the parental virus corresponding to the missing 60-kDa protein was excised from the gel, digested with trypsin and shown to be A26p by

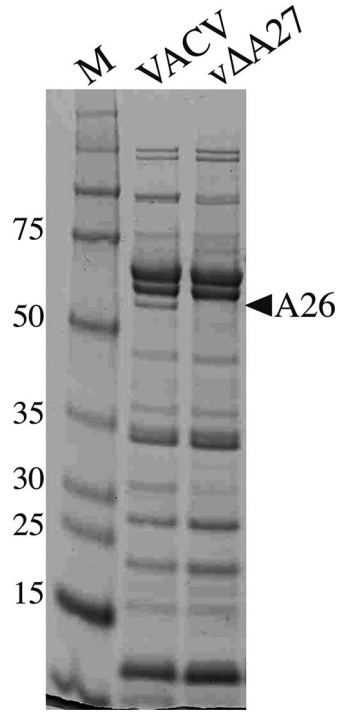

Figure 2-1. Absence of A26p in virions lacking A27p. Virions from cells infected with vΔA27 and the parental virus vA4-YFP (VACV) were purified by sucrose gradient sedimentation, disrupted with LDS and reducing agent, and analyzed by SDS-PAGE. Polypeptides were detected by staining them with Coomassie blue. The masses of marker proteins (M) are in kDa. The arrowhead labeled A26 points to the position of the 60-kDa band present in VACV and missing from vΔA27.

mass spectrometry. Our initial thought was that A27p was just required for incorporation of A26p into MVs. However, extracts of cells infected with vΔA27 had very low amounts of A26p compared to the amount from cells infected with the parental virus (Figure 2-2A). The deficiency of A26p was specific since the viral A3 protein and cellular glyceraldehyde-3-phosphate dehydrogenase were present in normal amounts. There was no reciprocal effect i.e. deletion of the ORF encoding A26p did not cause a decrease in A27 (Figure 2-2A).

A trivial explanation for the deficiency of A26p would be an unintentional mutation of the A26L promoter or ORF during the deletion of the neighboring A27L gene. However, DNA sequencing indicated that no such mutation had occurred. Furthermore, a normal amount of A26p was detected by Western blotting of extracts from cells infected with the revertant virus vΔA27Rev [204], in which a new copy of A27L with its natural promoter had been inserted into the VACV thymidine kinase locus thereby leaving unaltered the site of the original A27L deletion adjacent to A26L. Thus, the synthesis of A27p was necessary for normal amounts of A26p.

The above data suggested that A27p might be required for the stability of A26p. To investigate whether A26p was being actively degraded, cells were infected with vΔA27 and the specific proteasome inhibitor MG-132 was added 5 h later. The levels of A26p, determined by Western blotting, increased greatly over time in the presence of MG-132 (Figure 2-2B), indicating that A26p was being degraded by the proteosome in the absence of A27p. In contrast, MG-132 reduced A26p in the presence of A27p, presumably due to a general effect (data not shown). I also found that the amount of A26p in cells infected with vΔA27 could be increased by

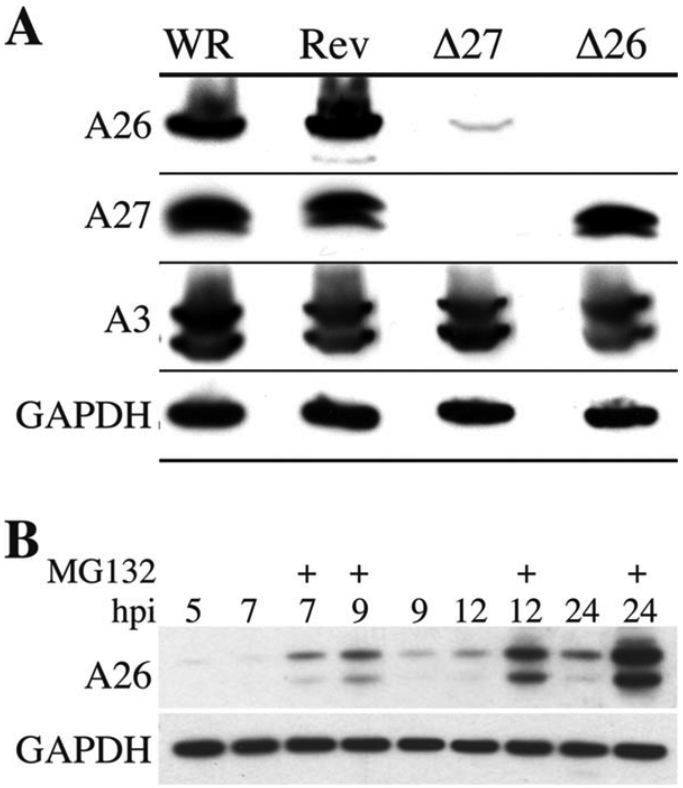

Figure 2-2. Decreased cytoplasmic A26p in the absence of A27p. (A) Western blot. Extracts of cells infected for 24 h with VACV WR (WR), vΔA27.Rev (Rev), vΔA27 (Δ27), or vΔA26 (Δ26) were reduced and analyzed by SDS-PAGE, and the proteins were identified by Western blotting using antibodies to A26p, A27p, A3p, and GAPDH as indicated. (B) Effect of proteasome inhibitor. Cells were infected with vΔA27. After 5 h, replicate cultures were treated with 10 μM MG-132 (+) or left untreated, and the incubation was continued. At the indicated times, lysates were prepared and analyzed by Western blotting with antibodies to A26p and GAPDH. hpi, hours post infection.

introduction of extra copies of the A26L gene by plasmid transfection and this strategy was used in some later experiments.

2.3.2 A26p and A27p physically interact.

A physical association between A26p and A2p7 could provide stabilization. This idea was supported by our finding of a 90-kDa complex, which reacted with antibodies to A26p and A27p, when VACV WR MVs were analyzed by SDS-PAGE and Western blotting in the absence of reducing agent (Figure 2-3A). Moreover, only faint bands corresponding to the A26p monomer and A27p multimers were detected under the latter conditions (Figure 2-3A). After treatment of VACV WR MVs with reducing agent, A26p and A27p were resolved as 60- and 14-kDa polypeptides, respectively (Figure 2-3A). Furthermore, when purified vΔA26 virions were analyzed, the 90-kDa band was absent and only multimeric forms of A27p were detected (Figure 2-3A).

Taken together, the above data suggested that the 90-kDa band was comprised of an A26p-A27p disulfide-bonded complex. Immunoprecipitation experiments were carried out to verify the A26p-A27p interaction. To facilitate such experiments, DNA encoding a V5 epitope tag was fused to the C-terminus of the A26L ORF and the recombinant vA26V5 was clonally isolated. Purified vA26V5 and control VACV WR virions were treated with 1% NP-40 to release membrane-associated proteins and incubated with V5 antibody that was conjugated to agarose beads. The unbound and bound proteins were resolved by SDS-PAGE under non-reducing conditions and detected by Western blotting with anti-A27p and -V5 antibodies. When the unbound fraction from the control VACV WR virions was probed with antibody to A27p, the

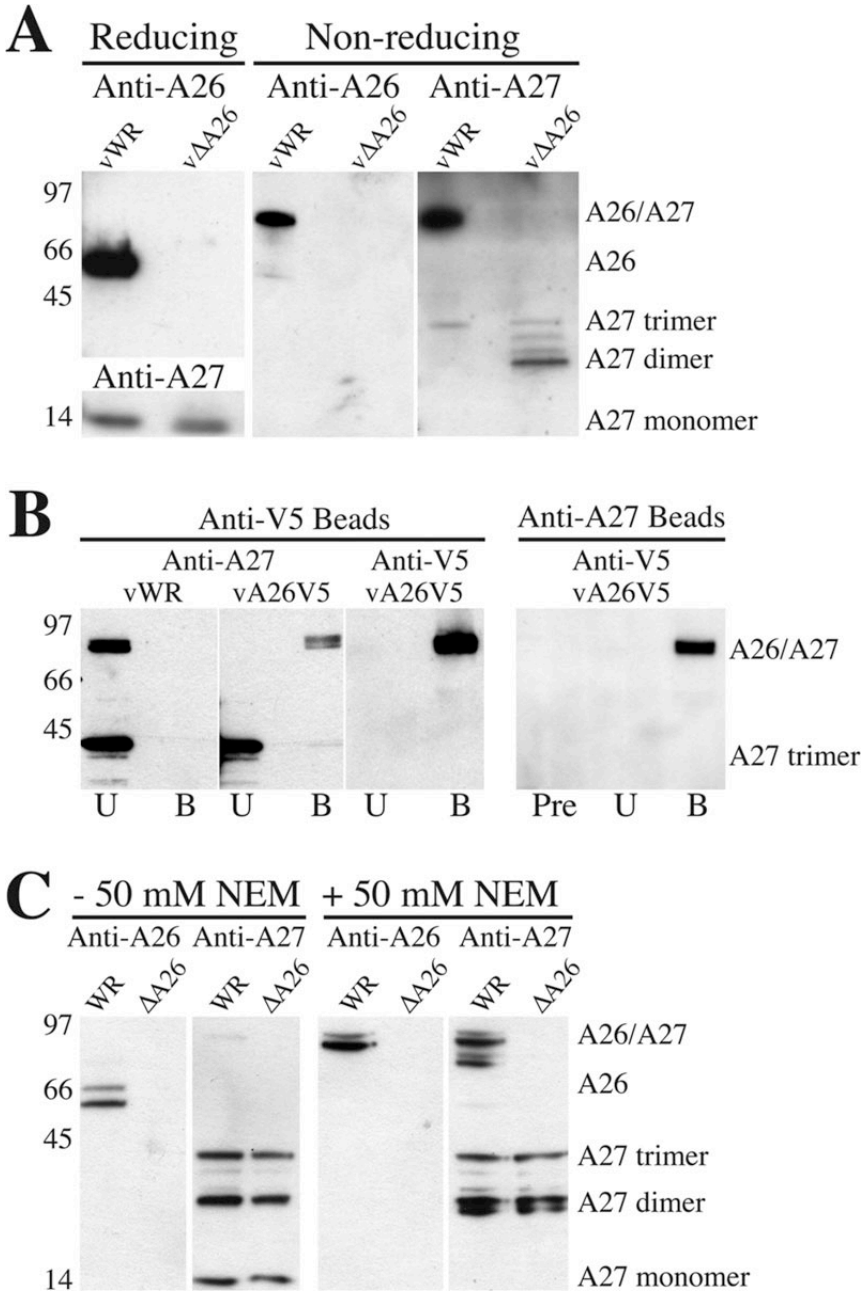

Figure 2-3. A26p and A27p form an SDS-stable complex. (A) Western blot analysis of virions. Virions from cells infected with VACV WR (vWR) and vΔA26 were purified by sucrose gradient sedimentation, dissociated with LDS in the presence or absence of reducing agent, and subjected to SDS-PAGE. The blots were probed with antibody to A26p and then stripped and reprobed with antibody to A27p. The positions of monomeric and oligomeric forms of A27p, monomeric A26p, and A26p/A27p complex are indicated. (B) Immunoaffinity purification of A26p/A27p complex. Purified virions from cells infected with VACV WR or vA26V5 MV were treated with 1% NP-40 detergent and incubated with antibody to V5 or A27p

immobilized on protein A beads. Bound (B) and unbound (U) fractions were resolved by SDS-PAGE under nonreducing conditions and probed successively with antibody to A27p and V5 (left) or with antibody to V5 (right). Pre, eluate from protein A-agarose beads unconjugated to antibody. (C) Western blot of cell lysates. Cells infected with VACV WR or vΔA26 were harvested after 24 h and lysed in the presence (+) or absence (-) of 50 mM NEM. The proteins were resolved by SDS-PAGE under nonreducing conditions, and Western blots were probed with antibody to A26p and A27p. In each panel, the numbers on the left are the masses in kDa of marker proteins.

major bands corresponded to the 90-kDa complex and trimeric A27p; no bands were detected in the "bound" fraction because of the absence of the V5 tag (Figure 3B). In contrast, the A27p antibody reacted with the 90-kDa complex in the bound fraction from vA26V5 virions, and only excess trimeric A27p was in the unbound fraction (Figure 2-3B). The 90-kDa species was detected in the bound fraction when the blot was stripped and re-probed with anti-V5 antibodies confirming that it was an SDS-stable complex of A26p and A27p (Figure 2-3B). When the reciprocal experiment was conducted by incubating NP-40 treated vA26V5 virions with A27p antibody-conjugated agarose beads, the 90-kDa complex was detected by antibody to A26p only in the bound fraction (Figure 2-3B). Taken together, these data indicate that A26p was physically associated with A27p in MVs. The Western blotting data obtained with VACV WR indicated that the majority of A26p and A27p were present as a complex (Figure 2-3A). The presence of substantial amounts of trimeric A27p in vA26V5 MVs indicated that the tagged A26V5 was present in lower amounts than A27p (Figure 2-3B). The A26p-A27p complex was sometimes detected as a doublet suggesting that A26p might be interacting with both A27p trimers and dimers.

2.3.3 Analysis of the A26p-A27p complex in infected cell lysates.

Initially, I was perplexed to find that the 90-kDa A26p-A27p complex was not detected when infected cell lysates were analyzed by SDS-PAGE and Western blotting in the absence of reducing agent; instead monomeric A26p and multimeric forms of A27p were resolved (Figure 2-3C). Since the A26p-A27p complex is held together by intermolecular disulfide bonds, I considered that these might be disrupted upon cell lysis by a process called disulfide interchange. For example, a free SH

group on A27p could displace the disulfide bond between A26p and A27p. An established way of preventing disulfide interchange is by adding NEM, which reacts with free sulfhydryl groups, prior to cell lysis. When NEM was added in this way, the 90-kDa complex was visualized by probing Western blots with antibodies to A26p and A27p (Figure 2-3C). There was still excess A27p in the cytoplasm, as shown by the A27p trimers and dimers, but now there was no free A26p. Therefore, it seems likely that the disulfide bond linking A26p and A27p was disrupted by disulfide interchange in the absence of NEM. This interchange may be catalyzed by some component in the cell extract in the presence of excess A27 since NEM was not needed to preserve the covalent A27p-A26p complex isolated from purified virions.

2.3.4 A26p-A27p complex formation is independent of other viral late proteins.

A26 and A27 have late promoters and are therefore synthesized following viral DNA replication. The following scheme allowed the synthesis of A26p and A27p in the absence of DNA replication and other late proteins. Cells were (i) untreated or treated with AraC, an inhibitor of DNA replication to prevent late gene expression, (ii) infected with vTF7.3, a recombinant VACV that expresses the T7 RNA polymerase under an early promoter, and (iii) transfected with pT7.A26V5 or pT7.A27HA, plasmids that have epitope tagged copies of A26p and A27p, respectively, regulated by a T7 promoter. The cells were lysed at 18 h after infection and incubated with beads that were conjugated with antibody to the V5 epitope tag on A26p. The unbound and bound fractions were treated with reducing agent, resolved by SDS-PAGE and analyzed by Western blotting with antibody to the HA tag of A27p (Figure 2-4). Comparison of the unbound and bound fractions indicated that

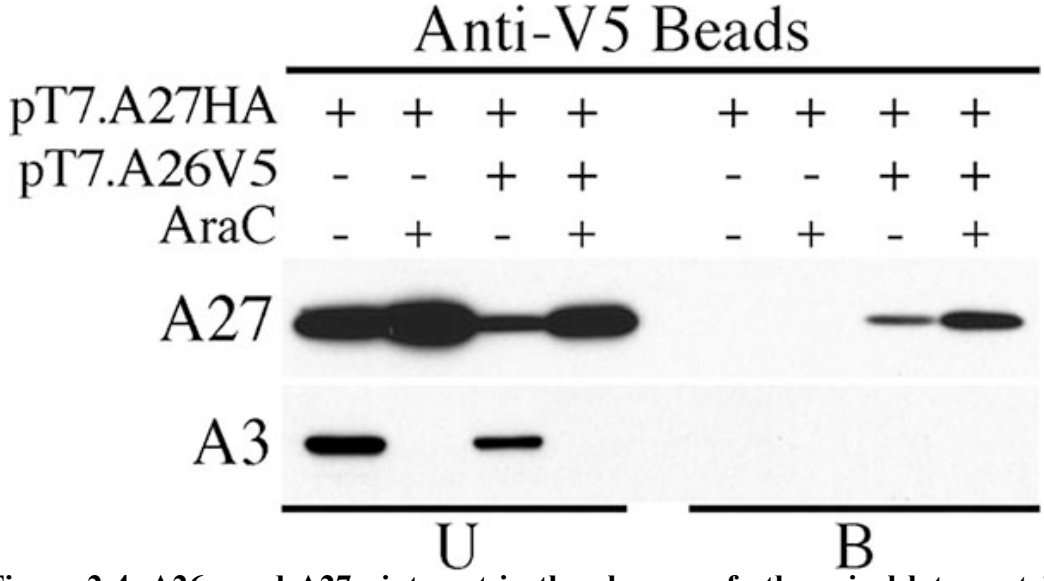

Figure 2-4. A26p and A27p interact in the absence of other viral late proteins. Cells were infected with a recombinant VACV that expresses bacteriophage T7 RNA polymerase in the presence (+) or absence (-) of AraC and transfected with plasmids encoding epitope-tagged A26p (pT7.A26V5) and A27p (pT7.A27HA) regulated by T7 promoters as indicated. After approximately 18 h, the cells were harvested, and the lysates were incubated with antibody to V5 attached to beads. The unbound (U) and bound (B) fractions were analyzed by SDS-PAGE and Western blotting with antibody to HA and the VACV A3 protein.

A27pHA was bound to A26pV5 in the absence or presence of AraC. Furthermore, there was no non-specific binding of A27pHA to the V5 antibody in the absence of A26pV5 expression (Figure 2-4). The higher expression of A26pV5 and A27pHA in the presence of AraC is probably due to the absence of competition by late mRNAs. The inhibition of late protein synthesis by AraC was shown by Western blotting with antibody to the A3 protein (Figure 2-4).

2.3.5 A26p is anchored to the MV membrane surface by A27p.

Since A27p is located on the exterior of the MV membrane, a similar location for A26p seemed likely. Indeed, previous studies had shown that the A26p (referred to then as 4c or P4c) could be labeled with iodine and released from purified virions by treatment with a non-ionic detergent [210, 211]. To confirm by another method that A26p was located on the MV surface, I carried out labeling experiments with a membrane-impermeable biotinylation reagent. Purified VACV WR virions were treated with sulfo-NHS-SS-biotin in the absence or presence of NP-40 detergent, which disrupts the MV membrane and exposes core proteins. Samples were incubated with NeutrAvidin beads to bind biotinylated proteins and then eluted with buffer containing DTT. The unbound and bound fractions were analyzed by SDS-PAGE and the Western blot was successively probed with antibody to A26p and A27p. A26p was predominantly present in the bound fraction, similar to A27p (Figure 2-5A). The A3 core protein was almost entirely in the unbound fraction, suggesting that the MV particles were intact and that the biotinylation reagent could not penetrate the viral membrane. The failure to biotinylate the A3 protein was not due to intrinsic unreactivity, since A3p was biotinylated after disruption of the MV membrane with

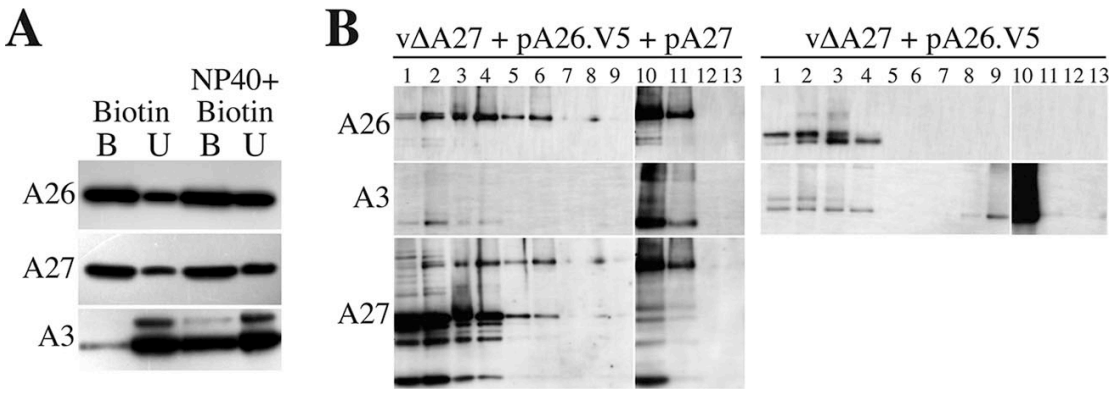

Figure 2-5. A26p is anchored to the MV membrane surface by A27p. (A) Biotinylation of A26p and A27p in intact virions. Sucrose gradient-purified virions from cells infected with VACV WR were treated with sulfo-NHS-SS-biotin and allowed to bind to NeutrAvidin beads. Bound (B) and unbound (U) fractions were analyzed by Western blotting with antibodies that recognized A26p, A27p, and A3p. As a positive control, purified virions were treated with NP-40 prior to biotinylation. (B) Incorporation of A26p into purified virions. Cells were infected with vΔA27 and transfected with pA26V5 with or without pA27. After approximately 24 h, the cells were harvested and virions were purified by sedimentation through sucrose cushions and CsCl gradient sedimentation. Fractions (1 ml) were collected from the top and analyzed by Western blotting using antibodies that recognized A26pV5, A27p, and A3p.

NP-40 and bound to NeutrAvidin beads (Figure 2-5A).

In our initial experiment (Figure 2-1), the absence of A26p in MVs produced in cells infected with vΔA27 could have been due mainly to the instability of A26p. It was important, therefore, to determine whether A27p was also required for the association of A26p with MVs. As mentioned above, I found that the amount of A26p in cells infected with vΔA27 could be increased by introduction of extra copies of the A26 gene by transfection. Cells were infected with vΔA27 and co-transfected with the plasmid pA26V5, which expresses a V5 epitope-tagged A26p, either alone or together with the plasmid pA27, which expresses A27p. Virions were purified from the cell lysate by two successive sedimentations through a 36% sucrose cushion followed by CsCl gradient centrifugation. Gradient fractions were analyzed by SDS-PAGE under non-reducing conditions and Western blotting. In the samples from the cells transfected with the two plasmids, both A26pV5 and A27p were detected in a 90-kDa band in fractions 10 and 11 with the A3 core protein, corresponding to the expected MV density of ~1.27g/ml (Figure 2-5B). Additional A26pV5 and A27p were present in the first several fractions near the top of the gradient. When A27p was not expressed, then A26pV5 was present in the upper fractions as a 60-kDa protein and was absent from the lower MV fractions containing the A3 core protein (Figure 2-5B). Thus, these data indicate that the association of A26p in the MV membrane is dependent upon A27p.

2.3.6 The A26-A27 complex is associated with A17 and A25.

Affinity purification was carried out to determine whether additional proteins were non-covalently associated with the A26p-A27p complex. I was particularly

interested in A17p, since the latter protein anchors A27p to the viral membrane [199]. Cells were infected with vA26V5 or VACV WR and lysates were incubated with antibody to V5 coupled to beads. The bound proteins were eluted and visualized by staining after SDS-PAGE (Figure 2-6). Several bands were specific for cells infected with vA26V5, whereas a few others were non-specific. The specific bands were excised and A25p, A26p, A17p and A27p were identified. Based on the intensity of the stain, A25p and A17p appeared to be present in lesser amounts than A26p and A27p (Figure 2-6). However, this may reflect the stability of the interactions rather than the stoichiometry of the complex. Proteins corresponding to other faint bands could not be identified by mass spectroscopy analysis.

Immunoprecipitation and Western blotting confirmed the association of A17p with the A26p-A27p complex in virions. MVs purifed from cells infected with vA26V5 were treated with NP-40 and then incubated with beads that were conjugated with antibody to A17p. A26pV5 was detected by Western blotting of proteins that were immunopurified with anti-A17p antibody (Figure 2-7A).

2.3.7 Association of A26p with A17p is mediated by A27p.

Since A27p is known to interact with A17p [199], the association of the latter with A26p could be indirect. Alternatively, A26p might also bind A17p directly. To investigate these alternatives, cells were infected with vΔA27 and transfected with combinations of plasmids expressing bacteriophage T7 RNA polymerase from a VACV promoter, and A26V5 and A27HA from T7 promoters. When all three plasmids were transfected, beads coupled to V5 antibody pulled down A26pV5, A27pHA and A17p (Figure 2-7B). However, when the plasmid expressing A27HA

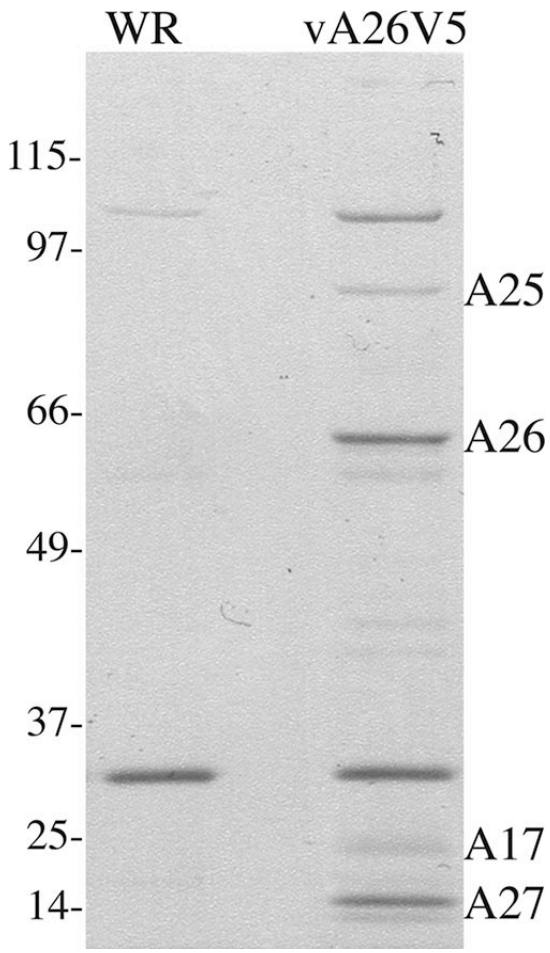

Figure 2-6. Association of A17p, A25p, and A27p with A26p determined by mass spectrometry. Sucrose gradient-purified virions from cells infected with vA26V5 or VACV WR were treated with NP-40 and then bound to V5-specific antibody bound to beads. The bound proteins were resolved by SDS-PAGE and stained with Coomassie blue. The bands were excised, digested with trypsin, and analyzed by mass spectrometry. Bands identified as A17p, A25p, A26p, and A27p are indicated.

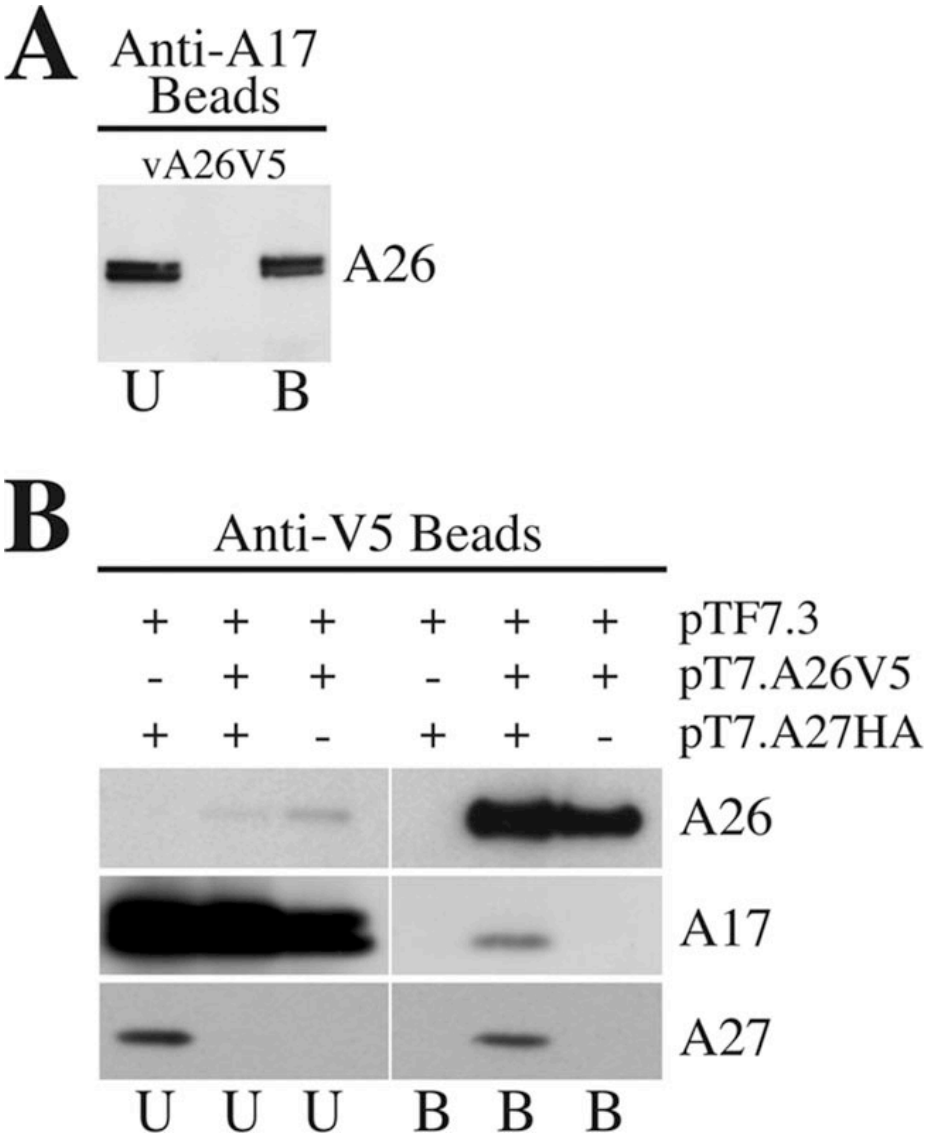

Figure 2-7. Association of A26p with A17p was dependent on A27p. (A) Immunopurification of A26 with immobilized A17. MVs purified from cells infected with vA26V5 were treated with NP-40 and incubated with antibody to A17 attached to protein A beads. Unbound (U) and bound (B) fractions were subjected to SDS-PAGE and Western blotting with antibody to the V5 epitope. (B) Immunoaffinity purification of A17 and A27 with A26. Cells were infected with vΔA27 and transfected with a plasmid expressing the T7 polymerase (pTF7.3) and plasmids expressing A26V5 (pT7.A26V5) and/or A27HA (pT7.A27HA) under the control of the T7 promoter. After approximately 24 h, the cells were harvested, lysed with NP-40, and incubated with antibody to V5 attached to beads. Proteins in the unbound and bound fractions were resolved by SDS-PAGE and analyzed by Western blotting with antibodies to V5, HA, and A17 as indicated.

was omitted, only A26pV5 was captured. Thus, A27p was required for the interaction of A26p with A17p.

2.3.8 The C-terminus of A26p mediates interactions with A27p.

The C-terminal region of A26p, from amino acids 441 to 472, shares a 44% amino acid identity with the A27p C-terminal, alpha helical "anchoring domain" through which A27p mediates interactions with A17p and the MV particle [212]. Two plasmids were constructed: pA26ΔNV5 expressed the C-terminal 270-500 amino acids and included the region of homology with A27p; whereas, pA26ΔCV5 coded for amino acids 1-409, excluding the region of homology to A27p (Figure 2-8A). Cells were infected with vΔA26 and transfected with either empty plasmid or plasmids expressing full length A26V5 or the deletion mutants. After 18 h, the cells were lysed with 1% NP40 and the soluble extract was incubated with anti-V5 conjugated beads. The unbound and bound fractions were resolved by SDS-PAGE under reducing conditions and probed with antibodies against A26p, A27p, and A17p. Full-length A26p and the C-terminal 220 amino acid fragment from pA26ΔNV5 pulled down A27p and A17p (Figure 2-8B). Neither A27p nor A17p, however, were present in the bound fractions from cells expressing the C-terminal deleted form of A26p from pA26ΔCV5 (Figure 2-8B). The region from amino acids 270 to 500 contains three cysteines, at least one of which may be involved in the disulfide bond with A27p.

2.3.9 Deletion of A26 does not increase EV formation.

The discovery that A26p is present in MVs but not EVs led to a suggestion

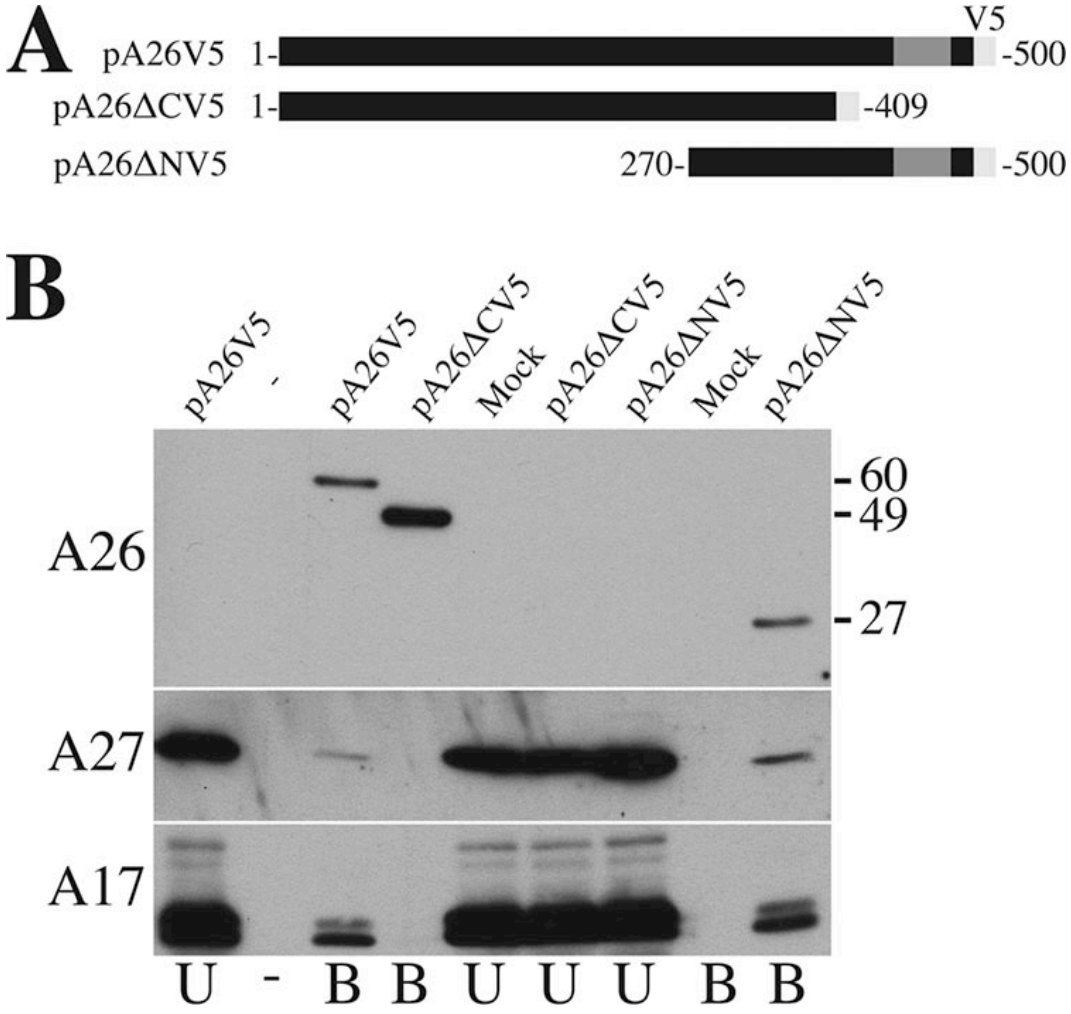

Figure 2-8. The C terminus of A26p interacts with A27p. (A) Schematic drawings of truncated A26 ORFs. pA26V5, pA26ΔCV5, and pA26ΔNV5 show the lengths of V5 epitope-tagged A26 plasmid inserts. Black shading, A26p sequence; dark gray, region of homology with A27p; light gray, V5 epitope tag. A26 amino acid residues are numbered. (B) Western blots of immunoaffinity-purified A26-associated proteins. Cells were infected with vΔA26 and mock transfected or transfected with pA26V5, pA26ΔCV5, or pA26ΔNV5. Lysates were incubated with antibody to V5 coupled to beads, and the unbound and bound fractions were analyzed by SDS-PAGE and Western blotting with antibody to V5, A17p, and A27p. The positions and masses in kDa of marker proteins are shown on the right.

that A26p negatively regulates wrapping [195]. Our finding that A26p interacted with A27p, which is required for wrapping, could have provided a mechanism for such a role. If this hypothesis were correct, then deletion of the A26L ORF should increase the amount of EVs. RK-13 and HeLa cells were infected with either vΔA26 or VACV WR and the cells and media were harvested separately after 48 h. The deletion of the A26L did not increase the amount of EV either released naturally into the medium (Figure 2-9A) or liberated from the surface of the cell with trypsin (Figure 2-9B). Furthermore, there was no discernible difference in plaque size or comet formation due to release of EVs in RK-13 cells infected with vΔA26 as compared to wild-type virus (not shown).

2.4 Discussion

The present study was initiated following our serendipitous observation that A26 was missing from MVs formed by an A27L deletion mutant. Further studies indicated that A27 was required for the stability of A26 as well as for its incorporation into MVs. The relationship between A26 and A27 was explained by the finding that the two proteins formed an SDS-stable complex in the absence of reducing agent. The complex migrated as a band of about 90-kDa, likely consisting of A26 (58-kDa) disulfide-bonded to A27 (12.6-kDa) trimers or dimers. Moreover, nearly all of the A26 and A27 in wild type MVs were in the complex. It was surprising, therefore, that this complex was not generally recognized during analysis of virion proteins, though it likely corresponds to the heterodimer of 54- and 16-kDa polypeptides described by Ichihashi [213]. I had trouble detecting the A26-A27 complex in cytoplasmic extracts until I realized the importance of adding NEM to

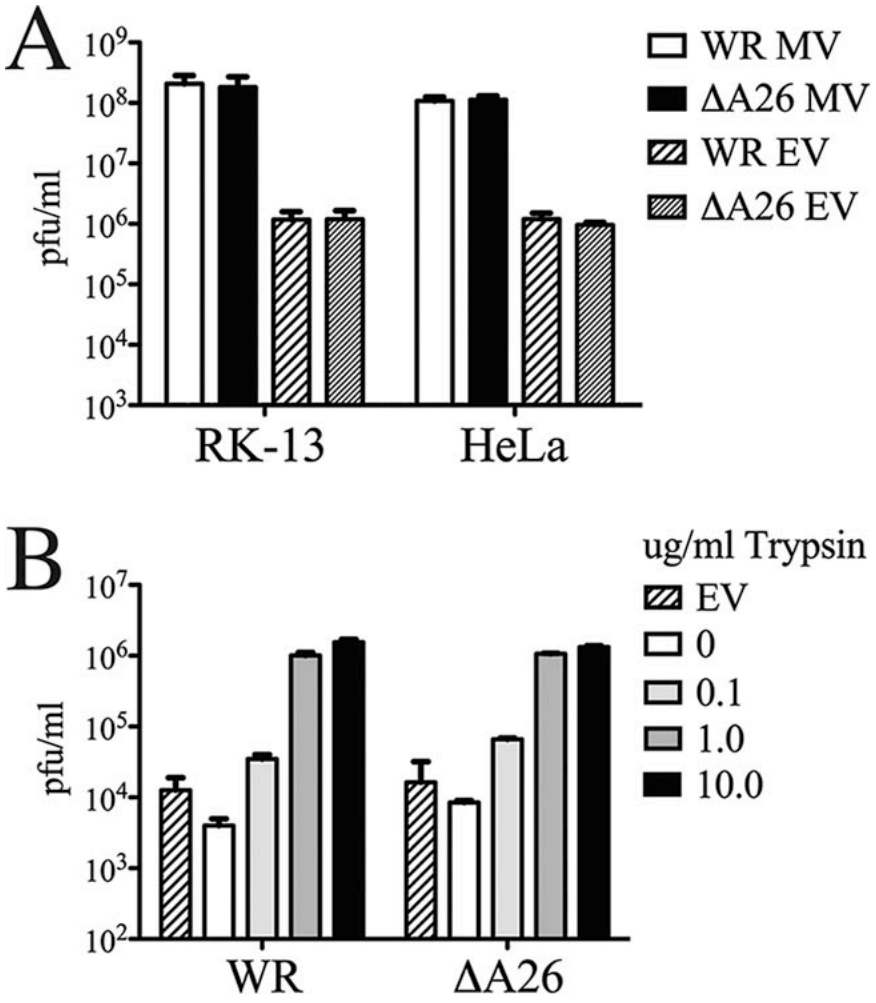

Figure 2-9. Intra- and extracellular virus production. (A) RK-13 and HeLa cells were infected with VACV WR or vΔA26 at a multiplicity of infection of 0.1 PFU per cell. After 48 h, the media were collected and the intra- and extracellular virus titers were determined. (B) The indicated concentrations of trypsin were used to release EVs from the surfaces of cells infected with VACV WR and ΔA26 for 24 h. Virus titers were determined by plaque assay. Error bars, standard error of the mean.

prevent disulfide interchange, perhaps providing an explanation for failure of others to observe the complex. Further studies indicated that no additional viral late proteins were required for the interaction of A26 and A27. Co-immunoprecipitation experiments indicated that the C-terminal segment of A26 interacted with A27. Interestingly, part of that region shares sequence homology with A27. These data are consistent with an observation that the C-terminal 75 amino acids of A26 are required for anchoring the latter protein to the MV particle, although an interaction with A27 was not proposed at the time [198].

The A26-A27 complex also associated non-covalently with the A17 and A25 proteins. A17, a transmembrane protein, had previously been shown to interact with A27 [199], and our study indicated that the association of A26 with A17 was indirect and dependent on A27. The inability of A26 to interact directly with A17 (or any other integral membrane protein) explains why A27 is needed for incorporation of A26 into MVs. Biotinylation studies confirmed that A26 and A27 were exposed on the surface of the MV-membrane

The finding of a multiprotein A17, A25, A26 and A27 complex has interesting implications. Previous studies have shown that the formation of the ATI is dependent on a full-length ortholog of the truncated A25 protein and that A26 is needed for the embedding of virions within them [197]. The role of A26 in this process has not been elucidated, although a role in retrograde transport on microtubules was suggested. The interaction of A26 with A25, shown here, suggests a direct role of A26 in attaching virions to the ATI. It is thought that the inclusions protect virions in a severe environment and allow for animal-to-animal transmission. However, a

reduction in EVs, which are important for cell-to-cell spread, appears to be a consequence of virion occlusion since this results in smaller size plaques [214, 215]. Ulateo and coworkers [195] suggested a related role for A26 in orthopoxviruses that do not make ATIs. Primarily because A26 was found in MVs but not EVs, they suggested that A26 might negatively regulate wrapping. Our finding that A26 interacts with A27, which is required for MV-wrapping [216], made the hypothesis that A26 modulates EV formation even more attractive. Nevertheless, I did not discern a change in the ratio of EVs to MVs when the A26L ORF was deleted. It remains possible, however, that the number of MVs lacking A26 were not limiting for wrapping in the two cell lines that were tested but that the situation would be different with other cells, other VACV strains or other incubation conditions. I did find a reduction in EV production when A26 was over expressed, but this was correlated with a reduction in expression of other viral proteins including A27 and was therefore difficult to interpret (our unpublished data).

A26 appears to have a role in cell attachment as it was shown that A26 binds laminin, an extracellular matrix protein, and soluble laminin partially blocks MV binding to cells [198]. Chiu et al. [198] reported that virions lacking A26 are still infectious and I confirmed this more directly with an A26L deletion mutant. Retention of infectivity was not surprising since VACV encodes other proteins that mediate cell attachment by binding glycosaminoglycans [217, 218]. Since A27 is one of the three glycosaminoglycan-binding proteins, there could be functional significance to the physical association of two membrane attachment proteins.

Chapter 3: Congregation of Orthopoxvirus Virions in Cytoplasmic A-type Inclusions is Mediated by Interactions of a Bridging Protein (A26p) with a Matrix Protein (ATIp) and a Virion Membrane-Associated Protein (A27p)

3.1 Introduction

The orthopoxviruses, which include the best characterized and medically most significant members of the poxvirus family, produce two major types of infectious particles known as mature virions (MVs) and enveloped virions [181]. MVs are assembled at cytoplasmic, juxtanuclear viral factories and consist of a core containing viral double-stranded genomic DNA, enzymes and factors necessary for early gene transcription, and structural proteins surrounded by a lipoprotein membrane. A population of MVs traffics along microtubules and acquires two additional membranes derived from trans-Golgi or endosomal cisternae to form wrapped virions. Wrapped virions traverse the cell along microtubules to the plasma membrane where the outer viral membrane fuses with the plasma membrane to allow exit of enveloped virions. However, the majority of MVs remain in the cytoplasm until cell lysis. The MVs of some orthopoxviruses, e.g. cowpox virus (CPXV), ectromelia virus and raccoonpox virus have an additional fate: they become embedded in dense, proteinaceous bodies called A-type inclusions (ATIs) that are distinguished from virus factories [146-148]. Orthopoxviruses that do not form A-type inclusions include vaccinia virus (VACV), the prototype of the poxvirus family, variola virus, the causative agent of smallpox, and monkeypox virus, an emerging pathogen. Inclusions with embedded virions also form in cells infected with

avipoxviruses and entomopoxviruses (3) and may protect virions from harsh environmental conditions during transmission between hosts.

ATIs form subsequent to viral DNA replication and the matrix consists of a single known viral late protein, the ATIp [151]. The ATIp is an abundant, high molecular weight (160 kDa in CPXV), hydrophobic protein that contains 14 repeats of about 30 amino acids each [151, 154]. Orthopoxviruses that do not form inclusion bodies have mutated ATI genes. An ATIp homolog encoded by the A25L gene (VACVWR148) of the Western Reserve (WR) strain of VACV contains a deletion of two adenylate residues resulting in synthesis of a C-terminally truncated, 94-kDa protein [151, 155, 156]. This A25 protein (A25p) contains the N-terminal half of ATIp including the first four ATIp repeats and six amino acids of the fifth repeat. The embedding of MVs in inclusions requires a protein encoded by homologs of the A26L gene, which is mutated in some orthopoxvirus strains (27, 42). Although VACV does not form inclusion bodies, the VACV A26L gene (VACVWR149) is intact, and the VACV A26 protein (A26p) can complement the defective A26p homolog in the Brighton red (BR) strain of CPXV (CPXV-BR) [160]. Whether VACV is missing other proteins needed for inclusion formation and occlusion was not known prior to the present study.

The mechanism by which A26p mediates occlusion had not been elucidated, although a role in retrograde transport of MVs was suggested [160]. Recently, A26p was shown to be anchored to the MV membrane through disulfide bonding with the A27 protein (A27p) [219, 220], which is in turn tethered to the MV membrane through interactions with the A17 transmembrane protein (A17p) [120, 123]. Our

finding that A26p also interacts with A25p (16), suggested that it might similarly interact with the intact ATIp, thereby localizing MVs in inclusion bodies. To investigate the role of A26p in mediating occlusion, I constructed recombinant VACV expressing the CPXV-BR ATIp in place of the truncated VACV-WR A25p. Remarkably, this single alteration allowed VACV to produce typical inclusions containing MVs. Occlusion of MVs by recombinant VACV was dependent on both A26p and A27p, even though inclusions formed without either of these proteins. A26p localized with inclusions in the absence of A27p or MV production, consistent with a direct interaction with ATIp. Separate domains of the ATIp were shown to be required for inclusion formation and association with A26p. Taken together, the data present a working model of occlusion in which A26p serves as a bridge between A27p on MVs and ATIp in inclusion bodies.

3.2 Materials and methods

3.2.1 Cells and viruses.

African green monkey kidney BS-C-1 and human HeLa cell cultures were maintained in minimum essential medium with Earle's salts (Quality Biological, Gaithersburg, MD) and 10% fetal bovine serum (FBS). The medium was further supplemented with 2 mM L-glutamine, 100 units/ml of penicillin, and 100 μg/ml of streptomycin. Cells were infected with viruses in medium containing 2.5% FBS and supplements listed above. Recombinant viruses were derived from the VACV-WR strain and the CPXV-BR strain and propagated as described previously [200].

3.2.2 Plasmid and recombinant virus construction.

The following recombinant viruses were constructed by standard methods: (i) vA25HA.A26V5, which expresses an influenza hemagglutinin (HA) epitope-tagged VACV A25p and a V5-tagged VACV A26p; (ii) vATIHA.A26V5, which encodes an HA-tagged CPXV ATIp and a V5-tagged A26p; and (iii) vATIHA.ΔA26, which has A26L deleted and expresses an HA-tagged ATIp. In the first step, the VACV WR A25L gene was replaced by the enhanced green fluorescent protein (GFP) gene to generate vΔA25.GFP. Plasmids were then constructed to insert the cassettes of interest into the GFP locus of vΔA25.GFP. Briefly, the plasmids used to make vA25HA.A26V5 and vATIHA.A26V5 contained the left flanking region of the A25L ORF with a *Pac*I site introduced immediately downstream of the A25L stop codon. The right flanking region was amplified with DNA encoding a V5 tag introduced into to the C-terminal coding region of A26L and a *Sal*I site immediately downstream of A26L and upstream of the A25L ORF. The two flanks were joined by overlap PCR using Accuprime *Pfx* (Invitrogen, Carlsbad, CA) and blunt-end ligated into pCR-BluntII-TOPO (Invitrogen) to generate the pFLANKS plasmid. pFLANKSΔA26 was constructed similarly to make vATIHA.ΔA26 except that the right flanking region was amplified from the A27L gene which is immediately upstream of the A26L ORF. The VACV-WR A25L and CPXV-BR ATI genes and native promoters were amplified with forward and reverse primers introducing an upstream *Sal*I site and DNA sequences coding for the HA tag with a downstream *Pac*I site, respectively. The PCR products were subcloned into pCR-BluntII-TOPO and the resulting plasmids designated as pA25HA and pATIHA. The ATIHA and A25HA inserts were

excised from pA25HA and pATIHA using *Sal*I and *Pac*I for ligation with linearized pFLANKS and pFLANKSΔA26 to generate pFLANKS.A25HA and pFLANKS.ATIHA and pFLANKSΔA26.ATIHA, respectively. vΔA25.GFP-infected cells were transfected with linearized pFLANKS.A25HA and pFLANKS.ATIHA and pFLANKSΔA26.ATIHA using Lipofectamine 2000 (Invitrogen) per the manufacturer's instructions. Control viruses with an A26L-A25L double deletion (vΔA25.ΔA26), an HA-fused A25L with a deleted A26L (vA25HA.ΔA26), and a deleted A25L with a V5-fused A26L (vΔA25.A26V5) were generated similarly as above. Recombinant viruses were clonally purified by consecutive rounds of white-plaque selection [221]. The A4:YFP fusion was introduced as previously described [108].

The A27L deletion (vΔA27) virus containing the yellow fluorescent protein (YFP) fused to the N-terminus of A4p was described previously [108]. vΔA27 forms small plaques, and vΔA26.A4:YFP was generated from vΔA27 by inserting a cassette that deleted A26L but restored A27L at the A27L-A26L locus and selecting for large plaques.

The ATI deletion mutants were amplified from the pATIHA plasmid and cloned into the pTOPO vector. N-terminal deletion mutants were amplified using forward primers containing the CPXV-BR ATI promoter and an introduced start codon adjacent to at least the first ten 5' nucleotides of the target sequence and a reverse primer to the HA tag. C-terminal mutants were amplified using a forward primer complementary to the ATI promoter and a reverse primer overlapping the HA tag and stop codon with at least ten nucleotides of the desired 3' target.

pATIFLAG was generated by amplifying the ATI gene with a reverse primer coding for the FLAG epitope tag with the amino acid sequence DYKDDDDK. pA27HA, pA26V5, pA26ΔNV5, and pA26ΔCV5 were described previously [219].

3.2.3 Antibodies.

Mouse monoclonal antibodies (MAbs) and rabbit polyclonal antibodies (PAbs) against the HA (YPYDVPDYA) and mouse MAbs against the V5 (GKPIPNPLLGLDST) epitope tags used for Western blotting were obtained from Covance (Princeton, NJ). Rabbit PAbs against A26p [219] and A3p (R. Doms and B. Moss, unpublished data) were also used for Western blotting. Immunofluorescence staining of the HA-tagged A25p, ATIp, and A27p was carried out using either rat MAbs (clone 3F10) from Roche Applied Sciences (Indianapolis, IN) or mouse MAbs or rabbit PAbs from Covance at 1:250 dilutions. Mouse MAbs and rabbit PAbs to V5 as well as mouse MAbs to FLAG were obtained from Sigma-Aldrich (St. Louis, MO). Mouse MAb to V5 from Abcam (Cambridge, MA) was also used. Alexa-conjugated anti-rat, anti-rabbit, and anti-mouse immunoglobulin G (IgG) were used at 1:250 (Invitrogen).

3.2.4 Immunoaffinity purification.

As described previously [219], cells were solubilized in lysis buffer (150 mM NaCl, 50 mM Tris-HCl pH 8.0, 1% NP40) by rotating at 4°C for 30 min. The extracts were cleared and incubated with unconjugated agarose A beads prior to incubation with mouse anti-V5 immunoaffinity beads (Sigma). Bound proteins were eluted by boiling beads in lithium dodecyl sulfate (LDS) loading buffer (Invitrogen). Following

the addition of reducing agent (Invitrogen), samples were resolved by sodium dodecyl sulfate-polyacrylamide gel electrophoresis (SDS-PAGE) using 4-12% NuPAGE Bis-Tris gels in NuPAGE MOPS running buffer (Invitrogen).

3.2.5 Western blotting.

Whole cell extracts for Western blotting were prepared by incubating virus-infected cells in 10 mM Tris-HCl, pH 7.4, 10 mM $CaCl_2$, 10 mM NaCl with 8 μg/ml micrococcal nuclease and 0.5% NP-40 for 30 min on ice followed by brief sonication [28]. LDS and reducing agent were added, and the samples were boiled prior to resolution by SDS-PAGE as described above. Proteins were transferred electrophoretically to a nitrocellulose membrane and detected using antibodies as described above and anti-rabbit or anti-mouse IgG conjugated to horse radish peroxidase (Pierce, Rockford, IL), which was developed using SuperSignal chemiluminescent substrates (Pierce).

3.2.7 Infection and transfection.

Dishes with 24-wells containing cover slips seeded with approximately 2.5 X 105 HeLa cells for confocal microscopy were infected at a multiplicity of infection of 0.1 PFU per cell in Opti-MEM (Invitrogen). After 1 h, cells were washed and transfected with 200 ng of plasmid using Lipofectamine 2000 (Invitrogen) per the manufacturer's recommendations [219].

3.2.8 Confocal microscopy.

HeLa cells were washed three times in room temperature Dulbecco's phosphate buffered saline (PBS) without Ca^{2+} and Mg^{2+} prior to fixing for 10 min in 4% paraformaldehyde in PBS. Cells were washed 4 times and permeabilized with 0.2% triton X for 7 min. Four 5 min washes in PBS were used to insure the removal of triton X. Prior to staining, cells were blocked in 10% FBS/PBS for 1 h. Primary staining was carried out at room temperature for 1 h in 10% FBS/PBS. Four 5 min washes in PBS were used to remove any unbound antibody, and secondary staining was carried out in 10% FBS/PBS for 45 min. Cells were subjected to four 5 min PBS washes, and coverslips were mounted onto slides using ProLong Gold with or without 4',6'-diamidino-2-phenylindole (DAPI) mounting medium (Invitrogen). A Leica SP2 inverted four-channel microscope was used for imaging. Select images were deconvolved using Huygens Essential version 3.5.0, 64 bit (Scientific Volume Imaging, Hilversum, Netherlands) and brightness and contrast were adjusted using either Imaris Bitplane Scientific Software version 6.4.2 (Saint Paul, MN) or Adobe Photoshop CS3 (Adobe Systems, San Jose, CA, USA).

3.2.9 Electron microscopy.

BS-C-1 cells in 60-mm-diameter dishes were infected with recombinant viruses at a multiplicity of infection of 10 PFU per cell. Cells were fixed with 2% glutaraldehyde at 22 h post infection and embedded in EmBed-182 resin (Electron Microscopy Sciences, Hatfield, PA). Samples were viewed with a FEI Tecnai Spirit transmission electron microscope (Hillsboro, OR).

3.3 Results

3.3.1 Restoration of full-length ATIp allows inclusion body formation in cells infected with recombinant VACV.

I was interested in determining whether replacement of the disrupted ATI gene of VACV with the full-length CPXV homolog would be sufficient to support inclusion body formation and occlusion for two main reasons: a negative result would suggest the need for additional CPXV genes, which I would then try to identify; a positive result would allow us to study occlusion in the VACV background, which is better characterized than CPXV. The region of CPXV-BR encoding the full length 1,284 amino acid ATIp (ORF 158) and the disrupted A26p homolog (ORFs 159, 160 and 161) is shown in Fig. 1A. In contrast, four smaller ORFs (145, 146, 147 and 148) comprise the disrupted ATIp homolog of VACV-WR whereas ORF 149 encoding A26p is intact (Figure 3-1A). VACV ORF 148, encoding the expressed 725-amino acid A25p, has a late promoter whereas ORFs 145, 146 and 147 are probably not expressed as they lack recognizable promoters. To avoid potential complications due to recombination during the reconstruction of the VACV genome, ORFs 145-148 were deleted from the VACV genome prior to insertion of the complete CPXV-BR ATI gene with a C-terminal HA epitope tag and the native ATI promoter. The VACV ORF encoding A26p was replaced with a V5-tagged version or deleted (Figure 3-1A.). Another recombinant virus was constructed encoding an HA-tagged VACV A25p and a V5-tagged VACV A26p to be used as a control that does not form inclusion bodies. In each case, the YFP ORF was fused to the ORF encoding the VACV core protein A4p (A4YFP) to visualize MV by confocal microscopy. The A4YFP fusion has been used previously to monitor virion localization and movement

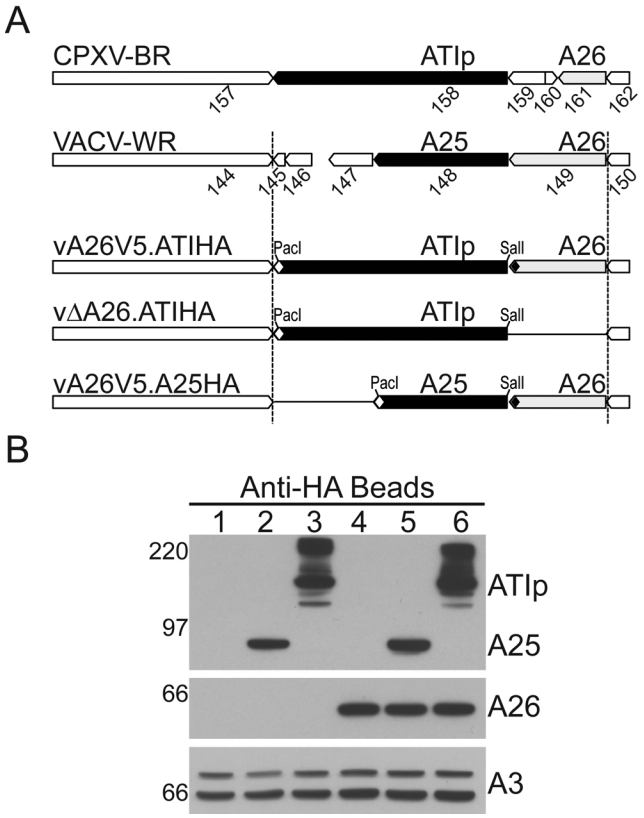

Figure 3-1. Construction of recombinant VACV expressing ATIp. (A) Schematic drawings of the ATI and neighboring loci in CPXV-BR, VACV-WR, and recombinant VACV-WR. Recombinant viruses were made by replacing the truncated A25L gene (VACVWR148) with the full-length ATI gene (CPXVBR158) containing a C-terminal HA-epitope tag or an A25L gene containing a C-terminal HA-epitope tag (white diamond). The VACV A26L gene (VACVWR149) was either deleted or given a C-terminal V5-epitope tag (black diamond). The ATI and A25L genes are flanked by introduced *Sal*I and *Pac*I sites. Additional control viruses with deletions of A25L or A26L are not shown. (B) Western blot confirming expression of ATIp or A25p from recombinant viruses. Extracts of HeLa cells infected with $vA25^{-}A26^{-}$ (lane 1), $vA25^{+}A26^{-}$ (lane 2), $vATI^{+}A26^{-}$ (lane 3), $vA25^{-}A26^{+}$ (lane 4), $vA25^{+}A26^{+}$ (lane 5), $vATI^{+}A26^{+}$ (lane 6) were resolved by SDS-PAGE under reducing conditions. ATIp and A25p were identified using anti-HA antibodies and A26p was detected with anti-A26p antibodies. Precursor and processed forms of VACV late protein A3p were detected with antibody as a loading control. The sizes in kDa and electrophoretic positions of marker proteins are shown on the left.

[108]. The recombinant viruses formed normal looking plaques (not shown) indicating that the genome alterations had little or no effect on replication. Because use of the full descriptive names of the recombinant viruses is cumbersome, I will generally omit reference to the epitope tags and YFP fusion and simply refer to recombinant viruses with intact ATIHA as ATI^{+}, A25HA as $A25^{+}$, and A26V5 as $A26^{+}$ as indicated in Table 1. Viruses with a deletion of A25 or A26 will be referred to as $A25^{-}$ or $A26^{-}$ (Table 3-1).

Whole cell lysates from cells infected with $vATI^{+}A26^{+}$ and $vA25^{+}A26^{+}$ or with control viruses missing one or two genes: $vATI^{+}A26^{-}$, $vA25^{+}A26^{-}$, $vA25^{-}A26^{+}$, and $vA25^{-}A26^{-}$ were analyzed by Western blotting to determine if the CPXV-BR ATIp was expressed in the VACV background. Proteins were resolved by SDS-PAGE under reducing conditions, and anti-HA antibodies revealed bands migrating to positions corresponding to the expected masses of approximately 94 and 160 kDa for A25p and ATIp, respectively (Figure 3-1B). Slower migrating bands, which presumably represent incompletely dissociated oligomeric forms of ATIp, were also detected in samples from $vATI^{+}A26^{+}$ and $vATI^{+}A26^{-}$-infected cells. In contrast, SDS-resistant oligomeric forms of A25p were not detected. Bands representing lower molecular weight processed species of both A25p and A26p were also detected by Western blotting (shown later). A26p was resolved as a 60-kDa protein detected by Western blotting using anti-A26p antibodies in lysates from cells infected with $vA25^{-}A26^{+}$, $vA25^{+}A26^{+}$, $vATI^{+}A26^{+}$ but not $vA25^{-}A26^{-}$, $vA25^{+}A26^{-}$, and $vATI^{+}A26^{-}$ (Fig.1B). Antibody to the A3p VACV core protein was used as a loading control.

After determining that ATIp was expressed in cells infected with $vATI^{+}A26^{+}$

Table 1. Abbreviated nomenclature for recombinant viruses.

Full Descriptive name	Abbreviated name
vA25HA.A26V5.A4YFP	$vA25^{+}A26^{+}$
vATIHA.A26V5.A4YFP	$vATI^{+}A26^{+}$
vA25HA.ΔA26.A4YFP	$vA25^{+}A26^{-}$
vATIHA.ΔA26.A4YFP	$vATI^{+}A26^{-}$
vΔA25.A26V5.A4YFP	$vA25^{-}A26^{+}$
vΔA25.ΔA26.A4YFP	$vA25^{-}A26^{-}$
vΔA27.A4YFP	$vA27^{-}$

and vATI^{+}A26^{-}, I investigated the formation of inclusion bodies by confocal microscopy. HeLa cells were infected with vA25^{+}A26^{+}, vATI^{+}A26^{+}, or vATI^{+}A26^{-} and fixed 18 h later. The cell nucleus and DNA factories, which were moderately dispersed at this late time, were visualized by DAPI staining. Anti-HA staining was used to detect A25p or ATIp, and anti-V5 staining was used for A26p localization. In cells infected with vA25^{+}A26^{+}, the A4:YFP core protein partially co-localized with virus factories and with punctate structures presumably representing virus particles distributed throughout the cytoplasm (Figure 3-2A, row 1). A26p co-localized with A4p:YFP, whereas the abundant A25p was diffusely distributed (Figure 3-2A, row 1). Western blotting and immunoprecipitation experiments carried out using purified vA25^{+}A26^{+}-virions showed that the HA tag did not disrupt either the virion association of A25 or the A26-A25 interaction (data not shown).

Optical sections of cells infected with vATI^{+}A26^{+} and stained with antibodies that recognized the HA tag on ATIp revealed distinct ring-like structures (Figure 3-2A, row 2) in contrast to the diffuse staining of A25p (Figure 3-2A, row 1). Similar peripheral staining patterns of inclusion bodies by anti-ATIp antibodies were seen in previous studies in which the authors suggested that inclusion bodies are impermeable to the antibody-conjugate [151]. MV particles, detected by the YFP fluorescence, were associated with ATI as early as 8 h (not shown) and encrusted and filled the inclusions by 18 h (Figure 3-2A, row 2). Anti-V5 staining showed that A26p was associated with the inclusions and non-occluded MVs (Figure 3-2A). The anti-V5 staining decorated the outside of the ATI bodies and was virtually

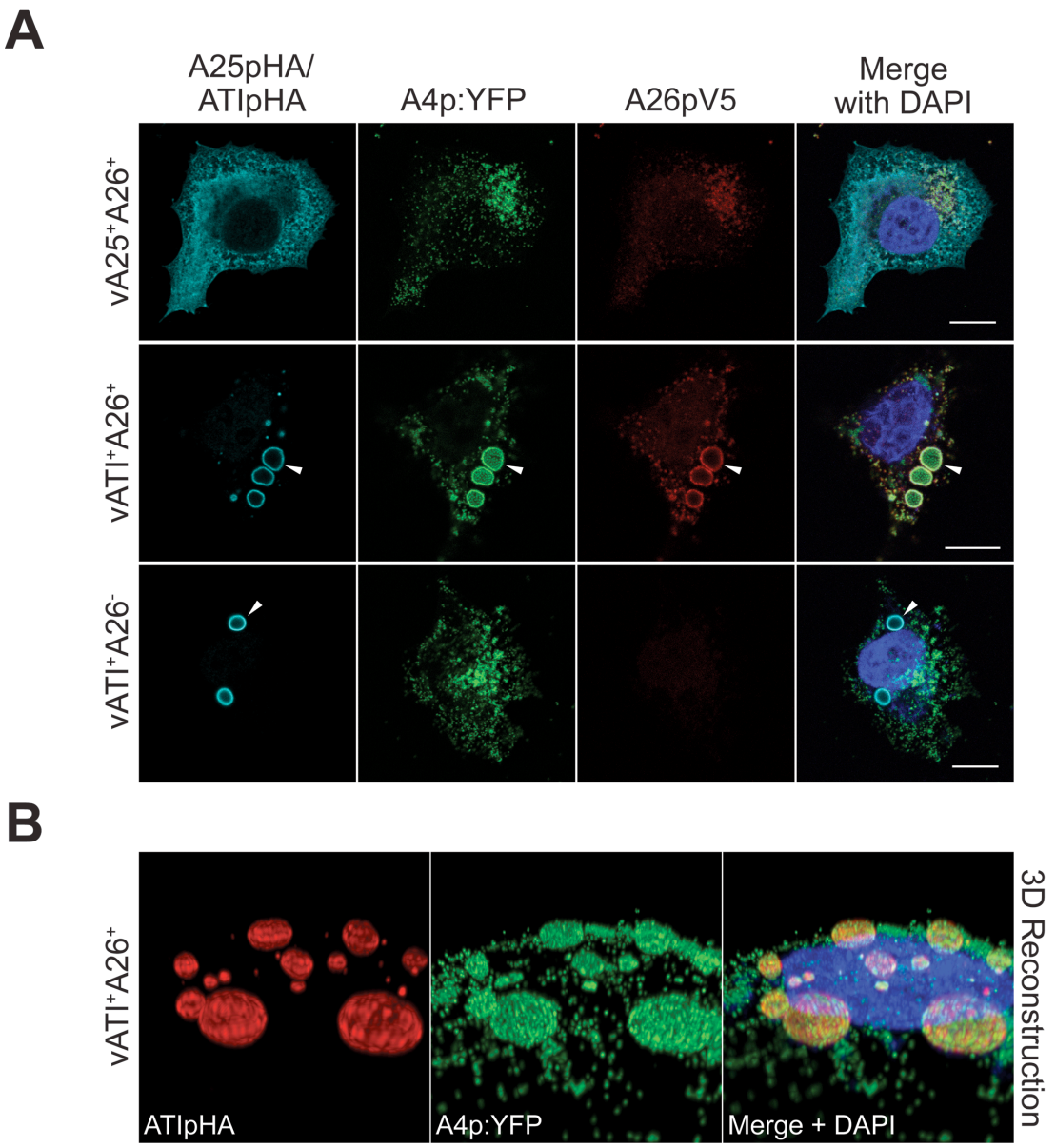

Figure 3-2. Recombinant VACV inclusion body formation and occlusion. (A) Confocal microscopic images of HeLa cells infected with vA25^{+}A26^{+} (first row), vATI^{+}A26^{+} (second row), and vATI^{+}A26^{-} (third row) were fixed, permeabilized, and stained at 18 h after infection. DAPI used to stain DNA in the nucleus and viral factories (blue) is shown in the merge. Rabbit anti-HA antibodies followed by Alexa 647-conjugated anti-rabbit IgG were used to stain A25p and ATIp (cyan). MV particles were visualized using YFP fluorescence (green). Mouse anti-V5 antibodies followed by Alexa 594-conjugated anti-mouse IgG was used to stain A26p (red). Inclusion bodies are denoted by arrowheads. Scale bars, 10 μm. (B) 3D reconstruction of cell infected with vATI^{+}A26^{+} at 18 h post infection and stained as above. ATIpHA (red) staining shows inclusion bodies are quasi-spherical and A4p:YFP fluorescence (green) reveals MV filling inclusions.

undetectable in their interior, presumably due to antibody inaccessibility. Three-dimensional reconstructions (Imaris Bitplane Scientfic Software, Saint Paul, MN) of optical sections of vATI^{+}A26^{+}-infected cells showed the peripherally stained inclusions as quasi-spherical bodies studded or packed with A4-YFP-fluorescing MV particles (Fig. 2B).

In cells infected with vATI^{+}A26^{-}, inclusion bodies formed but MV particles did not associate with them (Fig. 2A, row 3), confirming the requirement for A26p as observed previously for CPXV mutants [152, 157, 160, 222]. These experiments indicated that expression of the full length ATIp conferred upon VACV the ability to form inclusions and to occlude MVs. Thus, VACV-WR encodes all viral proteins needed for occlusion except for the full-length ATIp.

3.3.2 Fine structure of VACV inclusion bodies.

Transmission electron microscopy was used to visualize inclusion bodies and associated MVs at higher magnification. Sections were prepared from BS-C-1 cells infected with either vATI^{+}A26^{+}or vATI^{+}A26^{-} at 22 h post infection. In cells infected with vATI^{+}A26^{+}, characteristic large, electron-dense granular inclusion bodies were seen and MVs were embedded throughout the proteinaceous matrices of most (Figure 3-3A). Other forms of VACV including immature and wrapped virions were not closely associated with inclusion bodies. Inclusion bodies also formed in cells infected with vATI^{+}A26^{-}, but MVs were not occluded (Figure 3-3B).

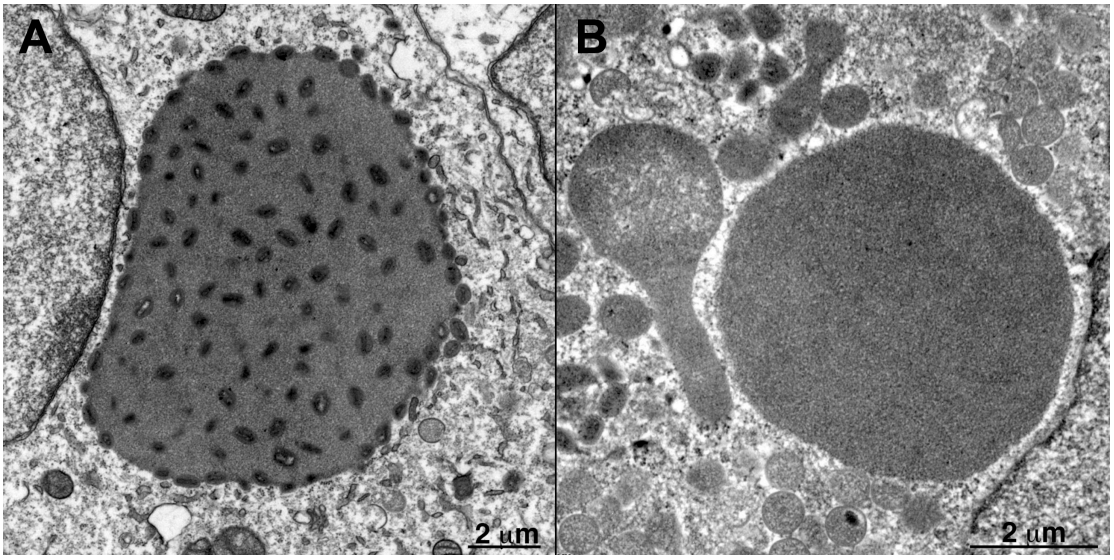

Figure 3-3. Transmission electron microscopy of inclusion bodies. BS-C-1 cells infected with 10 PFU of vATI^{+}A26^{+} (panel A) or vATI^{+}A26^{-} (panel B) per cell were fixed at 24 h after infection. Electron microscopic images of thin sections are shown. Representative MVs and immature virions (IV) are labeled. Scale bars, 2 μm.

3.3.3 Construction and expression of ATIp truncation mutants.

To distinguish the domains of ATIp necessary for formation of inclusion bodies and for occlusion of MVs, a panel of plasmids expressing N-terminal or C-terminal truncated ATIps was constructed. Each mutant ATIp had a C-terminal HA epitope tag to allow detection. Mutants ΔN1-100, ΔN1-300, and ΔN1-412 have N-terminal deletions of 100-, 300-, and 412-amino acids, respectively (Figure 3-4A). Mutants ΔNcc1, ΔNcc1/2, and ΔNcc1/2/3 have more extensive N-terminal deletions extending through the first, second, and third coil-coil domains, respectively (Fig. 4A). The entire N-terminal half of the protein including repeats 1- 4 was deleted in the mutant ΔNRep1-4'. A set of C-terminal truncations was made by incrementally deleting repeats up to the amino acid sequences included in A25p (Figure 3-4A).

To examine expression of the mutant proteins, BS-C-1 cells infected with $vA25^{-}A26^{+}$ were transfected with plasmids encoding the mutant ATIps regulated by the natural ATIp promoter. Proteins in whole cell lysates were resolved by SDS-PAGE under reducing conditions and transferred to nitrocellulose membranes for Western blotting with anti-HA antibodies. Prominent bands migrated to positions corresponding to the reported 160 kDa for ATIp and 94 kDa for VACV A25p as well as the predicted masses of the mutant proteins (Figure 3-4B). Multiple bands were detected for ATIp, A25p, and ATIp mutants presumably representing larger oligomeric and smaller processed forms of the proteins (Figure 3-4B).

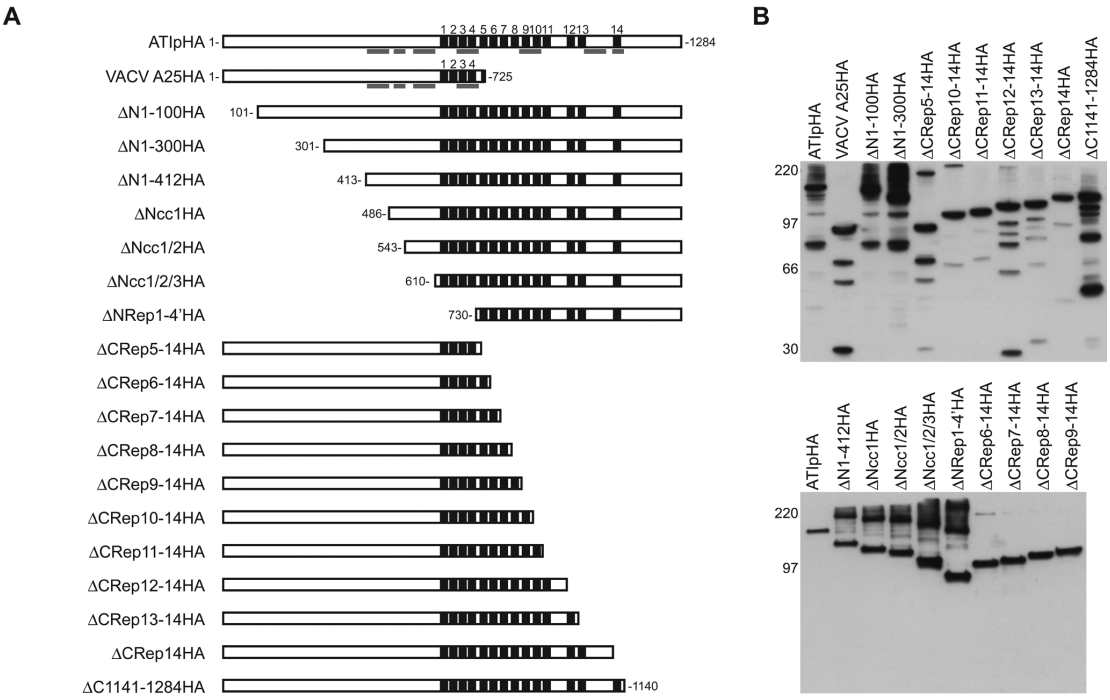

Figure 3-4. Construction and expression of truncated ATIps. (A) Schematic of ATIp and N- and C-terminal truncated versions with C-terminal HA tag. The 14 ATIp repeats (black boxes) are numbered. Gray bars represent predicted coil-coil domains. ΔN followed by numbers indicate the amino acids deleted from the N-terminus; ΔNcc followed by numbers indicate deletion of coil-coil domains from the N-terminus; ΔNRep followed by a numbers indicate the deletion of repeat sequences from the N-terminus; ΔCRep followed by numbers indicate deletion of repeat sequences from the C-terminus; ΔC followed by numbers indicate amino acids deleted from C-terminus. (B) Detection of HA-tagged ATIp and truncated forms by Western blotting. Proteins from BS-C-1 cells infected with $vA25^{-}A26^{+}$ and transfected with plasmids expressing ATIp and truncation mutants were resolved by SDS-PAGE under reducing conditions, transferred to a nitrocellulose membrane, and detected by chemiluminescence after probing with antibody to the HA epitope tag. The positions of marker proteins in kDA are shown on the left.

3.3.4 Effects of N- and C- terminal truncations of ATIp on inclusion formation.

The inability of VACV expressing the C-terminally truncated A25p to form inclusions and the repair of this defect by substituting the CPXV ATIp suggested the importance of the added repeats. To map the domains of ATIp required for inclusion formation and occlusion, HeLa cells were infected with vA25^{-}A26^{+} and transfected with the panel of plasmids shown in Figure 3-4A. Cells were fixed at 16 h after transfection, immunostained, and analyzed by confocal microscopy. The results of these experiments are summarized in Table 2 and confocal microscopy images of selected mutants are shown in Figure 3-5. In this section, I discuss the effects of the mutations on inclusion body formation; the effects on A26p and MV localization are noted in the following section. Typical inclusion bodies with ring-like antibody staining formed in all cells transfected with pATIpHA (Figure 3-5). N-terminal truncations of ATIp up to the repeats did not abrogate inclusion formation, although inclusions had an altered architecture appearing as lamellar structures (Figure 3-5:pΔN1-100HA; pΔN1-300HA; pΔNcc1/2/3HA) that sometimes occupied the bulk of the cytoplasm (data not shown). However, deletion of the first four repeats plus the first 6 amino acids of repeat 5 (pΔNRep1-4') disrupted inclusion formation even though the protein still contained nine intact repeats (Figure 3-5).

The C-terminal truncation mutants were analyzed similarly. Truncation through repeats 12-14 did not alter architecture of inclusion bodies (not shown). Inclusions formed by ATIp truncation through repeats 10 and 11 also resembled wild-type inclusions in shape, but staining revealed a greater amount of unincorporated protein in the cytoplasm (not shown). As additional repeats were deleted from the C-

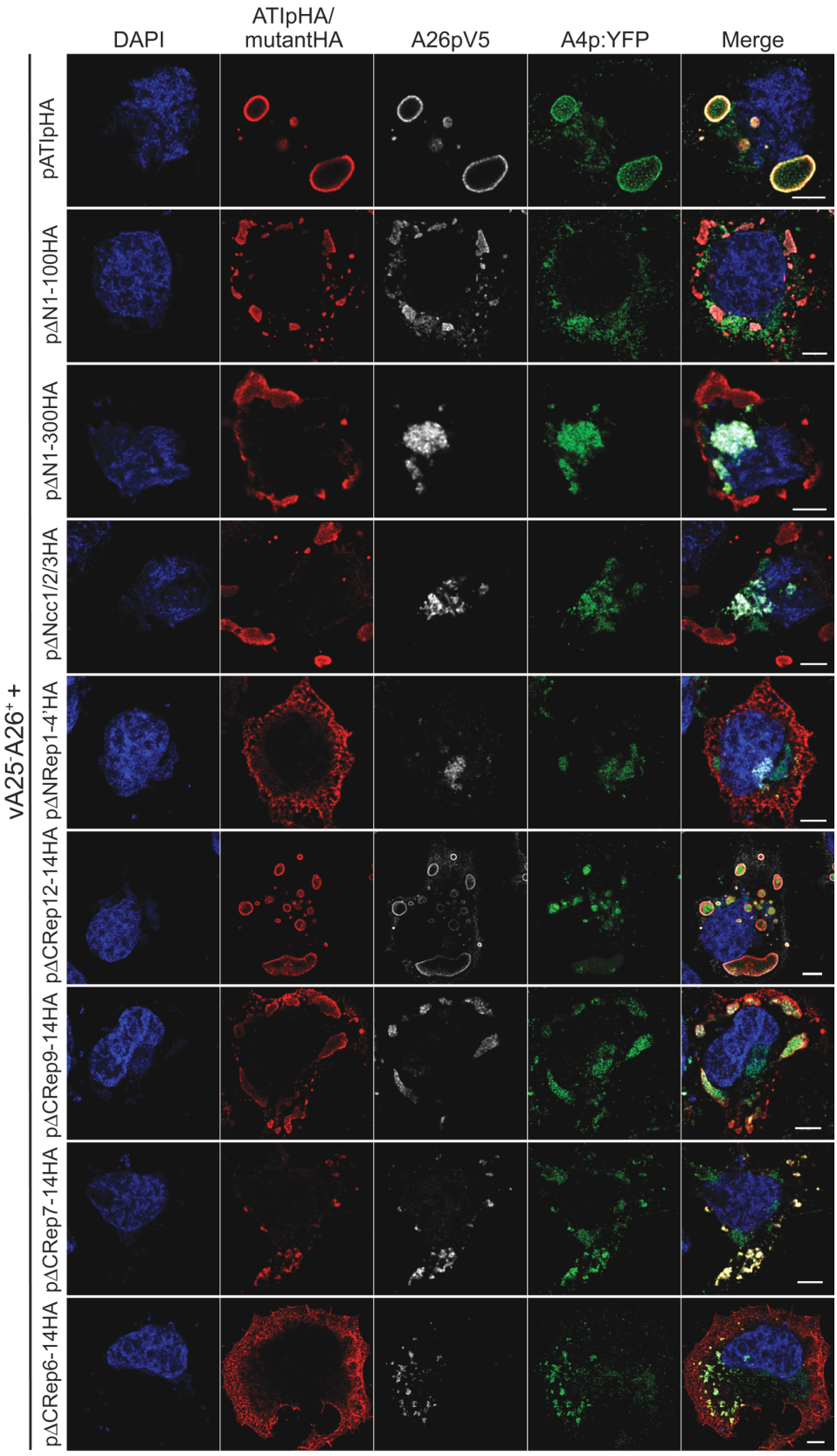
DAPI
ATIpHA/
mutantHA
A26pV5
A4p:YFP
Merge
vA25-A26+ +
pATIpHA
pΔN1-100HA
pΔN1-300HA
pΔNcc1/2/3HA
pΔNRep1-4'HA
pΔCRep12-14HA
pΔCRep9-14HA
pΔCRep7-14HA
pΔCRep6-14HA

Figure 3-5. Effects of ATIp mutations on inclusion formation, A26p localization, and MV occlusion. BS-C-1 cells were infected and transfected as described in the legend to Fig. 4. Representative confocal microscopic sections of selected N- and C-terminal deletion mutant ATIps are shown. Rabbit anti-HA antibodies followed by Alexa-594 conjugated anti-rabbit IgG were used to identify inclusion bodies. Mouse anti-V5 antibodies followed by Alexa-647 conjugated anti-rabbit IgG were used to visualize A26pV5. MVs were detected by YFP fluorescence due to A4 fusion protein. Blue, DAPI; red, Alexa 594; white, Alexa 647; green, A4:YFP.

terminal end of ATIp, the inclusions became smaller, less discrete, and were detected in a lower percentage of cells e.g. 60%, 32%, 22% and 8% of cells transfected with pΔCRep9-14, pΔCRep8-14, pΔCRep7-14, and pΔCRep6-14, respectively (Figure 3-5). The pΔCRep8-14HA and pΔCRep7-14HA proteins formed small, irregular inclusion bodies (Figure 3-5 and not shown). The pΔCRep6-14HA localization in the cell resembled that of A25HA (Figure 3-5). These results demonstrated a role for the N-terminal sequence of ATIp as well as repeats 1-4 (and possibly the first 6 amino acids of repeat 5) plus an additional 3 or more repeats of ATIp for inclusion formation.

3.3.5 Effects of N- and C-terminal truncations of ATIp on A26p association and occlusion.

In the experiments described above, A26p and MV localization were also examined. The first 100 amino acids of ATIp were dispensable for ATIp-A26p colocalization, even though the inclusions had an atypical appearance (Fig. 5, Table 2). However, the truncated ATI proteins pΔN1-300HA through pΔNRep1-4'HA did not co-localize with A26p demonstrating that ATIp-A26p interactions are mediated through the N-terminal half of the ATIp protein (Figure 3-5, Table 3-2). Furthermore, mutations that disrupted the ability of ATIp to interact with A26p disrupted MV occlusion as determined by A4p:YFP fluorescence (Figure 3-5, Table 3-2). Although A26p localized to inclusion bodies formed by pΔN1-100HA, MVs were not embedded in those bodies (Figure 3-5), perhaps due to the aberrant structure of the ATIs. A26p and MV localized to the C-terminal mutants of ATIp that retained the ability to form inclusion bodies (Figure 3-5, Table 3-2).

It was impossible to use immunoprecipitation to study interactions of A26p

Table 2. Summary of the effects of deletion mutations on inclusion formation, A26p localization, and MV occlusion.

Mutant	[a]Inclusion formation	[b]A26 localization	[b]MV occlusion
ΔN1-100HA	+	+	-
ΔN1-300HA	+	-	-
ΔN1-412HA	+	-	-
ΔNcc1HA	+	-	-
ΔNcc1/2HA	+	-	-
ΔNcc1/2/3HA	+	-	-
ΔNRep1-4’	-	-*	NA
ΔCRep5-14HA	-	+*	NA
ΔCRep6-14HA	-	+*	NA
ΔCRep7-14HA	+/-	+*	NA
ΔCRep8-14HA	+/-	+	+
ΔCRep9-14HA	+	+	+
ΔCRep10-14HA	+	+	+
ΔCRep11-14HA	+	+	+
ΔCRep12-14HA	+	+	+
ΔCRep13-14HA	+	+	+
ΔCRep14HA	+	+	+
ΔC1141-1284HA	+	+	+

[a]Approximately 100 cells infected with $vA25^{-}A26^{+}$ and transfected with plasmids expressing mutant ATIps were scored in at least two separate experiments. Inclusion formation was scored as +, +/-, or – based on the number of cells expressing the mutant protein that contained inclusion bodies: +, >50% cells contain inclusion bodies; +/-, <50% but >20%; -, <20%.

[b]A26 and MV localization were scored as + or –. NA, not analyzed.

*Proteins that did not form inclusion bodies or formed few inclusion bodies were tested for interaction with A26p by immunoprecipitation.

with ATIps that formed inclusions because of solubility problems even in the presence of non-denaturing detergents. However, I could employ immunoprecipitation to determine whether soluble ATIp mutants that did not form inclusion bodies were able to interact with A26p. BS-C-1 cells were infected with vA25^{-}A26^{-} and co-transfected with pA26V5 and plasmids expressing the N-terminal ATI truncations pΔNRep1-4'HA or the C-terminal ATI truncations pΔCRep5-14HA, pΔCRep6-14HA, or pΔCRep7-14, respectively. Detergent-disrupted cell lysates were incubated with mouse anti-V5 conjugated agarose beads to bind A26p and associated proteins, and unbound and bound fractions were resolved by SDS-PAGE and analyzed by Western blotting. The C-terminal truncated proteins pΔCRep5-14HA, pΔCRep6-14HA, and pΔCRep7-14 were associated with A26p and present in the bound fractions (Figure 3-6). However, the N-terminal truncated protein, pΔNRep1-4'HA, was absent from the bound fraction and present only in the unbound fraction confirming that A26p-ATIp interactions are mediated by the N-terminus of the ATIp (Figure 3-6).

3.3.6 A27p is required for congregation of MVs in inclusion bodies but not for localization of A26p.

VACV A27p anchors A26p to the MV particle through disulfide interactions with the C-terminus of A26p [219, 220]. The association of the VACV A25p with the A26p-A27p complex suggested that A26p bridges MV with inclusion bodies through interactions with A27p on the MV membrane and ATIp, respectively. To test whether A27p is required for occlusion, I infected cells with the A27 deletion mutant vA27^{-} (Table 3-1), which lacks an intact ATI gene and contains A4:YFP, and transfected plasmids expressing FLAG-tagged ATIp and V5-tagged A26p with or without

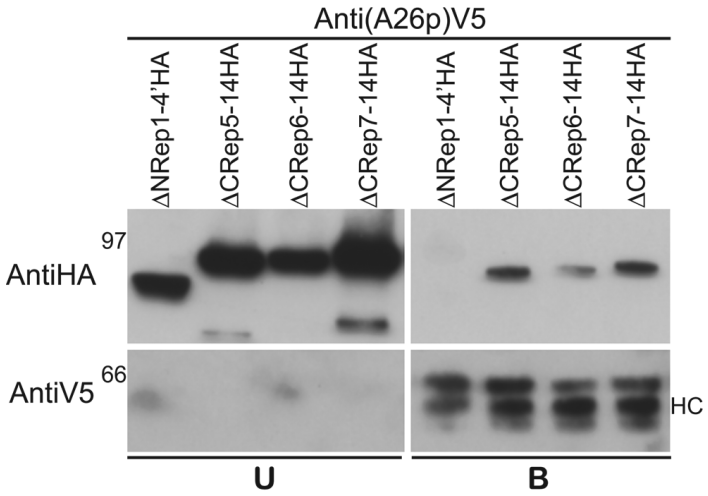

Figure 3-6. Coimmunoprecipitation of truncated ATIps with A26pV5. Cells were infected with vA25^{-}A26^{-} and cotransfected with pA26V5 and plasmids expressing an N-terminal (ΔNRep1-4'HA) or C-terminal (ΔCRep5-14HA, ΔCRep6-14HA, ΔCRep7-14) ATIp truncation mutants that do not form inclusion bodies. Cells lysates were cleared and incubated with mouse anti-V5 conjugated affinity agarose beads. Unbound (U) and bound fractions eluted from beads with LDS sample buffer (B) were resolved by SDS-PAGE, transferred to nitrocellulose membrane, and probed with mouse anti-HA antibody to detect ATIp (upper panels) and mouse anti-V5 antibody (lower panels) to detect A26p. Positions of 97- and 66-kDa marker proteins are on left. HC, IgG heavy chain.

plasmids expressing HA-tagged A27p. ATIpFLAG formed inclusion bodies when transfected into cells infected with vA27$^-$. However, the YFP fluorescent MV particles did not localize in inclusion bodies in the absence of A27p (Figure 3-7A). Occlusion was not rescued in cells infected with vA27$^-$ and transfected with a plasmid over expressing A26V5p in addition to ATIpFLAG, although A26V5p did localize to inclusion bodies under these conditions (Figure 3-7A). The ability of MV to embed within inclusion bodies in cells infected with vA27$^-$ was rescued by A27p expressed from plasmids co-transfected with pATIpFLAG and pA26V5 (Figure 3-7A). The data indicated a role for A27 in occlusion, likely by tethering A26p to the MV membrane.

The above experiment also demonstrated that A26p could traffic to inclusions in the absence of MVs. To confirm this result, cells were infected with vATI$^+$A26$^+$ for 9 h in the presence of the drug rifampin, which interrupts assembly at a stage prior to crescent membrane formation [223, 224]. A26p localized to inclusion bodies in the absence of virion assembly, demonstrating that A26p traffics to inclusions in the absence of MV-association (Figure 3-7B).

3.3.7 The MV anchoring domain of A26p is required but not sufficient for occlusion.

I previously determined that the C-terminal 100 amino acids of A26p are required for A26p-A27p disulfide interactions and anchoring to the MV membrane [219]. Subsequently, it was shown that two conserved cysteines in the A26p C-terminus specifically mediate A26-A27 interactions [20]. I employed two previously characterized truncated A26p mutants to test whether anchoring to the MV membrane is required for directing particle occlusion. The plasmid pA26ΔNV5

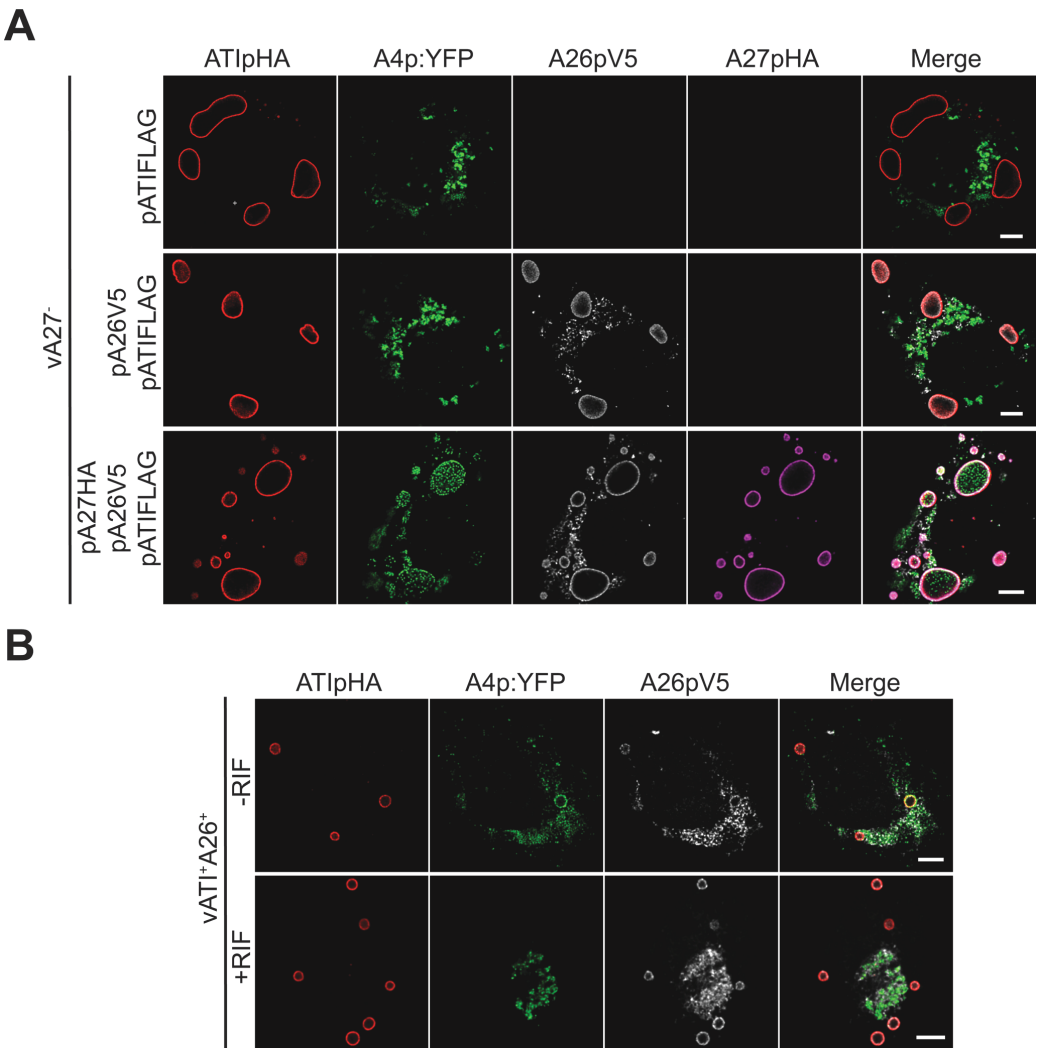

Figure 3-7. Requirement for A27p for virion occlusion. (A) HeLa cells were infected with an A27-deletion VACV expressing YFP fused to the core protein A4 and lacking an intact ATI gene (vA27$^-$, Table 1). Cells were transfected with pATIFLAG alone (top row), pATIFLAG and pA26V5 (middle row), or pATIFLAG, pA26V5 and pA27HA (bottom row). At 18 h after transfection, cells were fixed and permeabilized. ATIp (red) was detected with mouse anti-FLAG antibodies followed by Alexa 405 conjugated anti-mouse IgG. The A27pHA (magenta) and A26pV5 (white) proteins were visualized using rat anti-HA and rabbit anti-V5 antibodies followed by Alexa 647- and Alexa 594-conjugated anti-rat and anti-rabbit IgG, respectively. MVs were detected by YFP fluorescence (green). (B) Cells were infected with vATI$^+$A26$^+$ for 9 h in the presence of the drug rifampin, which blocks virion assembly. ATIpHA (red) and A26pV5 (white) were visualized using rat anti-HA and rabbit anti-V5 antibodies followed by Alexa 405 and -594, respectively. MVs were detected by A4p:YFP fluorescence (green). Scale bars, 5 μm.

expresses the C-terminal 270-500 amino acids of A26p and is sufficient for interaction with A27p, whereas pA26ΔCV5, which codes for amino acids 1-409 of A26p, is not. Cells were infected with the A25p and A26p double deletion virus expressing A4:YFP (vA25$^-$A26$^-$) and co-transfected with pATIHA and pA26V5, pA26ΔCV5, or pA26ΔNV5. Cells infected with vA25$^-$A26$^-$ and co-transfected with pATIHA and pA26V5 contained inclusion bodies to which A26pV5 and virions localized (Figure 3-8). A26ΔCpV5 localized to inclusion bodies but was not associated with virions demonstrating that A26-MV anchoring is required for the occlusion of MV within inclusion bodies. In contrast, A26ΔNpV5 was strongly coincident with virions, but neither A26ΔNpV5 nor MV localized to inclusion bodies (Figure 3-8) suggesting that the N-terminus, although dispensable for A26p-A27p interactions, was required for association with inclusion bodies.

3.4 Discussion

The embedding of virions in dense proteinaceous masses is a strategy used by some DNA viruses to enhance their stability upon release into the environment. This capability is preserved by some orthopoxviruses but lost by others. Previous studies had shown that CPXV inclusions consist predominantly or exclusively of the 160 kDa ATIp [151]. However, some CPXV mutants that have an intact ATIp and can form inclusions fail to occlude virions. This defect is due to a mutation of the CPXV homolog of the VACV A26p [160]. Nevertheless, how A26p mediates occlusion was not understood. The discovery that A26p interacts with both MV membrane bound

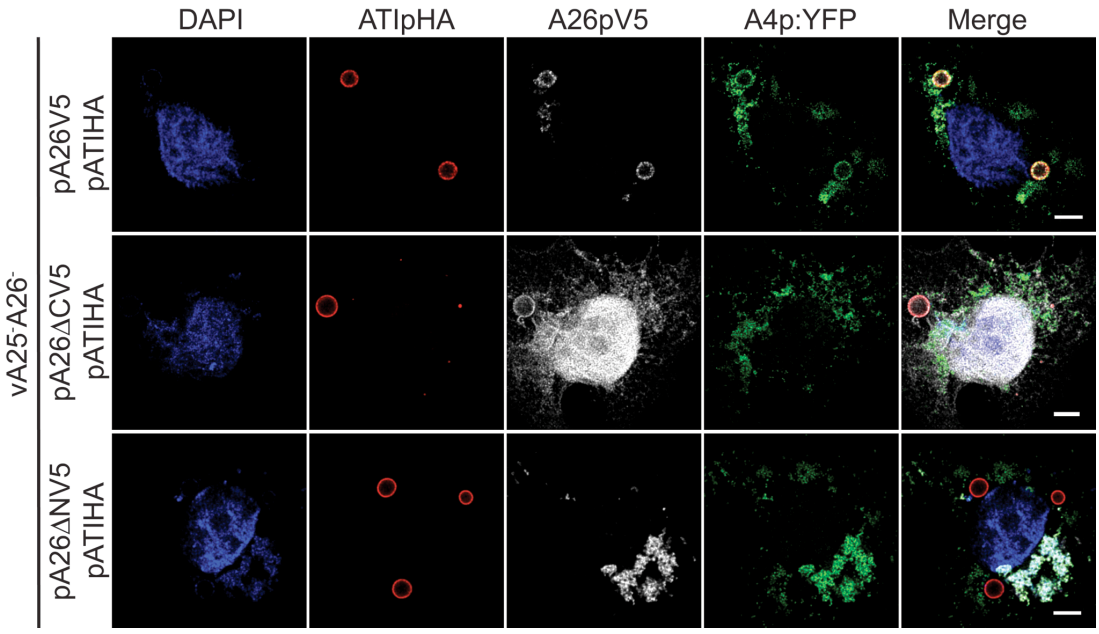

Figure 3-8. Requirements of A26p N- and C-terminal domains for virion occlusion. HeLa cells were infected with vA25^{-}A26^{-} and transfected with pATIpHA and cotransfected with pA26V5, pA26ΔCV5, or pA26ΔNV5. At 18 h after transfection, ATIpHA (red) was stained with rat anti-HA antibodies followed by Alexa 405 conjugated anti-mouse IgG, and A26pV5 and mutants (white) were visualized using rabbit anti-V5 followed by Alexa 594-conjugated anti-rabbit IgG. MV localization was monitored using A4p:YFP fluorescence (green). Blue, DAPI. Note that A26ΔCV5 also localized to nucleus. Scale bars, 5 μm.

A27p--A17p complex and the truncated VACV ATIp homolog A25p, suggested a bridging role for A26p in occlusion [219].

I explored the validity of the above occlusion model using recombinant VACV rather than CPXV for two main reasons. First, VACV is better characterized than CPXV and more mutants and reagents are available. Second, I wanted to determine whether restoration of the full length ATIp would be sufficient for occlusion as well as inclusion formation in VACV-infected cells. If restoration of the ATIp failed to allow occlusion, then it would suggest a role for additional viral proteins. Remarkably, exchanging the truncated A25p of VACV-WR with the full-length ATIp of CPXV-BR was sufficient for inclusion formation as well as occlusion of MVs. Indeed the VACV ATI were indistinguishable from CPXV ATI by electron microscopy.

A panel of plasmids expressing ATIp mutants was constructed to investigate the domains needed for inclusion formation, interaction with A26p, and occlusion of MVs. Mutational analysis of ATIp revealed that domains essential for inclusion formation are contained in the C-terminal ATI repeat region of the protein. Inclusion formation required ATI repeats 1-4 and possibly the first 6 amino acids of repeat 5, which are present in A25p, plus at least three additional repeats. In general, a higher percentage of cells formed inclusions with more ATI repeats. N-terminal deletions of ATIp did not prevent inclusion body formation but their appearance was altered and lamellar structures were observed. I found that the N-terminal region of ATIp was needed for interaction with A26p. Even though deletion of the entire repeat region of ATIp abrogated inclusion formation, the truncated protein was still able to interact

with A26p as determined by both microscopic localization studies and immunoprecipitation experiments. Furthermore, mutations in ATIp that prevented its interaction with A26p also blocked occlusion indicating an essential role for A26-ATIp interactions. Our data suggest that multiple ATI repeats are needed for aggregation of ATIp to form inclusions and that the N-terminal region of ATIp is needed for interaction with A26p.

I further investigated the need to anchor A26p to the MV particle for occlusion. Initial characterization of occlusion by Shida et al. [225] suggested that the p4c protein, subsequently shown to be A26p [160], functions to mediate occlusion as a virion component. Since I had shown that A26p is anchored to the MV by the A27p-A17p complex, I predicted that A27p would be required for occlusion. Indeed, A26p was not sufficient to direct occlusion in the absence of A27p. Moreover, an A26p C-terminal deletion mutant that does not interact with A27p did not mediate occlusion. Nevertheless, the mutant A26p still localized to inclusion bodies, even though it was not associated with virus particles, suggesting that the N-terminus of A26p interacts directly with ATIp. On the other hand, an N-terminal deletion mutant of A26p that does not disrupt A26p-A27p interactions localized to virions in the cytoplasm of infected cells but was unable to mediate occlusion or localize to inclusion bodies.

Our studies indicated that A26p has a bridging function enabling the association of MVs containing membrane-associated A27p with the ATIp in inclusions. This model can explain why immature virions are not occluded since A27p is incorporated into virions at a later stage [124], presumably after the D13

scaffold has been removed [91]. The large size of MVs and the distance between the sites of their assembly in factories and inclusion bodies make it unlikely that occlusion is a totally passive phenomenon. McKelvey et al. [160] suggested that A26p might be involved in retrograde movement of MVs in the cytoplasm.

Chapter 4: Formation of orthopoxvirus cytoplasmic inclusion bodies by *in situ* mRNA translation and the requirement of microtubules for their coalescence and occlusion of virions

4.1 Introduction

Poxviruses subvert the host cell infrastructure to create microenvironments in which viral and host proteins are sequestered for the regulation of distinct stages of the viral life cycle. Poxvirus transcription, genome replication, and assembly occur entirely in the cytoplasm of infected cells at organized, endoplasmic reticulum (ER)-bound bodies called viral factories (VFs) [79, 80, 83, 226]. Studies using vaccinia virus (VACV), the most characterized member of the orthopoxvirus genus, showed that VFs contain tunnel-like subdomains in which viral mRNAs and transcription factors localize [79]. In addition, translation initiation factors eIF4E and eIF4G and ribosomal proteins are recruited to these VF subdomains for the synthesis of viral proteins [79]. Consequently, VFs efficiently localize the components necessary for the assembly of progeny mature virions (MVs).

MVs consist of genomic DNA and enzymes necessary for early transcription packaged in a multi-protein core surrounded by a lipoprotein membrane [84]. A population of MVs segregates to sites at the trans-Golgi network (TGN) or late endosomes where they acquire two extra membranes to form the triple-membrane wrapped virions (WVs). WVs are transported to the periphery of the cell and exocytosed, losing the outermost membrane to become double-enveloped extracellular virions (EVs). Most MVs, however, are not destined to become EVs, but are instead retained in the cytoplasm until cell lysis. Alternatively, some

orthopoxviruses, including strains of cowpox (CXPV), ectromelia (ECTV), fowlpox, and raccoonpox, embed MVs in cytoplasmic, proteinaceous matrices called A-type inclusion (ATIs) [146-149], which are thought to provide protection after release into the environment. ATIs are composed of a single viral polypeptide, the ATI protein (ATIp)[151]. ATIp is a large protein (160-kDa in CPXV) containing C-terminal, highly hydrophobic repeats [151, 154] that are required for inclusion body assembly [227].

ATIs are localized throughout the cytoplasm and increase in size during infection. In electron microscopy studies of sections from cells infected with CPXV, polyribosomes and protein pulse-labeled with 3H-leucine were seen associated with the peripheries of ATIs [153]. Attempts to identify RNA associated with the polyribosomes surrounding ATIs suggested that the RNA was most likely viral in origin [153]. However, the specific RNA associated with ATIs was not identified. The A26 protein (A26p) is required for the embedment of MV within ATIs [160, 227]. A26p is an MV-specific protein anchored by disulfide bond mediated protein-protein interactions with the A27p-A17p complex to the MV membrane [20, 219, 220].

Orthopoxviruses hijack the cytoskeleton for entry, intracellular transport, and exit from the host cell. Modulation of the actin cytoskeleton facilitates virus entry [228], after which viral cores rapidly associate with microtubules facilitating migration to a juxtanuclear position [43, 229]. Progeny MVs traffic on microtubules to sites of wrapping [107, 108], and WVs use microtubules to move to the plasma membrane to release EVs [230], which can stimulate the polymerization of actin tails

at the cell surface for cell-to-cell dissemination [140]. Given their size (~360 X 270 X 250 nm), it is likely that the association of MVs with inclusion bodies is also dependent on active transport using the cytoskeleton. McKelvey et al. proposed that A26p might have a role in directing transport of MV from VFs to ATIs during occlusion [160].

Orthopoxviruses such as VACV that do not form ATI may encode a C-terminally truncated ATIp, A25p [231, 232]. I demonstrated that VACV could make ATI and occlude MVs if the CPXV ATIp gene was substituted for the mutated VACV homolog (14). As much more is known about the molecular biology of VACV than CPXV or other orthopoxviruses than make ATI naturally, I have used the reconstructed VACV system to study ATI formation and the mechanism of occlusion. I demonstrated that the direct association of A26p with both the A27p-A17p complex and the ATIp is required to mediate occlusion [227]. In the present study, I show that ATI enlargement is dependent on both new protein synthesis and coalescence of smaller ATI. mRNA encoding ATIp and the translation initiation factor, eIF4E, were localized to ATIs, indicating the existence of a mechanism for specific mRNA trafficking from transcription sites in the VF. Both the coalescence of ATI and occlusion required intact microtubules, and MVs move to ATIs at speeds characteristic of microtubular transport.

4.2 Methods and materials

4.2.1 Cells and virus infection.

HeLa, African green monkey kidney BS^{-}C^{-}1, and rabbit kidney RK13 cells were maintained in minimum essential medium (EMEM) (Quality Biological,

Gaithersburg, MD) containing 2 mM L-glutamine, 100 units/ml penicillin, 100 μg/ml streptomycin, and 10% fetal bovine serum (FBS). Virus infections of cells were carried out in medium as described above except for 2.5% FBS. VACV strain Western reserve (WR) and all recombinant viruses were propagated as previously described.

4.2.2 Recombinant viruses and plasmids.

The recombinant VACVs used in this study were described previously (ref). Briefly, $vATI^{+}A26^{+}$.A4:YFP is a recombinant VACV expressing a C-terminally HA-tagged CPXV ATIp (ATIpHA) and a C-terminally V5-tagged VACV A26p (A26pV5). $vA25^{+}A26^{+}$.A4:YFP expresses an HA-tagged VACV A25p (A25pHA) and A26pV5. $vA25^{+}A26^{-}$.A4:YFP expresses A25pHA but with the A26 gene deleted. In the above viruses, A4:YFP denotes the fusion of the A4 gene in frame with the gene expressing the yellow fluorescent protein (YFP). $vA25^{-}A26^{+}$ is an A25-deletion virus and expressing A26pV5. $vA25^{+}A26^{+}$, $vATI^{+}A26^{+}$, $vATI^{+}A26^{-}$ are as described above but the A4 gene was not fused to YFP.

To construct the plasmid pATIAU1, the ATI gene was amplified using Accuprime *Pfx* (Invitrogen, Carlsbad, CA) from CPXV-BR genomic DNA with a forward primer to the ATI promoter and reverse primer coding for the AU1 epitope tag (DTYRYI) and blunt-end ligated into pCR-BluntII-TOPO (Invitrogen).

4.2.3 Antibodies for immunofluorescence.

Both rabbit polyclonal antibodies (PAbs) and mouse monoclonal antibodies (MAbs) against the HA tag (YPYDVPDYA) were used for immunofluorescence

studies at a 1:250 dilution (Covance, Princeton, NJ). Mouse anti-AU1 (DTYRYI) antibodies (Covance) were used at a 1:250 dilution. Mouse anti-puromycin (PMY) MAb 12D10 was used at 1:100 and was provided by Alexandre David from the laboratory of Jonathan Yewdell and Jack Bennink. Mouse anti-eIF4E was obtained from Santa Cruz Biotechnology (Santa Cruz, CA) and was used 1:100. All Alexa Fluors conjugated anti-IgG were obtained from Invitrogen and used at dilutions of 1:250.

4.2.4 Preparation for confocal microscopy.

For confocal imaging of fixed cells, 24-well dishes containing 12 mm coverslips seeded with HeLa cells were infected at a multiplicity of infection (moi) of 0.1 PFU per cell in EMEM (Quality Biological) and incubated with rocking at room temperature for 1 h. Following adsorption, the inoculum was removed and the cells were incubated at 37°C. Cells were washed twice in Dulbecco's phosphate-buffered saline (PBS) and then fixed with 4% paraformaldehyde for 15 min. Cells were washed with PBS, permeabilized with 0.2% Triton X-100 in PBS for 7 min, washed (4 X 5 min) in PBS, and blocked with 10% FBS diluted in PBS. Primary antibodies and secondary Alexa Fluor-conjugated IgG were diluted as described above in 10% FBS/PBS and incubated with cells for 1 h and 45 min, respectively, at 37°C. Labeling with anti-eIF4E antibody was carried out as above except blocking and antibody incubation steps were in 1% bovine serum albumin, and cells were incubated with anti-eIF4E antibody overnight at 4°C. Cover slips were mounted using ProLong Gold mounting medium containing 4', 6'-diamidino-2-phenylindole (DAPI) from Invitrogen. For confocal live imaging, 35 mm, glass bottom dishes (ibidi GmbH,

München, Germany) were seeded with HeLa cells and infected at an moi of 0.1 PFU/cell for 1 h. The inoculum was removed and medium containing 10 μM ST-246 was added.

4.2.5 Fluorescence *in situ* hybridization (FISH).

An antisense probe to the nucleotide sequence encoding the HA tag was synthesized and conjugated to Alexa-594 (5'-/5Alex594N/TCA GGC GTA CTC GGG CAC GTC GTA GGG GTA-3') by Integrated DNA technologies (IDT) (Coralville, IA). FISH was carried out per the Singer lab online protocol (http://www.singerlab.org/protocols). Briefly, coverslips containing $vATI^{+}A26^{+}$.A4:YFP- or $vA25^{-}A26^{+}$.A4:YFP- infected cells were fixed and permeabilized using 70% ethanol overnight at 4°C. Hybridization was carried out at 37°C overnight in 40 μl hybridization buffer containing 2 mM vanadyl-ribonuclease complex, 0.02% RNAase-free bovine serum albumin, 100X *E. coli* tRNA (Roche Applied Sciences, Indianapolis, IN), 2XSSC (300 mM NaCl, 30 mM sodium citrate, pH 7.0), 50% formamide, and 40 ng of probe. Cells were washed 2X in 2XSSC for 30 min at 37°C.

4.2.6 PEGylation experiments.

HeLa cells (1X12-well per cover slip) were infected with $vA25^{-}A26^{+}$ and transfected with pATIAU1 using Lipofectamine 2000 per the manufacturers instructions (Invitrogen); HeLa cells on coverslips were infected with $vATI^{+}A26^{+}$.A4:YFP. 4 hpi, the cells infected with $vA25^{-}A26^{+}$ and transfected with pATIAU1 were scraped into 200 μl EMEM and added to coverslips. The coverslips

were centrifuged for 10 min at 1500 x g at room temperature. The EMEM was aspirated and cell were incubated in 250 µl of the polyethylene glycol (PEG) solution containing a 10% DMSO in 50% (w/v) PEG (Av. Mol. Wt. 1450) (Sigma-Aldrich, St. Louis, MO) in DPBS without calcium.

4.2.7 Puromycin labeling.

Method provided by Alexandre David (publication in submission).

4.2.8 Confocal microscopy and image processing.

For fixed cell imaging, a Leica SP2 inverted four-channel microscope was used. A Leica SP5 inverted 5-channel confocal microscope with high speed scanning using a resonant scanner was used for live imaging experiments. Cells were imaged on a stage containing an incubation chamber that maintained cells at 37°C with 5% CO_2. Representative images and time series were deconvolved using Huygens Essential version 3.5.0, 64 bit (Scientific Volume Imaging, Hilversum, Netherlands). Z-sections were reconstructed as 3D images using IMARIS Bitplane Scientific Software version 7.0 (Saint Paul, MN) using surpass mode with an orthogonal view. The IMARIS Spots feature was used to track MV in 4D (X, Y, X, and time[t]) and to extract statistical analyses of particle dynamics.

4.3 Results

4.3.1 Time course of ATIp synthesis and ATI formation.

ATIp is a highly expressed late protein and CPXV inclusion bodies are visible by phase contrast microscopy by 9 h post infection (hpi) [151, 152]. I employed the

high sensitivity and resolution provided by immunofluorescent confocal microscopy to monitor ATIp synthesis using a previously characterized recombinant VACV that expresses the CPXV-BR ATI protein with a C-terminal HA tag and the A4 protein fused to YFP ($vATI^{+}A26^{+}$.A4:YFP). HeLa cells were infected with $vATI^{+}A26^{+}$.A4:YFP and fixed at 3-, 5-, 7-, 9-, and 11 hpi, and ATIp localization was monitored using anti-HA antibody. VFs were stained with DAPI and appear as amorphous juxta-nuclear bodies that appear compact early in infection and less structured at later time points (Figure 4-1). The core protein, A4p, fused to YFP was used as a control to monitor protein synthesis in VFs [79]. Numerous punctate bodies containing ATIp were distributed throughout the cell as early as 3 hpi, whereas A4p:YFP was in or adjacent to VFs (Figure 4-1). By 5 hpi, although A4p:YFP was detected throughout VFs, ATIp was not seen in VFs in any of the infected cells viewed (n=50). The ATI were larger than those seen at 3 hpi and had a characteristic donut appearance due to peripheral antibody staining (Figure 4-1). ATIs continued to increase in size throughout infection as previously observed, although some small inclusions were still seen at 9 h (Figure 4-1, arrowheads). MVs were at the periphery of ATIs at 7 hpi but were dispersed throughout the bodies at 11 hpi (Figure 4-1, lower panels).

4.3.2 ATI mRNA is translated at inclusion bodies.

Previous studies provided evidence for the synthesis of VACV late proteins within subdomains of the VF in which viral RNA and cellular translation factors were localized. The absence of ATIp in VFs (Figure 4-1) combined with previous studies showing polyribosomes associated with nascent protein and RNA surrounding

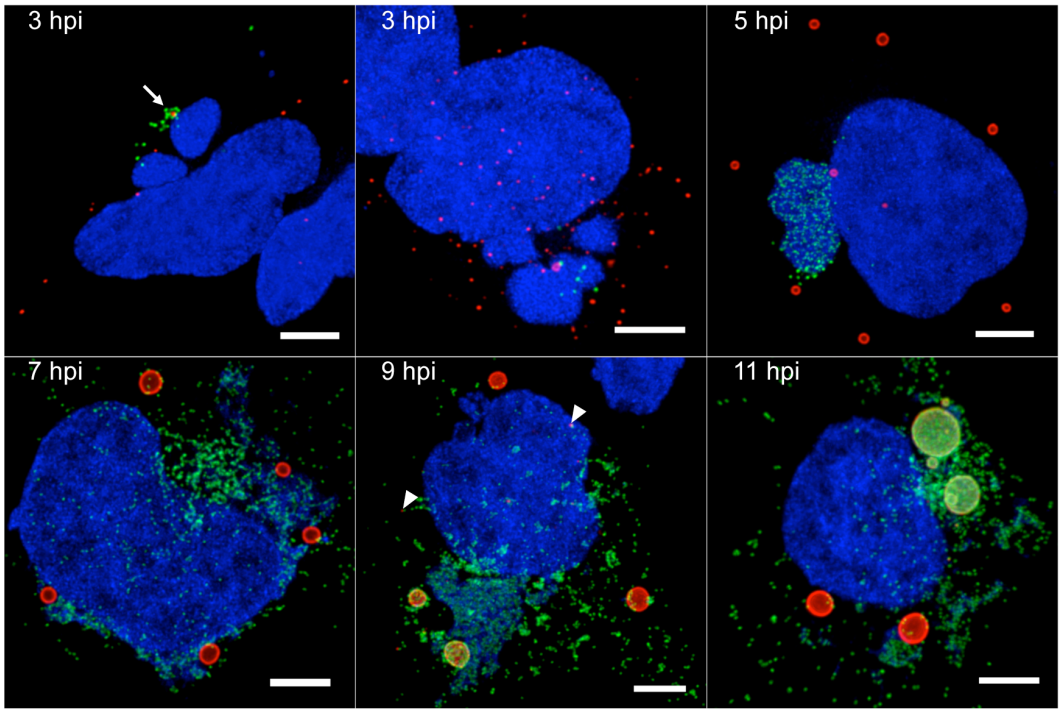

Figure 4-1: Time course of ATI formation. Representative confocal images of Hela cells infected with vATI^{+}A26^{+} and fixed at 3-, 5-, 7-, 9-, and 11 hpi. Rabbit anti-HA antibodies, followed by Alexa-568 conjugated anti-rabbit IgG, were used to visualize ATIpHA (red, Alexa-568). A4p:YFP (green) was monitored using YFP fluorescence. The nucleus and viral factories (VF) were visualized by DAPI staining (blue). Arrow indicates ATIpHA coincident with A4:YFP at the VF, and arrow heads indicate ATI puncti formed 9 hpi. Scale bars, 5 μm.

inclusion bodies [153] led us to investigate whether ATI mRNA is translated at inclusion bodies. The translation initiation factor eIF4E, which binds the 5' cap of mRNAs [234], was previously shown to localize within VF subdomains at 8 hpi in cells infected with VACV that does not form ATI. To determine whether eIF4E might be recruited to inclusion bodies, I infected HeLa cells with vATI^{+}A26^{+}.A4:YFP for 8 h and looked for the coincidence of anti-HA and anti-eIF4E staining. Cells were observed by confocal microscopy and scored for localization of eIF4E to both VFs (arrowheads) and inclusion bodies (arrows). eIF4E localized to VFs and/or inclusion bodies in 73% and 76% of cells (n=30), respectively (Figure 4-2A). This result suggested that translation was occurring in ATIs as well as in VFs.

Having shown that eIF4E was recruited to inclusion bodies, I next sought to determine whether active translation was occurring there. I addressed this question by employing an assay similar to the one developed by Schmidt et al (2009) that uses puromycin followed by fluorescent puromycin antibody to stain actively translating ribosomes [235]. Puromycin inserts at the A-site of ribosomes and is covalently linked to the growing, C-terminal end of nascent peptides causing cessation of translation [236, 237]. HeLa cells were infected with vATI^{+}A26^{+}.A4:YFP for 22 h, treated with puromycin, and then fixed. Mouse anti-puromycin MAb and rabbit anti-HA antibodies were used to visualize actively translating ribosomes and ATIs,

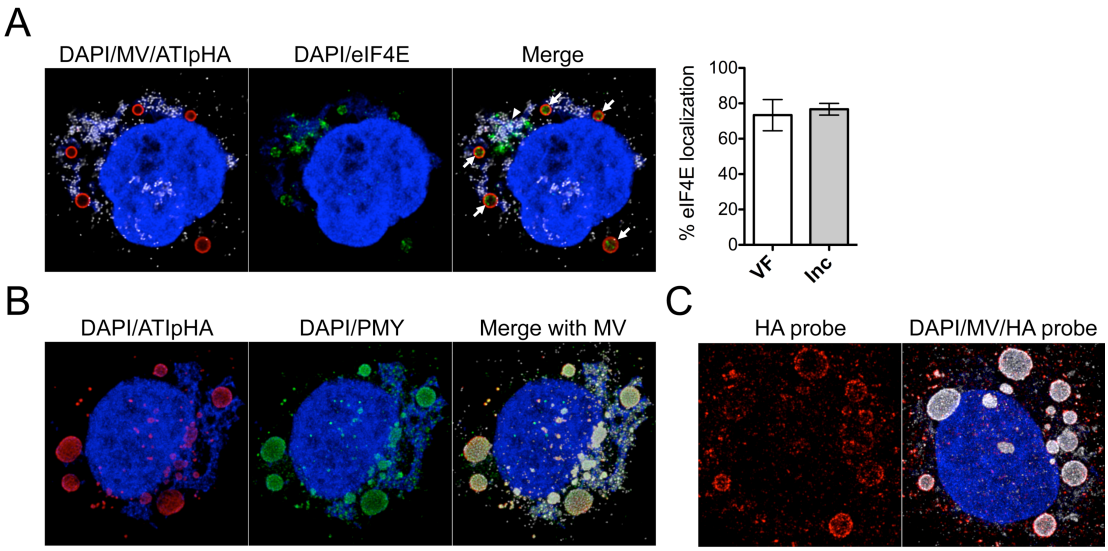

Figure 4-2: Translation and ATIp mRNA localization at ATIs. (A) Images of Hela cells infected with vATI^{+}A26^{+}.A4:YFP and processed 8 hpi for immunostaining using antibodies against eIF4E (green, Alexa-568) and the HA-tag on the ATIp (red, Alexa-647). The nucleus and viral factories (VFs) were visualized by DAPI staining (blue), and MVs were localized using A4-YFP-fluorescence (white). Cells were monitored for localization of eIF4E to VFs (arrowheads) and/or ATIs (arrows). Bar graph shows percent localization of eIF4E to VFs and/or ATIs in ten cells from three independent studies. Error bars, SEM. (B) 3D reconstruction of Z-sections from a vATI^{+}A26^{+}.A4:YFP-infected Hela cell labeled with puromycin (PMY) 22 hpi. Labeled cells were permeabilized with digitonin, fixed, and stained with mouse anti-PMY antibody (green, Alexa-568). ATIs were visualized using rabbit anti-HA antibodies (red, Alexa-647). Blue, DAPI; white, A4p:YFP. (C) *In situ* hybridization of ATIHA mRNA using an Alexa-594 labelled antisense oligonucleotide probe (red) specific to the HA tag. vATI^{+}A26^{+}.A4:YFP-infected Hela cells were fixed 12 hpi when ATIs could be visualized by YFP-fluorescence (white) from embedded MVs. Images are presented as 3D reconstructions. Blue, DAPI.

respectively. Anti-puromycin and anti-HA (ATIp) staining were coincident supporting the conclusion that active translation occurs at ATI (Figure 4-2B).

I next sought to determine whether ATIp mRNA is associated with ATI. I designed an anti-sense oligonucleotide probe conjugated to Alexa-594 specific to the HA tag that was fused to the ATIp and performed fluorescence *in situ* hybridization on cells infected for 12 h with $vATI^{+}A26^{+}$.A4:YFP. ATIs were identified using A4p:YFP fluorescence of embedded MVs. The HA probe labeled ATIs, although some signal was detectable in cytoplasm and coincident with virions (Figure 4-2C). Taken together, the data indicate that ATIp mRNA is translated at inclusion bodies.

4.3.3 Enlargement of ATIs is due to protein synthesis and ATI coalescence.

As the ATIs increased in size, I noted that their number appeared to decrease. To quantify this impression, I measured the diameters of inclusion bodies and determined their number during the course of infection. HeLa cells were infected with $vATI^{+}A26^{+}$.A4:YFP and fixed at 5-, 7-, 9-, and 11 hpi. Inclusion bodies were visualized using anti-HA staining of the fixed cells, which were imaged as Z-stacks. IMARIS Bitplane software was used to measure the diameter of each ATI in the Z-section at which the diameter was greatest. The lowest threshold of ATI diameters was set at 0.3 μm given the limits of resolution; therefore, ATIs that measured less than 0.3 μm in diameter were not scored. The mean size of ATIs increased from 0.66±0.02 to 1.36±0.04 from 5 to 11 hpi, respectively (Figure 4-3A). During the same time, the mean number of ATIs in infected cells decreased (Figure 4-3A). Plotting the distribution of individual ATI diameters provided further insight. At 5 hpi, inclusion body diameters distributed as a sharp peak indicating relative uniformity of sizes

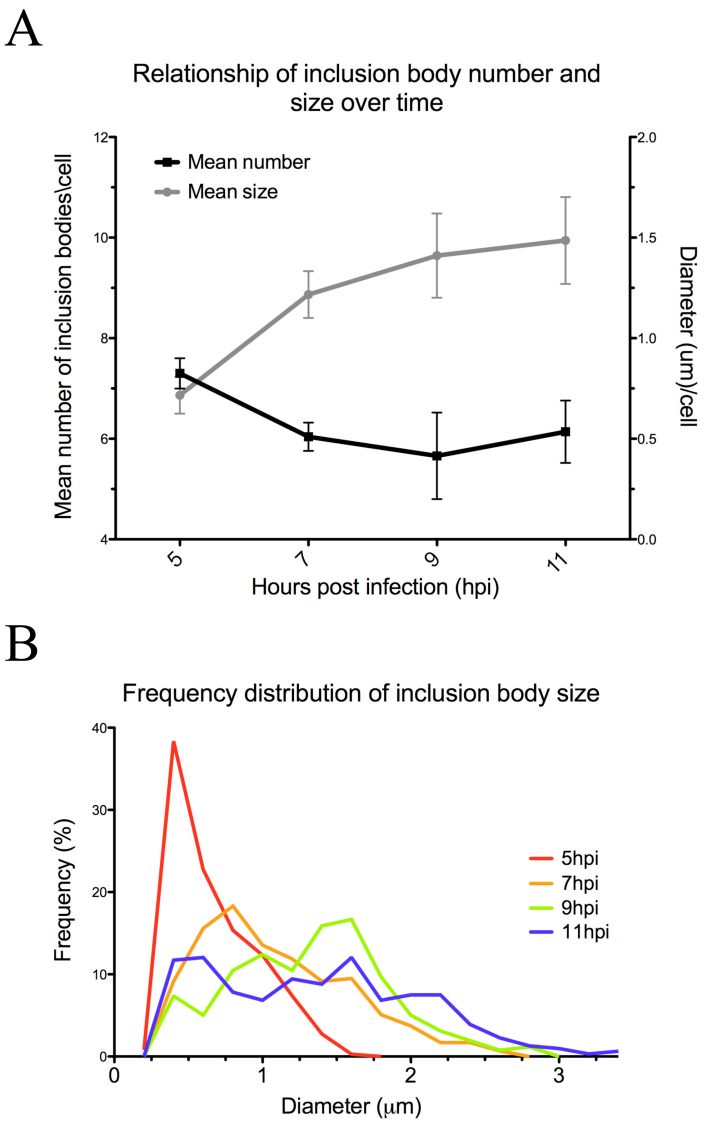

Figure 4-3: Time course of ATI diameter and number. Cells were infected with vATI+A26+ and fixed at 5-, 7-, 9-, and 11 hpi. Twenty five cells in two independent experiments were imaged as Z-stacks by confocal microscopy, and ATI diameters were measured at the largest diameter in section using Imaris Bitplane software. Only ATI $\geq$ 0.3 μm in diameter were enumerated. (A) The mean number of ATIs was compared to the mean size as expressed as diameter (μm) for several time points. Error bars represent the means ± the standard error of the means (SEM) of duplicate experiments. (B) The distribution of the diameters of the all of ATIs monitored from the two experiments were graphed for each time point. 365, 295, 258, and 307 inclusion bodies were measured at 5-, 7-, 9-, and 11 hpi, respectively.

(Figure 4-3B). By 7 hpi, the main peak shifted indicating the population as a whole had larger diameters, however the distribution was more heterogeneous than at 5 hpi. At 9 and 11 hpi, larger diameter ATIs predominated (Figure 4-3B). The data suggested that the increase in ATI size and reduction in number were due to coalescence as well as ATIp synthesis and that new ATIp continued to form.

I next examined the effects of blocking protein synthesis on the formation of ATI. I infected HeLa cells with vATI^{+}A26^{+}.A4:YFP, and after 5 h replaced the medium with either untreated medium or medium containing cycloheximide (CHX), an inhibitor of protein synthesis. Infected cells were incubated in the presence of CHX for an additional 4 and 6 h and then fixed at 9 and 11 hpi, respectively. Anti-HA antibody was used to stain ATI, which were imaged as Z-stacks using confocal microscopy. ATI were enumerated and the diameters measured as described above. Frequency distributions of the diameters at both 9 and 11 hpi in cells incubated without CHX showed a peak shift relative to diameters at 9 and 11 hpi with CHX, demonstrating that new protein synthesis contributes to ATI size (Figure 4-4A, histograms). However, ATI diameters at 9 and 11 hpi from cells incubated with CHX were larger than ATI diameters from cells fixed at 5 hpi or time zero. Thus, ATI increased in size even in the absence of new protein synthesis (Figure 4-4A, histograms). In addition, the average inclusion body number per cell still decreased in the presence of CHX (Figure 4-4A, bar graphs).

I considered that the changes in ATI size and number in the presence of ÇHX might be due to coalescence and require microtubules. Microtubules might also be involved in the transport of ATIp mRNAs from the VFs to the ATIs. Therefore, I

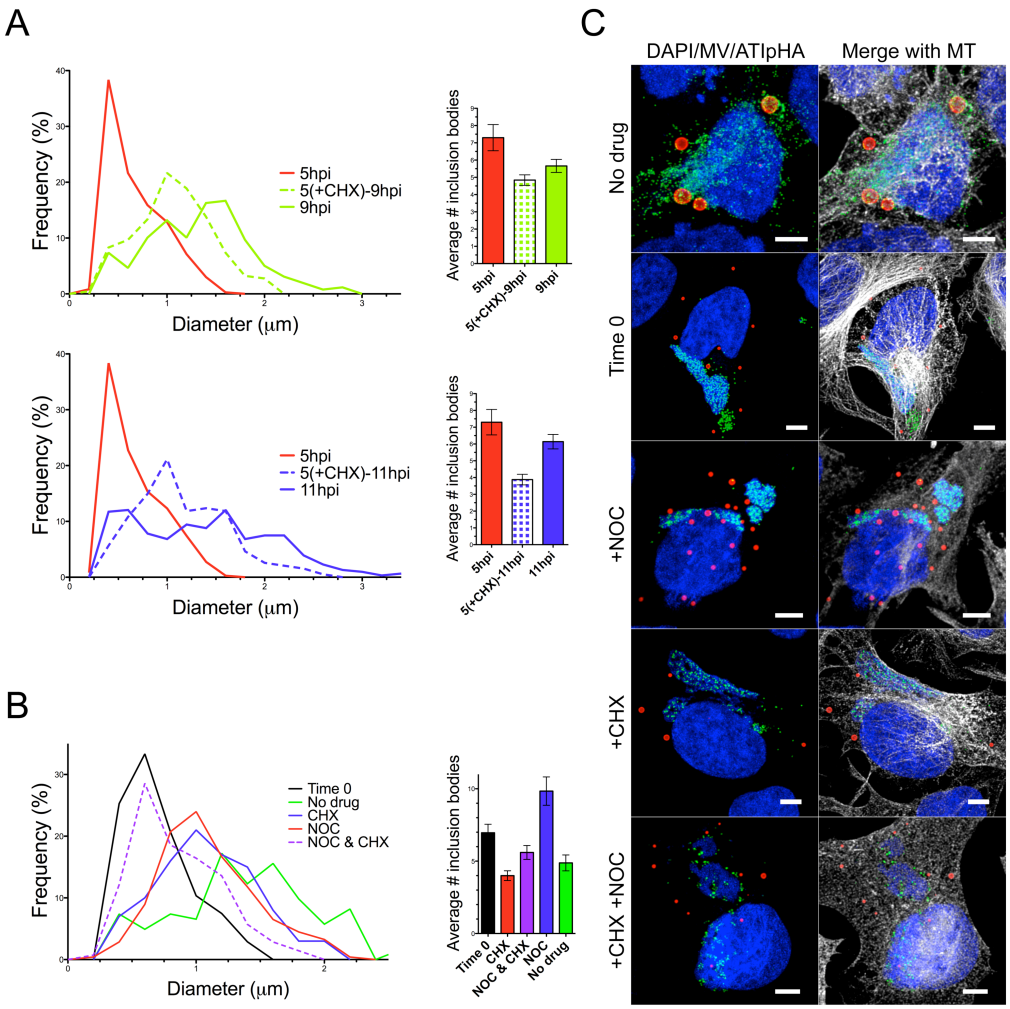

Figure 4-4: Contribution of new protein synthesis and microtubules to ATI size and number. (A) Histograms showing frequency distributions of ATIs (μm) in the presence and absence of cycloheximide (CHX). Bar graphs showing the effects of CHX on average ATI number per cell. Hela cells were infected with vATI^{+}A26^{+}.A4:YFP and ATIs at 5-, 9-, and 11 hpi were compared to ATIs from cells to which 10 μg/mL CHX was added at 5 hpi and fixed at 9 or 11 hpi [5+(CHX)-9 or -11 hpi]. Data represents two separate experiments of 25 cells each. Error bars, SEM. (B) Histogram showing the effects of CHX alone or with 30 μm NOC on ATI size, and bar graph of the effects of CHX and NOC on the average ATI numbere per cell. Drugs were added to vATI^{+}A26^{+}.A4:YFP-infected Hela cells at 4 hpi (Time 0) and fixed at 9 hpi. Error bars, SEM. (C) Representative confocal images from experiments in (B). ATIs were visualized using rabbit anti-HA antibodies (red, Alexa-568), and microtubules (MT) were stained using both mouse anti-α- and mouse anti-β-tubulin antibodies (white, Alexa-647). Blue, DAPI; green, A4p:YFP. Scale bars, 5 μm.

monitored ATI enlargement in the presence of the drug nocodazole, which depolymerizes microtubules. HeLa cells were infected with vATI^{+}A26^{+}.A4:YFP and at 4 hpi, were either fixed (time zero) or the media were replaced with media containing the following: (1) no drug, (2) nocodazole, (3) CHX, or (4) nocodazole plus CHX. The cells were incubated for an additional 5 h and fixed 9 hpi. At 4 hpi, there were numerous, small ATIs (Figure 4-4B and C). The diameters distributed as a narrow peak suggested that ATIs were relatively homogenous in size (Figure 4-4B, histogram). By 9 hpi in medium without drugs, cells contained fewer ATIs (Figure 4-4B, bar graph). ATI diameters distributed into multiple peaks indicating cells contain both small and large inclusion bodies (Figure 4-4B, histogram). In contrast, treatment with nocodazole, which disrupted microtubules (Figure 4-4C), resulted in a one main, relatively narrow peak representing more uniform ATIs of smaller diameter (Figure 4-4B, histogram). In addition, the cells treated with nocodazole contained large numbers of ATIs (Figure 4-4B, bar graph). As described above for Figure 4-4A, there was some increase in ATI size and reduction in number in the presence of CHX (Figure 4-4B). Incubation with both nocodazole and CHX, however, drastically reduced ATI diameters relative to treatment with medium containing no drugs and nocodazole or CHX alone (Figure 4-4B, histogram). The distribution peak resembled the peak of diameters in cells fixed at 4 hpi or time zero. With CHX and nocodazole, the mean number of ATIs per cell was slightly reduced compared to time zero reflecting the inhibition of new ATI formation and prevention of coalescence (Figure 4-4B, bar graph). The data suggest that both new protein synthesis and intact microtubules contribute to ATI formation.

4.3.4 Further evidence for coalescence.

The finding that ATI enlarge in size while the mean number per cell decreases between 5 and 9 hpi suggested that inclusion bodies might be merging together or coalescing by a microtubule-dependent mechanism. Visual evidence for coalescence is shown in a 3D reconstruction and sections of a Z-stack of adjacent ATIs in a HeLa cell infected with vATI^{+}A26^{+}.A4:YFP. The junction between ATIs appears continuous in sections 5-8 (Figure 4-5).

To further test for ATI mixing, I used polyethylene glycol (PEG) to fuse two cell populations expressing differentially tagged ATIps. HeLa cells on cover slips were infected with vATI^{+}A26^{+}.A4:YFP, which expresses an HA-tagged ATIp. I next infected another population of HeLa cells with vA25^{-}A26^{+}, which does not express YFP fused to A4p, and transfected plasmids expressing the ATI gene with an AU1 tag (pATIAU1). At 4 h after transfection, the cells expressing ATIpAU1 were scraped and spinoculated onto the cover slips containing the vATI^{+}A26^{+}.A4:YFP-infected cells and incubated with PEG to induce cell fusion. Following washout of PEG, the fused cells were incubated in medium with or without CHX for 12 h prior to fixation and staining with antibodies against the HA and AU1 epitope tags. Cells were scanned for A4p:YFP expression and AU1 staining to identify fused clusters, and the ATIs were imaged and measured as described for previous experiments.

In cells fixed at 4 hpi immediately following PEG-fusion, representing time zero, anti^{-}HA staining was not coincident with AU1 staining in fused cell clusters (Figure 4-6A). ATIpHA formed smaller inclusion bodies than those composed of ATIpAU1, although both genes were expressed under the endogenous viral promoter.

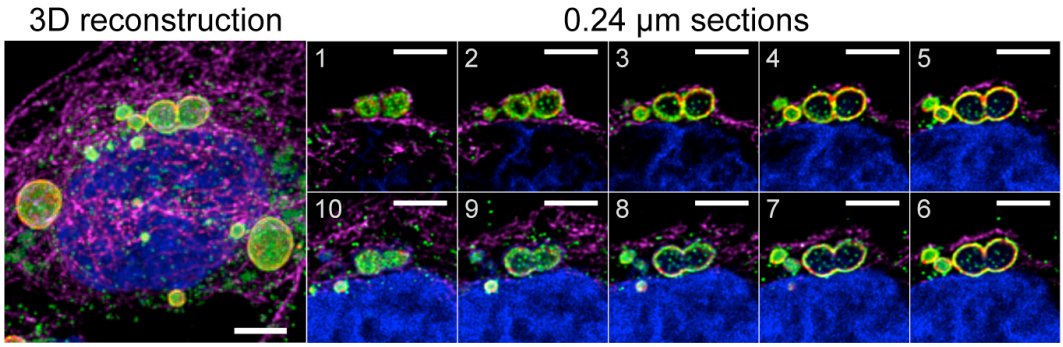

Figure 4-5: Visualization of partially coalesced ATIs. Large panel shows a 3D reconstruction of 0.21 µm Z-sections through a cell containing adjacent ATIs. The optical sections are presented in panels 1-10. Hela cells were fixed after overnight infection with vATI^{+}A26^{+}.A4:YFP, and ATIs were visualized using rabbit anti-HA antibody (red, Alexa-568). Mouse anti-α- and -β-tubulin antibodies were used to stain microtubules (magenta, Alexa-647). Green, A4p:YFP; blue, DAPI. Scale bars, 5 µm.

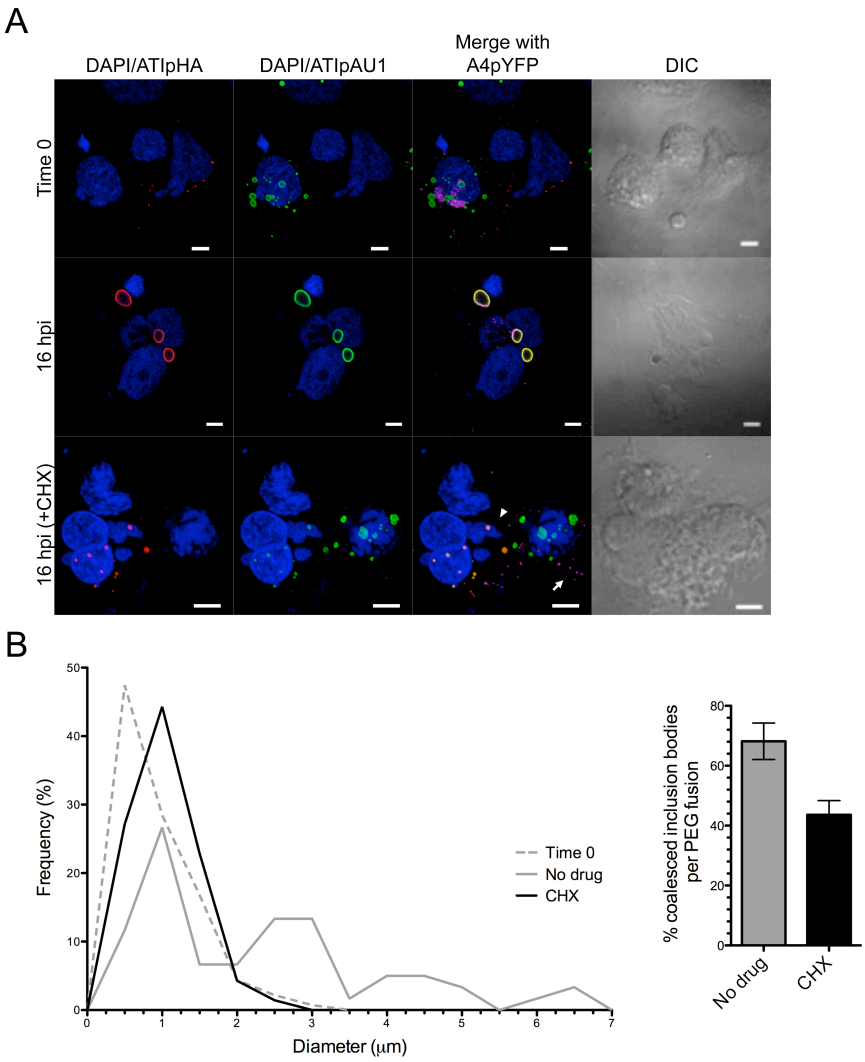

Figure 4-6: Inclusion bodies coalesce in PEG-fused cells. (A) Images of polyethylene glycol (PEG)-fused cells expressing HA-tagged ATI (red, Alexa-647) and AU1-tagged (green, Alexa-568) ATI proteins. $2.5X10^5$ Hela cells were infected with $vATI^-A26^+$ and transfected with plasmids expressing the ATI protein with a C-terminal AU1 tag (pATIAU1). 4 hpt, the cells were scraped and added in the presence of 50% (w/v) PEG to $vATI^+A26^+$.A4:YFP -infected Hela cells on coverslips 4 hpi. Fused cells were either fixed (Time 0) or incubated at 37°C for 12 h in EMEM with or without CHX [16 hpi and 16 hpi (+CHX), respectively]. Time zero and 16 hpi (+CHX) are 3D reconstructions of multiple Z-sections and 16 hpi and DIC images are 0.24 μm Z-sections. Blue, DAPI; magenta, A4p:YFP. Scale bars, 5 μm. (B) Frequency distribution of inclusion body sizes in PEGylated cell clusters. ATIpHA- and ATIpAU1-containing unmerged inclusion bodies were measured for Time 0. Merged inclusion body sizes in the presence or absence of CHX were measured for No drug and CHX, respectively. Bar graph shows the percent of fused cell clusters expressing both ATIpHA and ATIpAU1 that contained merged inclusion bodies in the presence or absence of CHX. Error bars, SEM.

perhaps transfection resulted in a higher level of ATIpAU1 expression. In cell clusters fused and incubated in untreated medium for 16 h, ATIpHA and ATIpAU1 staining was coincident in almost 70% of the cell clusters viewed (Figure 4-6B, bar graph and Figure 4-6C). At 16 h, the ATIs had increased in diameter and showed multiple peaks (Figure 4-6B, histogram). To eliminate the possible addition of ATIp monomers post-cell-fusion, the experiment was also carried out in the presence of CHX. About 44% of cell clusters contained inclusion bodies with coincidental anti-HA and -AU1 staining providing evidence for coalescence (Figure 4-6B, bar graph). The inclusion bodies co-staining for HA and AU1 had smaller diameters than those incubated in the absence of CHX, consistent with the absence of ATIp synthesis in the fused cells (Figure 4-6, histogram).

4.3.5 MVs use microtubules for embedment within inclusion bodies.

I was interested in investigating MV movement to inclusion bodies. To this end, I infected HeLa cells with vATI^{+}A26^{+}.A4:YFP in the presence of 10 μm ST-246 (4-trifluoromethyl-N-(3,3a,4,4a,5,5a,6,6a-octahydro-1,3-dioxo-4,6-etheno-cyclo-prop[f]isoindol-2(1H)-yl)-benzamide) to prevent the wrapping of MVs to form WVs, which traffic on microtubules [126]. Infected cells were imaged at 8 hpi, a time at which I could visually identify ATIs encrusted with YFP-fluorescing MVs. MV-studded ATIs had a characteristically spherical pattern that was easily distinguishable from clusters of virions seen in cells infected with a wild-type VACV expressing A4p:YFP (data not shown). To track MVs I imaged in X, Y, and Z at 1 frame/1.573 s by confocal microscopy. The IMARIS 'Spots' tracking function was used to track

MVs that visibly adhered to inclusion bodies for at least ten time points following contact. MVs moved to inclusion bodies at an average speed of 0.501±0.637 (SEM) (Table 4-1), which is consistent for the transport of MV on microtubules [108]. Particle velocities alternated between fast and slow, but particles did not pause as often as MV observed moving between VFs and sites of wrapping [108].

To further investigate the movement of MVs to ATI, I infected HeLa cells with $vATI^{+}A26^{+}$.A4:YFP in the presence of rifampicin, which does not block inclusion body formation [152, 227] but reversibly prevents virus assembly [224, 238]. After 10 h, the rifampicin was washed out and the cells were incubated either in the presence of cytochalasin D, which inhibits actin polymerization, or nocodazole for an additional 10 h. Cells were fixed and stained for ATIp using anti-HA antibodies, and occlusion was monitored using A4p:YFP fluorescence (Figure 4-7A). The effects of the drugs on microtubules and actin were visualized using both mouse anti-α- and anti-β-tubulin antibody staining and 594-phalloidin staining, respectively (data not shown). ATIs in randomly selected cells in three separate experiments were scored as positive (+) or negative (-) for occlusion (Figure 4-7A). Cytochalasin D caused cells to shrink and have a misshapen appearance but did not have a statistically significant effect on occlusion (Figure 4-7B). Nocodazole, however, decreased occlusion by a statistically significant level (Figure 4-7B), providing additional evidence that microtubules are required for embedment of MVs.

Frame-by-frame measurements[a] for four individual virions

	MV particle					
Frame no.[b]	A	B	C	D		Frame no.[b]
1	2.381	2.089	1.160	0.592	0.932	16
2	1.267	0.450	0.875	0.248	0.603	17
3	0.892	0.200	0.589	0.422	0.634	18
4	0.587	0.253	0.277	0.705	0.541	19
5	0.221	0.467	1.094	0.649	0.310	20
6		0.399	0.234	0.893	0.362	21
7		0.297	1.497	0.618	0.144	22
8			0.456	0.432	0.473	23
9			0.462	0.636	1.065	24
10			1.178	0.490	0.831	25
11			0.677	0.532	0.224	26
12			0.705	0.866	0.957	27
13			0.893	0.868	1.323	28
14			0.393	0.474	0.338	29
15				1.238	0.146	30
No. Time points	5	7	14	25		
Total Time	7.865	11.011	22.022	39.325		
Total distance (μm)	5.348	4.156	10.491	18.547		
Average speed (μm/s)	0.680	0.377	0.476	0.472		

[a]Measurements are displayed in μm; [b]Frame rate equals 1 frame/1.573 s

Table 4-1: Frame-by-frame measurements of four individual virions. 4D (X, Y, Z, and t) live cell imaging of MV trafficking to ATIs. HeLa cells were adsorbed with $vATI^{+}A26^{+}$.A4:YFP for 1 h at room temperature and then incubated for 8 to 10 h in EMEM containing 10 μm ST-246 to prevent WV formation. Particles and occluded inclusion bodies were visualized using YFP fluorescence. Imaris Spots software was used to track MV observed to associate with inclusion bodies for at least ten subsequent time frames post visualized contact.

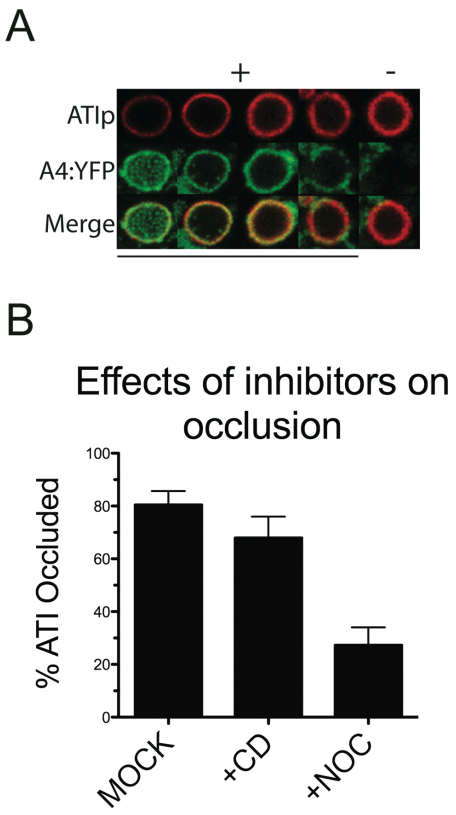

Figure 4-7: Effects of cytoskeletal inhibitors on occlusion. (A) Representative confocal Z-section images of occluded (+) and non-occluded (-) ATIs. Rabbit anti-HA antibodies were used to identify inclusion bodies (red, Alexa-594), and A4p:YFP fluorescence (green) was used to visualize MV particles. (B) Bar graph depicting the effects of cytoskeletal inhibitors on percent occlusion, which is the number of ATIs positive for virion occlusion relative to the total number of ATIs viewed. HeLa cells were infected with $vATI^{+}A26^{+}$.A4:YFP in the presence of 100 μg/ml rifampicin to inhibit virion morphogenesis. After 10 h, the rifampicin was removed and replaced with untreated medium (mock) or medium containing 30 μm nocodazole (NOC) or 1 μm cytochaslasin D (CD) for an additional 10 h. Data represents two separate experiments of 10 randomly selected cells per condition. Error bars, SEM.

4.3.6 A26p is not required for MV movement but contributes to particle velocity.

Previously, I observed that A26p associates with ATIs even in the absence of incorporation into MV particles [227]. Given the requirement of microtubules for occlusion, I next examined whether microtubules are required for A26p localization to ATIs. Cells were infected with vATI^{+}A26^{+}.A4:YFP for 4 h prior to the addition of medium containing nocodazole as not to inhibit movement of entering viral cores and establishment of VFs. At 16 hpi, cells were fixed, permeabilized, and stained using anti-V5 antibodies to localize A26p and anti-HA antibodies to visualize ATIs. Cells were selected at random and ATIs were scored for both MV and A26p localization (Figure 4-8B). As shown previously [227], in the absence of nocodazole A26p strongly colocalized with inclusion bodies and as well as unembedded virions (Figure 4-8A, top panel). Almost 90% of ATIs viewed contained embedded MVs, and A26p localized to almost 100% of the ATIs viewed (Figure 4-8B). Furthermore, nocodazole did not disrupt A26p localization to inclusion bodies as seen in two representative images (Figure 4-8A). While nocodazole greatly disrupted MV embedment, A26p localized to almost 80% of the inclusion bodies studied (Figure 4-8B). A26p was also strongly localized to MV (Figure 4-8B, bottom two panels), which aggregate near factories in the presence of nocodazole.

The above data showing that A26p associates with ATIs in the presence of nocodazole suggest that A26p is not a movement protein for MVs. Nevertheless, I decided to examine MV particle dynamics in the absence of A26p to see if I could detect a defect in movement. HeLa cells were infected with a VACV expressing an HA-tagged A25p and a V5-tagged A26p (vA25^{+}A26^{+}.A4:YFP) or an A26-deletion

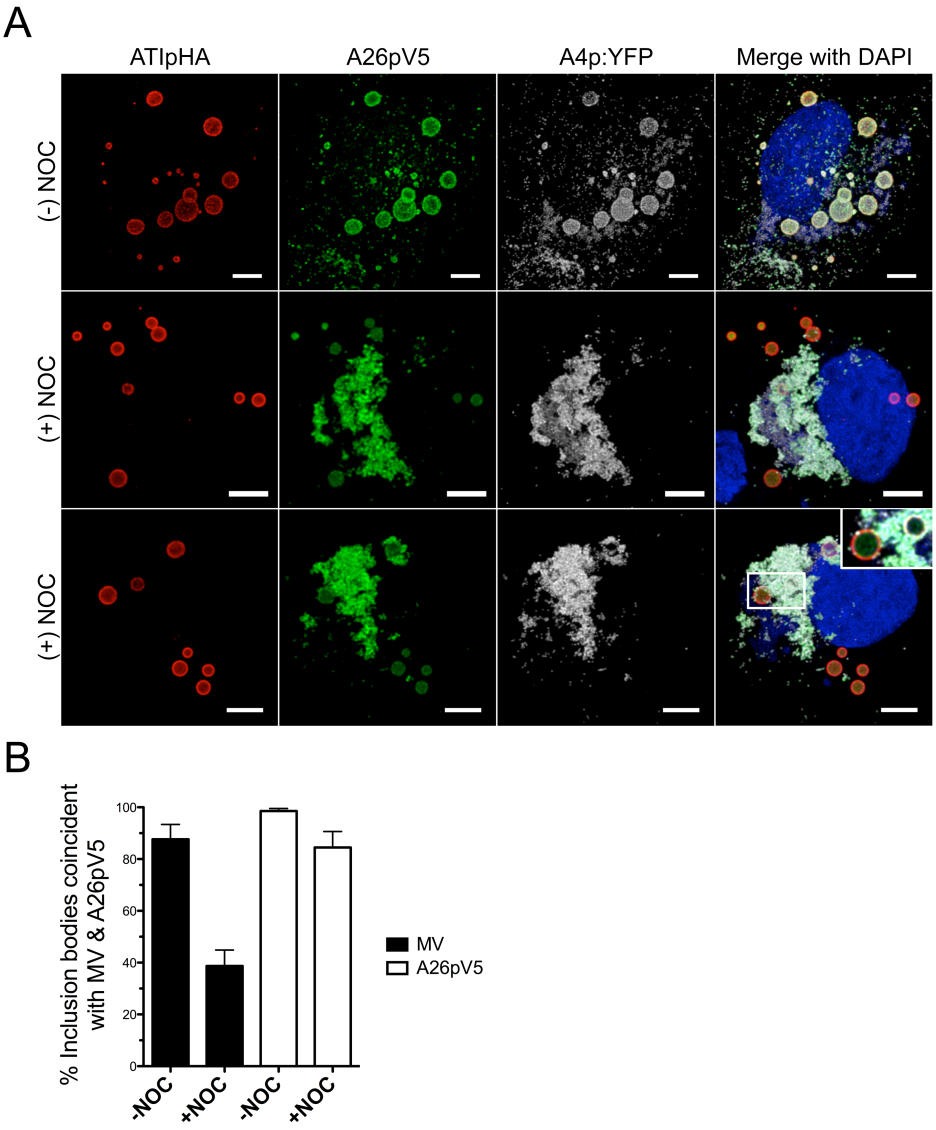

Figure 4-8: Effects of nocodazole on localization of A26p to ATIs. (A) Media from vATI^{+}A26^{+}.A4:YFP-infected Hela cells were replaced 4 hpi with untreated medium (-NOC) or medium containing 30 μm NOC (+NOC) and incubated overnight. ATIs were visualized and enumerated using anti-HA antisera (red, Alexa-647). A26pV5 (green, Alexa-568) and MV (white) were localized using anti-V5 antibodies and A4p:YFP-fluorescence, respectively. Blue, DAPI. Scale bars, 5 μm. (B) Bars represent percent of inclusion bodies positive for MV and A26pV5 localization +/-NOC. Error bars, SEM.

VACV expressing an HA-tagged A25p (vA25^{+}A26^{-}.A4:YFP). Following adsorption, the medium was replaced with medium containing ST-246 to prevent WV formation and movement. At 7 to 8 hpi, MVs were live imaged in 4D using a Leica SP5 inverted confocal microscope with a resonant scanner. Regions of interest in cells distal from factories and from aggregates of virions were visualized to allow tracking of individual particles. Tracking was carried out as described above using IMARIS "Spots" software, and the movement statistics of MV in the presence and absence of A26p were compared. The deletion of A26 did not affect overall track length, however, mean particle speeds were significantly reduced (Figure 4-9A, B).

4.3.7 Occlusion does not sequester MV from wrapping.

In early studies on occlusion, a strain of ectromelia that encoded an intact A26p and did not embed MV into ATIs produced smaller plaques than a strain that encoded an intact A26p and embedded MV within ATIs [157]. Small plaque phenotypes can be indicative of less EV production, suggesting that occlusion sequesters MV from the wrapping pathway. To test this hypothesis, I infected cells with vATI^{+}A26^{+}, vATI^{+}A26^{-}, and vA25^{+}A26^{+} and compared the plaques produced. Inclusion body formation did not alter the plaque phenotype on two different cell types and, furthermore, occlusion did not result in small plaque formation (Figure 4-10A). I also compared EV titers from two cell types infected with vATI^{+}A26^{+}, vATI^{+}A26^{-}, and vA25^{+}A26^{+} and did not find a correlation between EV production and ATI formation or occlusion (Figure 4-10B).

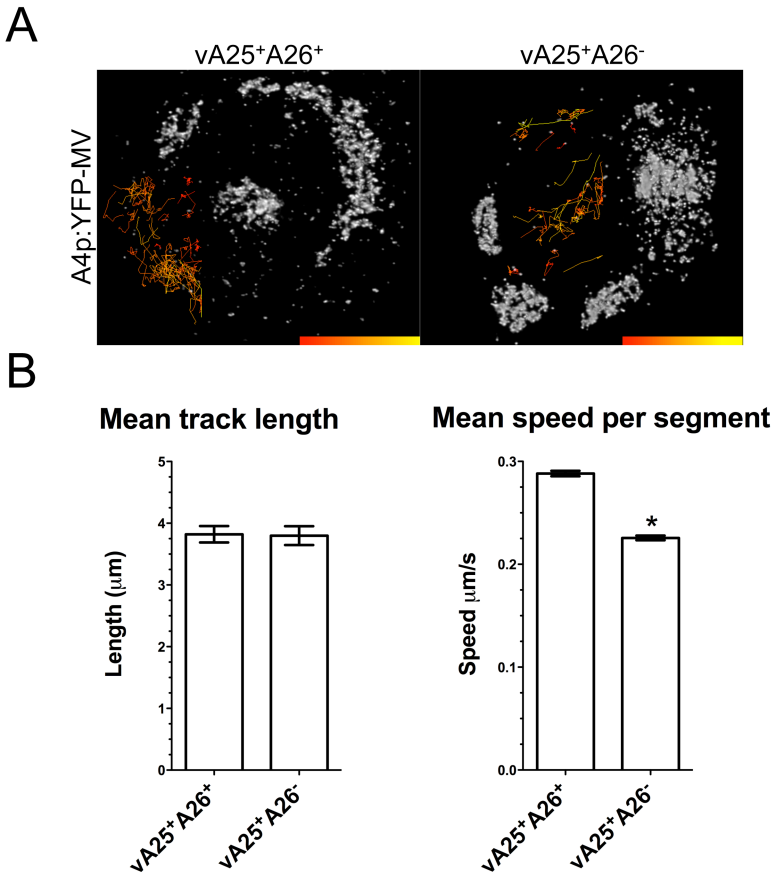

Figure 4-9: MV movement dynamics in the absence of A26p. (A) Images of tracks in two representative cells are shown statistics-coded by color for speed. Hela cells were infected with vA25^{+}A26^{+}- or vA25^{+}A26^{-}-.A4:YFP in media containing 10 μm ST-246 for 7 h, and live imaged at 1.399s/frame in 4D using a Leica SP5 inverted microscope with a resonant scanner. Particles were tracked from regions distal from virion aggregates using Imaris Spots software. Colorbar, low (red) to high (yellow) speeds (μm/s). (B) Bar graphs showing movement dynamics for 1129 and 982 particle tracks in 4 each vA25^{+}A26^{+}- and vA25^{+}A26^{-}-infected cells, respectively. Track length is the total length (μm) of recorded movement for each particle. The mean speed (μm/s) includes the instantaneous velocities for all particles. Asterisk, P-value < 0.0001. Error bars, SEM.

4.4 Discussion

The formation of VFs allows orthopoxviruses to coordinate gene expression, replication, and assembly [79]. Consequently, viral proteins required for late functions are often observed within the VFs. The ATIp is an abundant late protein that assembles into large proteinaceous masses called ATIs that are distributed widely in the cytoplasm of infected cells. In previous confocal microscopy studies, I did not detect ATIp in VFs suggesting either rapid translocation of the protein or an external site of ATIp synthesis. In earlier electron microscopic studies polyribosomes were detected at the periphery of ATI, consistent with the latter interpretation [153]. Since the double stranded DNA genome is located in the VF, these observations suggested a model in which the ATIp mRNA is transported out of the VF and translated at the site of ATI formation. The subcellular localization of cellular mRNAs has been described and there is mounting evidence to indicate the importance of this process [239].

To test an mRNA translocation model, I initially monitored ATIp expression and inclusion body formation over time in cells infected with a recombinant VACV expressing an HA-tagged ATIp. I detected ATIp in small puncti throughout the cytoplasm, rather than in VFs, as early as 3 hpi. With time, these puncti enlarged into typical ATI. ATIp was never observed as diffuse cytoplasmic staining, unassociated with inclusion bodies. To assess whether ATI mRNA is translated at ATIs, I carried out three additional experiments. First, I demonstrated that the translation initiation factor, eIF4E, was associated with ATIs as well as VFs. Second, a puromycin-immunodetection assay demonstrated that active translation occurs at the ATI. Finally, using FISH, I identified the ATIp mRNA associated with ATIs. To our

knowledge, this is the first demonstration of an orthopoxvirus late mRNA that is transported and translated at specific sites outside of the VF. Presumably the ATIp monomers self assemble very rapidly into insoluble aggregates. For this reason, I imagine that synthesis of ATIp in the VF would be detrimental to other viral processes that take place there.

To further study ATI formation, I performed quantitative analyses on the diameters and mean number of ATIs per cell over the course of infection. I found that the mean ATI diameter increased in size from 5 to 11 hpi, whereas the number of ATIs decreased. Frequency distributions of ATI diameters revealed that at 5 and 7 hpi, there was relative uniformity of ATI size. By 9 and 11 hpi, however, there existed populations of small, intermediate, and large ATIs. Treatment with CHX prevented the emergence of small ATIs at 9 and 11 hpi demonstrating that inclusion bodies continuously form throughout infection. More interesting, however, was the finding that the size of ATIs increased and the number decreased in the presence of CHX, though to a lesser extent than in the absence of the drug. This led us to consider that that individual ATI were merging or coalescing. This finding was supported by optical sectioning of adjacent ATIs, which in some cases showed a continuum between the bodies. To test directly for inclusion body coalescence, PEG was used to fuse one cell population expressing an HA-tagged ATIp with another cell population expressing an AU1-tagged ATIp. I found that ATI stained for both tags even in the presence of CHX, which was added to prevent ATIp monomers synthesized post-cell fusion. Anti-HA and -AU1 co-staining was uniform versus patchwork suggesting that coalescence results in content mixing rather than just aggregation. In view of the large

size of the ATIs, I suspected that the cytoskeleton might be required for their merger. I found that the decrease in ATIs was inhibited by nocodazole, implicating microtubules in the process.

I was also interested in how MVs localize to the ATI. MV movement to ATI was investigated using a confocal microscope for live imaging at about 1.57 frames/s. Cells were infected with a recombinant VACV expressing the CPXV ATI and the A4 core protein fused to YFP. ST-246, an inhibitor of MV wrapping, was used to prevent movement of WVs on microtubules, which would interfere with our confocal microscopy analysis. MV movement was monitored in four dimensions with Z-stacks that were typically about 4 μm. Some MVs were observed to associate and then disassociate and move away from inclusion bodies. The mean speeds of 4 indivdually tracked MVs were similar to mean speeds seen for MV movement to sites of wrapping along microtubules [108]. To test whether microtubules are required for occlusion, I monitored inclusion bodies for embedment in the presence of cytochalasin D and nocodazole, which are drugs that disrupt actin and microtubules, respectively. I found that while cytochalasin D did not disrupt occlusion, nocodazole drastically reduced the frequency of embedment.

To date, the viral protein(s) required for MV movement to sites of wrapping have not been identified. The A27 protein was initially implicated as an MV-movement factor [240], but live imaging studies showed that MV of an A27-deletion VACV could move bidirectionally between VFs and sites of wrapping. In the absence of A27p, A26p is unstable [108], suggesting that A26p is not required for MV movement. Nevertheless, A26p has been implicated as a potential movement factor

during occlusion [160]. The primary observation supporting this hypothesis came from studies using electron microscopy that showed there exits a visible boundary between MV and inclusion bodies in cells infected with viruses expressing ATIp and a non-functional A26p [160]. Our finding that A26p is capable of associating with inclusion bodies in the absence of virion-anchoring or assembly lent support to the idea that A26p might function as a movement protein. Because occlusion requires microtubules, I rationalized that if A26p might also use microtubules to actively transport to inclusion bodies. However, although the addition of nocodazole to the medium of infected cells abrogated occlusion, A26 localization to inclusion bodies was not disrupted.

To further test whether A26p is required for MV movement I compared the particle dynamics of an A26-deletion VACV with a VACV encoding an intact A26p using live imaging. Cells were infected in the presence of ST-246 to arrest WV movement, and particle movement over time was recorded. The number of particles moving in cells infected with the A26 deletion VACV appeared similar to the number moving in cells infected with wild-type VACV. The deletion of A26 also did not affect total track length. However, MV lacking A26p moved with statistically slower velocities. One possibility is that within cells there exist two populations of MV. One population lacks A26p and moves to sites of wrapping to become EV, and the other population has A26p and moves to inclusion bodies using a different motor with greater velocities.

In early experiments, recombinant strains of CPXV that formed inclusion bodies but did not embed MV into them formed larger plaques than strains that

embedded MV in infected cell monolayers [225]. A large plaque phenotype is indicative of a greater production of EV, and thus the data suggested that MV were sequestered in inclusion bodies from the wrapping pathway. I compared VACV expressing the ATI protein in the presence or absence of the occlusion factor, A26p, and did not see a difference in plaque phenotype or EV production. It is therefore likely that the phenotypic differences in plaque sizes observed previously among the recombinant CPVX were due to some other genetic differences among the viruses tested.

Chapter 5: Conclusions and future directions

5.1 Incorporation of A26p into MV

The A26 protein was of especial interest because it is one of only three known MV-specific proteins [145, 241]. A26p lacks a transmembrane domain, and prior to this study nothing was known about how it becomes incorporated into the MV particle. The instability of A26p in the absence of A27p led us to investigate a potential interaction between the two proteins. I found that A26 forms a disulfide-bonded complex with A27p and this interaction is required for the stability of A26p. The A26p-A27p interaction depends on a C-terminal segment of A26p with 45% amino acid identity to a region within the A27 protein. The region of homology between the two proteins contains two adjacent cysteine residues that were subsequently found by another group to be required for the A26p-A27p interaction [242]. A27p not only confers stability to A26p but also incorporates it into the viral membrane. A27p is anchored to the membrane by a transmembrane protein, A17p [123], and I found that A26p interacts with A17p indirectly through the A27p. The A27p-A17p complex was thus determined as the anchor for the localization of A26p on the surfaces of MVs. One interesting question remaining is the mechanism by which A26p is excluded from EV/CEVs.

5.2 A26p-mediated MV embedment into ATIs

Interestingly, while investigating the mechanism of A26p incorporation into MVs, I discovered that the A26p-A27p-A17p complex interacted with the A25 protein. VACV A25p is also an MV-specific protein [145]. Although the function of A25p in VACV is not known, the A25p homolog, ATIp, forms inclusion bodies. Some orthopoxviruses, e.g. cowpox and ectromelia viruses, form large, discrete cytoplasmic inclusions within which MVs are embedded by a process called occlusion. These inclusions are composed of aggregates of the ATIp, and the ATIp homolog, A25p, is truncated in orthopoxviruses such as VACV that fail to form inclusions [151, 154, 232]. Occlusion requires an intact A26p, and although VACV does not form inclusion bodies it encodes a functional A26p [160]. The role of A26p in the embedment of MV into ATIs had not been demonstrated prior to this study. As discussed above, I showed that A26p is anchored to the MV membrane through disulfide bonding with the A27 protein [219, 220], which is in turn tethered to the MV membrane through interactions with the A17 transmembrane protein [219]. Our discovery that the VACV multiprotein complex A26p-A27p-A17p interacted with A25p suggested that it might similarly interact with the intact ATIp, thereby embeding MVs in inclusion bodies.

Given that VACV is the most characterized of the orthopoxviruses, I investigated the requirements for occlusion by expressing the CPXV full-length ATIp in the VACV background. I found that restoration of the full-length ATI gene was sufficient for VACV inclusion formation and the occlusion of MVs. A26p was present in inclusions even when virion assembly was inhibited, suggesting a direct

interaction of A26p with ATIp. Analysis of a panel of ATIp mutants indicated that the N-terminal domain was required for the interaction with A26p and occlusion and the C-terminal repeat region was required for inclusion formation. Interestingly, the N-terminus of A25p is conserved among orthopoxviruses expressing truncated ATIps. The conservation of the N-terminus suggests an additional function for the A25p and the A25p-A26p interaction in the virus life cycle. The recent report that A26p and A25p cause MV to preferentially enter through fusion within endosomes by suppressing fusion at the plasma membrane might be one reason for this conservation [243]. The C-terminal truncation of VACV, VARV, and MPXV ATIp homologs suggests that the formation of ATIs might be detrimental for these viruses.

After determining that A26p interacts with ATIp and that this interaction is necessary for occlusion I investigated the requirement of A26p-anchoring to the MV particle for occlusion. I found that A27p was not needed for association of A26p with ATIp, but was indispensable for occlusion. In addition, the C-terminal domain of A26p, which mediates A26p-A27p interactions [20, 219, 220], was necessary but insufficient for occlusion. The N-terminus of the A26 protein localized to ATIs but as shown previously did not associate with A27p or MV. A26p therefore has two function domains in occlusion: the N-terminus mediates interactions with ATIp and the C-terminus attaches A26p to the MV membrane. Taken together, the data suggest a model for occlusion in which A26p has a bridging role between ATIp and A27p, and A27p provides a link to the MV membrane.

5.3 ATI mRNA transport and ATI enlargement

While studying occlusion, I did not see unincorporated ATIp localized to VFs, which prompted us to investigate inclusion body formation. Inclusion body formation was previously monitored using electron microscopy and phase contrast microscopy. Imaging ATIs formed by our recombinant VACV expressing an HA-tagged ATIp and a core protein (A4p) fused to YFP by immunofluorescence confocal microscopy achieves greater sensitivity and resolution than phase contrast microscopy, and the reconstruction of optical Z-sections gave us a 3D perspective not provided by electron microscopy.

It was reported previously that ATIs form late in infection at ~9-12 hpi [151, 157, 225], but time course experiments of ATI formation and ATIp synthesis revealed that ATIs are dispersed throughout the cytoplasm as early as 3 hpi. Additionally, I did not see unincorporated ATIp either in the VFs or the cytoplasm of infected cells. Because late transcription occurs in the VF, this suggested to us that ATIp is either shuttled rapidly out of VFs or that the ATI mRNA is shuttled out of the VF for translation in the cytoplasm at sites of inclusion body nucleation. Supporting the latter scenario, previous studies demonstrated the presence of ribosomes at ATI peripheries [153]. I localized the translation initiation factor eIF4E, which is also recruited to VFs, as well as actively translating ribosomes to the peripheries of inclusion bodies. Using FISH, I furthermore determined that the ATI mRNA is associated at the peripheries of ATIs. To our knowledge, this is the first report of an orthopoxvirus late mRNA that is translated out of the VF.

Orthopoxviruses regulate translation of ATI mRNAs by transporting them out of the VF to sites within the cytoplasm. A reason for the translation of ATIp outside of VFs could be the hydrophobic properties of the protein, which cause it to assemble into insoluble aggregates that might perturb other processes in the VF. Given the abundance of ATIp, perhaps ATI mRNA is segregated to prevent depletion of resources necessary for the translation of other late viral proteins. Additionally, perhaps the polyribosomes at the ATI periphery function in amplifying translation of the ATI mRNA message for rapid assembly.

An exciting future project would be to study the requirements of ATI mRNA transport from the VFs to sites in the cytoplasm. To this end, I could use the bacteriophage MS2-GFP system. The coat protein is fused to GFP (MS2-GFP) and selectively binds hairpin RNAs. These hairpins can be engineered into a gene of interest and coexpressed with MS2-GFP in cells for live tracking of individual mRNAs. It would be of interest to demonstrate directly the transport of ATI mRNA from VFs to the cytoplasm. This system could also be used to define ATI mRNA sequences and host factors involved in the transport of ATI mRNA. It is likely the ATI mRNA contains a 'cis-acting element' or zipcode recognized by mRNA binding proteins for transport out of the VF [244]. Typically, zipcodes are found in the 3' and 5' UTRs of mRNAs. One method to identify zipcodes is by using antisense oligonucleotides targeting specific sequences within the mRNA and then to look for the mislocalization of those mRNAs.

It would be interesting to identify the RNA binding partners and motor proteins required for ATI mRNA transport. Presumably, the RNA-binding proteins

that shuttle ATI mRNAs out of the VF use motor proteins to move along the cytoskeleton to specific sites in the cytoplasm [245]. To identify the motor protein that transports ATI mRNAs, one could use dominant negative inhibitors of motor proteins and look for mislocalization of the ATI mRNA. Interestingly, in pilot experiments studying the effects of kinesin-1 and dynein dominant negative inhibitors on occlusion, I noted that the kinesin-1 inhibitor, which competes with cargo for kinesin-1 binding, localized within inclusion bodies but the dynein inhibitor did not (data not shown).

The time course of ATI formation revealed that ATIs enlarge over time as previously reported, and enlargement requires new protein synthesis. Interestingly, enlargement of ATIs corresponded to a decrease in ATI number in the presence of CHX. This suggested that ATIs were enlarging by merging together or coalescing. Supporting this notion, I observed continua between adjacent ATIs by fixed cell microscopy. Pegylation experiments fusing separate cell populations each expressing an ATIp with a different tag revealed ATIs expressing both tags in multinucleated cell clusters even in the presence of CHX. The staining of the tags was uniform rather than patchwork suggesting that ATI coalescence results in content mixing between ATIs rather than aggregation. Although the matrices of ATIs are selective, content mixing among ATIs suggests that they are also fluid. The role of coalescence is not clear, but I observed by live imaging that MVs appeared to be transferred between two coalescing inclusion bodies.

Given the size of ATIs, it was likely that the cytoskeleton is required for their fusion. Experiments showed that microtubules were required for the merging of ATIs,

which suggests that ATIs are motile bodies. ATIs appeared by live imaging as dynamic structures that exhibited a rolling motion. The movement of large protein aggregates along microtubules is reminiscent of the formation of cellular aggresomes. Protein aggregates of misfolded proteins between ~4 and 50 nm use dynein motors for retrograde movement along microtubules to the microtubule-organizing center (MTOC) where they coalesce and become surrounded by vimentin cages that immobilize them for proteasome-mediated degradation [246]. Interestingly, vimentin collapses to form cages around VFs during VACV infections [247]. I did not, however, observe vimentin cages surrounding ATIs (data not shown).

5.4 Role of A26p in MV movement and wrapping

Electron micrographs from a previous study showed small masses of granular material thought to be newly forming ATIs associated with MVs and polyribosomes. This observation led authors to suggest that MVs might nucleate the formation of ATIs [153]. Contradictory to this notion, ATIs still form when A26p is truncated and MVs do not become embedded. Additionally, ATIs formed in the presence of the drug rifampicin, which blocks virion assembly but not late protein synthesis, and ATIs were dispersed in the cytoplasm by 3 hpi, prior to MV assembly and the subsequent movement out of the VFs. Since ATIs do not nucleate around MVs, it suggested MVs must localize to ATIs for embedment. Given the distance of ATIs from VFs and the large size of MV (~360 X 270 X 250 nm), it was likely that the localization of MV to ATIs required active transport along the cytoskeleton. Using drugs that perturb the actin and microtubule networks, I found that MVs use

microtubules for embedment within inclusion bodies. I also observed using live imaging that the MVs moved to inclusion bodies at speeds similar to those observed in the movement of MVs to sites of wrapping [108].

McKelvey et al. proposed that A26p might be a movement protein that transports MV from VFs to ATIs during occlusion [160]. In the absence of intact A26p, electron microscopy reveals that there exists a spatial separation between MVs and ATIs [160]. This suggests MVs that do not have intact A26p do not move ATIs. Further support for a role of A26p in MV movement to ATIs came from our finding that A26p associates with inclusion bodies in the absence of virus assembly or anchoring to the MV particle. This finding implied that A26p might move along microtubules independently from other viral proteins. Because microtubules were required for occlusion, I investigated the dependence of microtubules for A26p localization. I found that A26p associated with ATIs even in the presence of nocodazole suggesting that A26p localizes to ATIs by passive diffusion.

Our finding that A26p is unstable in the absence of A27p, suggested that A26p is dispensable for MV movement. The A27 protein was initially implicated as an MV-movement factor [240], but live imaging studies showed that MV of an A27-deletion VACV could move bidirectionally between VFs and sites of wrapping. Nevertheless, although A26p does not move independently of the virus, it is possible that A26p might contribute to movement. For example, the VACV F12 and A36 proteins cooperate in the egress of WVs. F12p binds the kinesin-1 motor for movement along microtubules but requires A36p for anchoring to the WV membrane and regulating its dissociation from motors [136, 137]. To further assess a role for

A26p in MV movement, I examined MV particle dynamics in the absence of A26p to see if I could detect a defect in movement. Using live imaging, I compared the movement dynamics of wild-type VACV and A26 deletion VACV MVs and found that a similar number of particles moved for each virus. However, interestingly, MVs lacking A26p moved with statistically slower velocities.

The significance of the defect in MV speeds in the absence of A26p is unclear. I could speculate that within cells there exist two populations of MVs. One population lacks A26p and moves to sites of wrapping to become EVs, and the other population has A26p and moves to inclusion bodies using a different motor that moves with greater velocities. Analogously, VACV MVs lacking A26p would move to sites of wrapping, whereas, MVs containing A26p would move away from sites of wrapping for retention in the cell until lysis. The specificity of A26p for MV membranes makes it an attractive candidate for the negative regulation of wrapping either as a directional movement protein or in some other capacity. Toward the latter, it is possible that MVs containing A26p move to sites of wrapping but are excluded from the wrapping pathway. This is plausible since A27 is required for EV formation [248], and A26p interacts with A27p but is excluded from EVs. It has been suggested that A27p mediates wrapping by interacting with either a viral protein such as F13p or with a host protein at the wrapping proteins for wrapping. The finding that an ECTV strain that embeds MVs within ATIs forms smaller plaques than a strain that encodes a truncated A26p and does not embed MVs within ATIs suggested that occlusion might represent an oppositional fate to wrapping and further implicated A26p in the negative regulation of wrapping [157].

Taken together, the potential role of A26p in MV movement, the exclusion of A26p from wrapped particles, and its association with the wrapping protein, A27p, suggested A26p might negatively regulate wrapping. However, the deletion of VACV A26L did not affect the plaque phenotype in two cell lines. Moreover, when I titered the EVs released in the cell media, I did not detect an increase in their production. Similarly, recombinant VACVs expressing the ATIp in the presence of A26p did not produce smaller plaques than recombinant VACVs expressing ATIp but with a deleted A26L gene. The simplest interpretation is that A26p does not have a role in the differentiation of MVs into EVs either as a movement factor or by some other mechanism. However, I did not measure the production of WVs in the absence of A26p, and it is possible that more WVs were produced but not released as EVs. EV production could be limited by other factors such as the availability of wrapping membranes, viral proteins, and other host proteins required for egress and release. I did find a reduction in EV production when A26p was overexpressed, but this was correlated with a reduction in the expression of other viral proteins, including A27p, and was therefore difficult to interpret (our unpublished data).

An interesting question is how A26p becomes excluded from EV/CEVs. The A27p-A17p complex is found in MV, WV, and EV/CEV particles, however A26p is only found in MVs. There are three main scenarios of exclusion that seem likely: (1) MVs containing A26p do not move to sites of wrapping, (2) MVs containing A26p move to sites of wrapping but do not become wrapped, or (3) A26p is removed from MVs at sites of wrapping. It is unknown whether A26p is present at sites of wrapping, which would eliminate the first scenerio and implicate the latter two, but it is likely

that were A26p present at sites of wrapping it would be highly transitory and difficult to detect by methods such as immunogold labeling electron microscopy or fixed cell microscopy. If MV containing A26p moved to sites of wrapping and failed to wrap as is proposed in scenario two, it is unlikely that they would accumulate because MVs have been observed to move bidirectionally between VFs and sites of wrapping. In the third scenario, A26p would likely not be detectable because it is unstable when not associated with the A27 protein. Therefore, the most plausible method would be to monitor the localization of MV containing A26p relative to sites of wrapping using live imaging confocal microscopy.

The wrapping membrane protein, B5p, is functional as a GFP fusion protein [131, 249]. Were A26p to be functional as a fusion protein, I could simultaneously track the core (A4p:YFP), A26p (A26p:mCherry), and B5p (B5p:CFP) while using a DNA marker to monitor for coincidence at VFs and sites of wrapping. This technique could also be applied to further investigate a role for A26p in MV movement. I could not only localize MVs containing A26p but also compare the particle dynamics of MVs that have or do not have A26p. In general, the generation of a recombinant VACV expressing an A26p:fluorescent protein would be effective tool in other studies allowing the specific localization of MVs.

Bibliography

1. Iyer, L.M., L. Aravind, and E.V. Koonin, *Common origin of four diverse families of large eukaryotic DNA viruses.* J Virol, 2001. **75**(23): p. 11720-34.
2. Iyer, L.M., et al., *Evolutionary genomics of nucleo-cytoplasmic large DNA viruses.* Virus Res, 2006. **117**(1): p. 156-84.
3. Koonin, E.V. and N. Yutin, *Origin and evolution of eukaryotic large nucleo-cytoplasmic DNA viruses.* Intervirology. **53**(5): p. 284-92.
4. Fauquet, C., International Committee on Taxonomy of Viruses., and International Union of Microbiological Societies. Virology Division., *Virus taxonomy : classification and nomenclature of viruses : eighth report of the International Committee on the Taxonomy of Viruses*. 2005, San Diego, Calif. ; London: Elsevier Academic Press. viii, 1259 p.
5. Moss, B., *Poxviridae: The viruses and their replication.* Fields Virology, 2007. **2**: p. 2905-2946.
6. Di Giulio, D.B. and P.B. Eckburg, *Human monkeypox: an emerging zoonosis.* Lancet Infect Dis, 2004. **4**(1): p. 15-25.
7. Roos, N., et al., *A novel immunogold cryoelectron microscopic approach to investigate the structure of the intracellular and extracellular forms of vaccinia virus.* EMBO Journal, 1996. **15**(10): p. 2343-2355.
8. Griffiths, G., et al., *Structure and assembly of intracellular mature vaccinia virus: isolated-particle analysis.* J Virol, 2001. **75**(22): p. 11034-55.
9. Cyrklaff, M., et al., *Cryo-electron tomography of vaccinia virus.* Proceedings of the National Academy of Sciences of the United States of America, 2005. **102**(8): p. 2772-2777.
10. Zwartouw, H.T., *The chemical composition of vaccinia virus.* J. Gen. Microbiol., 1964. **34**: p. 115-123.
11. Goebel, S.J., et al., *The complete DNA sequence of vaccinia virus.* Virology, 1990. **179**(1): p. 247-66, 517-63.
12. Garon, C.F., E. Barbosa, and B. Moss, *Visualization of an inverted terminal repetition in vaccinia virus DNA.* Proc Natl Acad Sci U S A, 1978. **75**(10): p. 4863-7.
13. Baroudy, B.M., S. Venkatesan, and B. Moss, *Structure and replication of vaccinia virus telomeres.* Cold Spring Harb Symp Quant Biol, 1983. **47 Pt 2**: p. 723-9.
14. Baroudy, B.M., S. Venkatesan, and B. Moss, *Incompletely base-paired flip-flop terminal loops link the two DNA strands of the vaccinia virus genome into one uninterrupted polynucleotide chain.* Cell, 1982. **28**(2): p. 315-24.
15. McCarron, R.J., et al., *Structure of vaccinia DNA: analysis of the viral genome by restriction endonucleases.* Virology, 1978. **86**(1): p. 88-101.
16. Law, M., et al., *Ligand-induced and nonfusogenic dissolution of a viral membrane.* Proc Natl Acad Sci U S A, 2006. **103**(15): p. 5989-94.
17. Chung, C.S., et al., *A27L protein mediates vaccinia virus interaction with cell surface heparan sulfate.* J Virol, 1998. **72**(2): p. 1577-85.

18. Hsiao, J.C., C.S. Chung, and W. Chang, *Vaccinia virus envelope D8L protein binds to cell surface chondroitin sulfate and mediates the adsorption of intracellular mature virions to cells.* J Virol, 1999. **73**(10): p. 8750-61.
19. Lin, C.L., et al., *Vaccinia virus envelope H3L protein binds to cell surface heparan sulfate and is important for intracellular mature virion morphogenesis and virus infection in vitro and in vivo.* J Virol, 2000. **74**(7): p. 3353-65.
20. Chiu, W.-L., et al., *Vaccinia virus 4c(A26L) protein on intracellular mature virus binds to the extracellular cellular matrix laminin.* Journal of Virology, 2007. **81**(5): p. 2149-2157.
21. Carter, G.C., et al., *Entry of the vaccinia virus intracellular mature virion and its interactions with glycosaminoglycans.* J Gen Virol, 2005. **86**(Pt 5): p. 1279-90.
22. Huang, C.Y., et al., *A novel cellular protein, VPEF, facilitates vaccinia virus penetration into HeLa cells through fluid phase endocytosis.* J Virol, 2008. **82**(16): p. 7988-99.
23. Townsley, A.C., et al., *Vaccinia virus entry into cells via a low-pH-dependent endosomal pathway.* J Virol, 2006. **80**(18): p. 8899-908.
24. Mercer, J. and A. Helenius, *Vaccinia virus uses macropinocytosis and apoptotic mimicry to enter host cells.* Science, 2008. **320**(5875): p. 531-5.
25. Senkevich, T.G., et al., *Poxvirus multiprotein entry-fusion complex.* Proc Natl Acad Sci U S A, 2005. **102**(51): p. 18572-7.
26. Ojeda, S., T.G. Senkevich, and B. Moss, *Entry of vaccinia virus and cell-cell fusion require a highly conserved cysteine-rich membrane protein encoded by the A16L gene.* J Virol, 2006. **80**(1): p. 51-61.
27. Ojeda, S., A. Domi, and B. Moss, *Vaccinia virus G9 protein is an essential component of the poxvirus entry-fusion complex.* J Virol, 2006. **80**(19): p. 9822-30.
28. Townsley, A.C., T.G. Senkevich, and B. Moss, *Vaccinia virus A21 virion membrane protein is required for cell entry and fusion.* J Virol, 2005. **79**(15): p. 9458-69.
29. Senkevich, T.G., B.M. Ward, and B. Moss, *Vaccinia virus entry into cells is dependent on a virion surface protein encoded by the A28L gene.* J Virol, 2004. **78**(5): p. 2357-66.
30. Izmailyan, R.A., et al., *The envelope G3L protein is essential for entry of vaccinia virus into host cells.* J Virol, 2006. **80**(17): p. 8402-10.
31. Senkevich, T.G. and B. Moss, *Vaccinia virus H2 protein is an essential component of a complex involved in virus entry and cell-cell fusion.* J Virol, 2005. **79**(8): p. 4744-54.
32. Townsley, A.C., T.G. Senkevich, and B. Moss, *The product of the vaccinia virus L5R gene is a fourth membrane protein encoded by all poxviruses that is required for cell entry and cell-cell fusion.* J Virol, 2005. **79**(17): p. 10988-98.
33. Satheshkumar, P.S. and B. Moss, *Characterization of a newly identified 35-amino-acid component of the vaccinia virus entry/fusion complex conserved in all chordopoxviruses.* J Virol, 2009. **83**(24): p. 12822-32.

34. Bisht, H., A.S. Weisberg, and B. Moss, *Vaccinia virus l1 protein is required for cell entry and membrane fusion.* J Virol, 2008. **82**(17): p. 8687-94.
35. Brown, E., T.G. Senkevich, and B. Moss, *Vaccinia virus F9 virion membrane protein is required for entry but not virus assembly, in contrast to the related L1 protein.* J Virol, 2006. **80**(19): p. 9455-64.
36. Nichols, R.J., et al., *The vaccinia virus gene I2L encodes a membrane protein with an essential role in virion entry.* J Virol, 2008. **82**(20): p. 10247-61.
37. Moss, B., *Poxvirus entry and membrane fusion.* Virology, 2006. **344**(1): p. 48-54.
38. Yang, Z., et al., *Simultaneous high-resolution analysis of vaccinia virus and host cell transcriptomes by deep RNA sequencing.* Proc Natl Acad Sci U S A. **107**(25): p. 11513-8.
39. Baldick, C.J., Jr., J.G. Keck, and B. Moss, *Mutational analysis of the core, spacer, and initiator regions of vaccinia virus intermediate-class promoters.* J Virol, 1992. **66**(8): p. 4710-9.
40. Davison, A.J. and B. Moss, *Structure of vaccinia virus early promoters.* J Mol Biol, 1989. **210**(4): p. 749-69.
41. Davison, A.J. and B. Moss, *Structure of vaccinia virus late promoters.* J Mol Biol, 1989. **210**(4): p. 771-84.
42. Broyles, S.S., *Vaccinia virus transcription.* J Gen Virol, 2003. **84**(Pt 9): p. 2293-303.
43. Carter, G.C., et al., *Vaccinia virus cores are transported on microtubules.* J Gen Virol, 2003. **84**(Pt 9): p. 2443-58.
44. Mallardo, M., S. Schleich, and J. Krijnse Locker, *Microtubule-dependent organization of vaccinia virus core-derived early mRNAs into distinct cytoplasmic structures.* Mol Biol Cell, 2001. **12**(12): p. 3875-91.
45. Yang, Z. and B. Moss, *Interaction of the vaccinia virus RNA polymerase-associated 94-kilodalton protein with the early transcription factor.* J Virol, 2009. **83**(23): p. 12018-26.
46. Keck, J.G., C.J. Baldick, Jr., and B. Moss, *Role of DNA replication in vaccinia virus gene expression: a naked template is required for transcription of three late trans-activator genes.* Cell, 1990. **61**(5): p. 801-9.
47. Sanz, P. and B. Moss, *Identification of a transcription factor, encoded by two vaccinia virus early genes, that regulates the intermediate stage of viral gene expression.* Proc Natl Acad Sci U S A, 1999. **96**(6): p. 2692-7.
48. Katsafanas, G.C. and B. Moss, *Vaccinia virus intermediate stage transcription is complemented by Ras-GTPase-activating protein SH3 domain-binding protein (G3BP) and cytoplasmic activation/proliferation-associated protein (p137) individually or as a heterodimer.* J Biol Chem, 2004. **279**(50): p. 52210-7.
49. Kovacs, G.R. and B. Moss, *The vaccinia virus H5R gene encodes late gene transcription factor 4: purification, cloning, and overexpression.* J Virol, 1996. **70**(10): p. 6796-802.
50. Wright, C.F., et al., *A vaccinia virus late transcription factor copurifies with a factor that binds to a viral late promoter and is complemented by extracts from uninfected HeLa cells.* J Virol, 1998. **72**(2): p. 1446-51.

51. Wright, C.F., B.W. Oswald, and S. Dellis, *Vaccinia virus late transcription is activated in vitro by cellular heterogeneous nuclear ribonucleoproteins.* J Biol Chem, 2001. **276**(44): p. 40680-6.
52. Oda, K.I. and W.K. Joklik, *Hybridization and sedimentation studies on "early" and "late" vaccinia messenger RNA.* J Mol Biol, 1967. **27**(3): p. 395-419.
53. Ahn, B.Y. and B. Moss, *Capped poly(A) leaders of variable lengths at the 5' ends of vaccinia virus late mRNAs.* J Virol, 1989. **63**(1): p. 226-32.
54. Wright, C.F. and B. Moss, *In vitro synthesis of vaccinia virus late mRNA containing a 5' poly(A) leader sequence.* Proc Natl Acad Sci U S A, 1987. **84**(24): p. 8883-7.
55. Yuen, L. and B. Moss, *Oligonucleotide sequence signaling transcriptional termination of vaccinia virus early genes.* Proc Natl Acad Sci U S A, 1987. **84**(18): p. 6417-21.
56. Rohrmann, G., L. Yuen, and B. Moss, *Transcription of vaccinia virus early genes by enzymes isolated from vaccinia virions terminates downstream of a regulatory sequence.* Cell, 1986. **46**(7): p. 1029-35.
57. Mahr, A. and B.E. Roberts, *Arrangement of late RNAs transcribed from a 7.1-kilobase EcoRI vaccinia virus DNA fragment.* J Virol, 1984. **49**(2): p. 510-20.
58. Parsons, B.L. and D.J. Pickup, *Transcription of orthopoxvirus telomeres at late times during infection.* Virology, 1990. **175**(1): p. 69-80.
59. Patel, D.D. and D.J. Pickup, *Messenger RNAs of a strongly-expressed late gene of cowpox virus contain 5'-terminal poly(A) sequences.* EMBO J, 1987. **6**(12): p. 3787-94.
60. D'Costa, S.M., et al., *Post-transcription cleavage generates the 3' end of F17R transcripts in vaccinia virus.* Virology, 2004. **319**(1): p. 1-11.
61. Antczak, J.B., et al., *Site-specific RNA cleavage generates the 3' end of a poxvirus late mRNA.* Proc Natl Acad Sci U S A, 1992. **89**(24): p. 12033-7.
62. Howard, S.T., et al., *A 43-nucleotide RNA cis-acting element governs the site-specific formation of the 3' end of a poxvirus late mRNA.* Virology, 1999. **255**(1): p. 190-204.
63. Parrish, S. and B. Moss, *Characterization of a vaccinia virus mutant with a deletion of the D10R gene encoding a putative negative regulator of gene expression.* J Virol, 2006. **80**(2): p. 553-61.
64. Parrish, S. and B. Moss, *Characterization of a second vaccinia virus mRNA-decapping enzyme conserved in poxviruses.* J Virol, 2007. **81**(23): p. 12973-8.
65. Lee-Chen, G.J., et al., *Structure of the transcription initiation and termination sequences of seven early genes in the vaccinia virus HindIII D fragment.* Virology, 1988. **163**(1): p. 64-79.
66. Shors, T., J.G. Keck, and B. Moss, *Down regulation of gene expression by the vaccinia virus D10 protein.* J Virol, 1999. **73**(1): p. 791-6.
67. Evans, E. and P. Traktman, *Characterization of vaccinia virus DNA replication mutants with lesions in the D5 gene.* Chromosoma, 1992. **102**(1 Suppl): p. S72-82.
68. De Silva, F.S. and B. Moss, *Vaccinia virus uracil DNA glycosylase has an essential role in DNA synthesis that is independent of its glycosylase activity:*

catalytic site mutations reduce virulence but not virus replication in cultured cells. J Virol, 2003. **77**(1): p. 159-66.
69. Stuart, D.T., et al., *A poxvirus-encoded uracil DNA glycosylase is essential for virus viability.* J Virol, 1993. **67**(5): p. 2503-12.
70. Garcia, A.D. and B. Moss, *Repression of vaccinia virus Holliday junction resolvase inhibits processing of viral DNA into unit-length genomes.* J Virol, 2001. **75**(14): p. 6460-71.
71. Tattersall, P. and D.C. Ward, *Rolling hairpin model for replication of parvovirus and linear chromosomal DNA.* Nature, 1976. **263**(5573): p. 106-9.
72. Pogo, B.G. and M.T. O'Shea, *The mode of replication of vaccinia virus DNA.* Virology, 1978. **84**(1): p. 1-8.
73. De Silva, F.S. and B. Moss, *Origin-independent plasmid replication occurs in vaccinia virus cytoplasmic factories and requires all five known poxvirus replication factors.* Virol J, 2005. **2**: p. 23.
74. Paran, N., et al., *Cellular DNA ligase I is recruited to cytoplasmic vaccinia virus factories and masks the role of the vaccinia ligase in viral DNA replication.* Cell Host Microbe, 2009. **6**(6): p. 563-9.
75. Gaylord, W.H., Jr. and J.L. Melnick, *Intracellular forms of pox viruses as shown by the electron microscope (Vaccinia, Ectromelia, Molluscum Contagiosum).* J Exp Med, 1953. **98**(2): p. 157-72.
76. Dales, S., *The uptake and development of vaccinia virus in strain L cells followed with labeled viral deoxyribonucleic acid.* J Cell Biol, 1963. **18**: p. 51-72.
77. Morgan, C., et al., *Serial sections of vaccinia virus examined at one stage of development in the electron microscope.* Exp. Cell Res., 1955. **9**: p. 572-578.
78. Cairns, H.J.F., *The initiation of vaccinia infection.* Virology, 1960. **11**: p. 603-623.
79. Katsafanas, G.C. and B. Moss, *Colocalization of transcription and translation within cytoplasmic poxvirus factories coordinates viral expression and subjugates host functions.* Cell Host Microbe, 2007. **2**(4): p. 221-8.
80. Tolonen, N., et al., *Vaccinia virus DNA replication occurs in endoplasmic reticulum-enclosed cytoplasmic mini-nuclei.* Molecular Biology of the Cell, 2001. **12**(7): p. 2031-2046.
81. Schramm, B. and J.K. Locker, *Cytoplasmic organization of POXvirus DNA replication.* Traffic, 2005. **6**(10): p. 839-846.
82. Lin, Y.C. and D.H. Evans, *Vaccinia virus particles mix inefficiently, and in a way that would restrict viral recombination, in coinfected cells.* J Virol. **84**(5): p. 2432-43.
83. Dales, S. and L. Siminovitch, *The development of vaccinia virus in Earle's L strain cells as examined by electron microscopy.* J. Biophys. Biochem. Cytol., 1961. **10**: p. 475-503.
84. Condit, R.C., N. Moussatche, and P. Traktman, *In a nutshell: structure and assembly of the vaccinia virion.* Adv Virus Res, 2006. **66**: p. 31-124.
85. Husain, M., A.S. Weisberg, and B. Moss, *Existence of an operative pathway from the endoplasmic reticulum to the immature poxvirus membrane.* Proc Natl Acad Sci U S A, 2006. **103**(51): p. 19506-11.

86. Husain, M., A.S. Weisberg, and B. Moss, *Sequence-independent targeting of transmembrane proteins synthesized within vaccinia virus factories to nascent viral membranes.* J Virol, 2007. **81**(6): p. 2646-55.
87. Szajner, P., et al., *External scaffold of spherical immature poxvirus particles is made of protein trimers, forming a honeycomb lattice.* J Cell Biol, 2005. **170**(6): p. 971-81.
88. Heuser, J., *Deep-etch EM reveals that the early poxvirus envelope is a single membrane bilayer stabilized by a geodetic "honeycomb" surface coat.* Journal of Cell Biology, 2005. **169**(2): p. 269-283.
89. Betakova, T., E.J. Wolffe, and B. Moss, *Membrane topology of the vaccinia virus A17L envelope protein.* Virology, 1999. **261**(2): p. 347-56.
90. Betakova, T. and B. Moss, *Disulfide bonds and membrane topology of the vaccinia virus A17L envelope protein.* Journal of Virology, 2000. **74**(5): p. 2438-2442.
91. Bisht, H., et al., *Assembly and disassembly of the capsid-like external scaffold of immature virions during vaccinia virus morphogenesis.* J Virol, 2009. **83**: p. 9140-9150.
92. DeMasi, J. and P. Traktman, *Clustered charge-to-alanine mutagenesis of the vaccinia virus H5 gene: isolation of a dominant, temperature-sensitive mutant with a profound defect in morphogenesis.* J Virol, 2000. **74**(5): p. 2393-405.
93. da Fonseca, F.G., et al., *Vaccinia virus mutants with alanine substitutions in the conserved G5R gene fail to initiate morphogenesis at the nonpermissive temperature.* J Virol, 2004. **78**(19): p. 10238-48.
94. Resch, W., A.S. Weisberg, and B. Moss, *Vaccinia virus nonstructural protein encoded by the A11R gene is required for formation of the virion membrane.* Journal of Virology, 2005. **79**(11): p. 6598-6609.
95. Satheshkumar, P.S., A. Weisberg, and B. Moss, *Vaccinia virus H7 protein contributes to the formation of crescent membrane precursors of immature virions.* J Virol, 2009. **83**(17): p. 8439-50.
96. Wang, S. and S. Shuman, *Vaccinia virus morphogenesis is blocked by temperature-sensitive mutations in the F10 gene, which encodes protein kinase 2.* J Virol, 1995. **69**(10): p. 6376-88.
97. Traktman, P., et al., *Temperature-sensitive mutants with lesions in the vaccinia virus F10 kinase undergo arrest at the earliest stage of virion morphogenesis.* J Virol, 1995. **69**(10): p. 6581-7.
98. Szajner, P., A.S. Weisberg, and B. Moss, *Evidence for an essential catalytic role of the F10 protein kinase in vaccinia virus morphogenesis.* J Virol, 2004. **78**(1): p. 257-65.
99. Betakova, T., E.J. Wolffe, and B. Moss, *Regulation of vaccinia virus morphogenesis: phosphorylation of the A14L and A17L membrane proteins and C-terminal truncation of the A17L protein are dependent on the F10L kinase.* J Virol, 1999. **73**(5): p. 3534-43.
100. Szajner, P., et al., *A complex of seven vaccinia virus proteins conserved in all chordopoxviruses is required for the association of membranes and viroplasm to form immature virions.* Virology, 2004. **330**(2): p. 447-59.

101. Szajner, P., A.S. Weisberg, and B. Moss, *Physical and Functional Interactions between Vaccinia Virus F10 Protein Kinase and Virion Assembly Proteins A30 and G7.* Journal of Virology, 2004. **78**(1): p. 266-274.
102. Bisht, H., E. Brown, and B. Moss, *Kinetics and intracellular location of intramolecular disulfide bond formation mediated by the cytoplasmic redox system encoded by vaccinia virus.* Virology. **398**(2): p. 187-93.
103. Senkevich, T.G., et al., *Expression of the vaccinia virus A2.5L redox protein is required for virion morphogenesis.* Virology, 2002. **300**(2): p. 296-303.
104. Senkevich, T.G., A.S. Weisberg, and B. Moss, *Vaccinia virus E10R protein is associated with the membranes of intracellular mature virions and has a role in morphogenesis.* Virology, 2000. **278**(1): p. 244-252.
105. White, C.L., T.G. Senkevich, and B. Moss, *Vaccinia virus G4L glutaredoxin is an essential intermediate of a cytoplasmic disulfide bond pathway required for virion assembly.* J Virol, 2002. **76**(2): p. 467-72.
106. Hollinshead, M., et al., *Vaccinia virus intracellular mature virions contain only one lipid membrane.* J Virol, 1999. **73**(2): p. 1503-17.
107. Smith, G.L., A. Vanderplasschen, and M. Law, *The formation and function of extracellular enveloped vaccinia virus.* J Gen Virol, 2002. **83**(Pt 12): p. 2915-31.
108. Ward, B.M., *Visualization and characterization of the intracellular movement of vaccinia virus intracellular mature virions.* J Virol, 2005. **79**(8): p. 4755-63.
109. Sanderson, C.M., M. Hollinshead, and G.L. Smith, *The vaccinia virus A27L protein is needed for the microtubule-dependent transport of intracellular mature virus particles.* Journal of General Virology, 2000. **81**(1): p. 47-58.
110. Hiller, G. and K. Weber, *Golgi-derived membranes that contain an acylated viral polypeptide are used for vaccinia virus envelopment.* J Virol, 1985. **55**(3): p. 651-9.
111. Tooze, J., et al., *Progeny vaccinia and human cytomegalovirus particles utilize early endosomal cisternae for their envelopes.* Eur J Cell Biol, 1993. **60**(1): p. 163-78.
112. Roper, R.L., L.G. Payne, and B. Moss, *Extracellular vaccinia virus envelope glycoprotein encoded by the A33R gene.* J Virol, 1996. **70**(6): p. 3753-62.
113. Duncan, S.A. and G.L. Smith, *Identification and characterization of an extracellular envelope glycoprotein affecting vaccinia virus egress.* J Virol, 1992. **66**(3): p. 1610-21.
114. Shida, H., *Variants of vaccinia virus hemagglutinin altered in intracellular transport.* Mol Cell Biol, 1986. **6**(11): p. 3734-45.
115. Wolffe, E.J., S.N. Isaacs, and B. Moss, *Deletion of the vaccinia virus B5R gene encoding a 42-kilodalton membrane glycoprotein inhibits extracellular virus envelope formation and dissemination.* J Virol, 1993. **67**(8): p. 4732-41.
116. Wolffe, E.J., et al., *The A34R glycoprotein gene is required for induction of specialized actin-containing microvilli and efficient cell-to-cell transmission of vaccinia virus.* J Virol, 1997. **71**(5): p. 3904-15.

117. Blasco, R. and B. Moss, *Extracellular vaccinia virus formation and cell-to-cell virus transmission are prevented by deletion of the gene encoding the 37,000-Dalton outer envelope protein.* J Virol, 1991. **65**(11): p. 5910-20.
118. Engelstad, M., S.T. Howard, and G.L. Smith, *A constitutively expressed vaccinia gene encodes a 42-kDa glycoprotein related to complement control factors that forms part of the extracellular virus envelope.* Virology, 1992. **188**(2): p. 801-10.
119. Rodriguez, J.F. and G.L. Smith, *IPTG-dependent vaccinia virus: identification of a virus protein enabling virion envelopment by Golgi membrane and egress.* Nucleic Acids Res, 1990. **18**(18): p. 5347-51.
120. Rodriguez, D., J.R. Rodriguez, and M. Esteban, *The vaccinia virus 14-kilodalton fusion protein forms a stable complex with the processed protein encoded by the vaccinia virus A17L gene.* Journal of Virology, 1993. **67**(6): p. 3435-3440.
121. Rodriguez, J.F., E. Paez, and M. Esteban, *A 14,000-Mr envelope protein of vaccinia virus is involved in cell fusion and forms covalently linked trimers.* J Virol, 1987. **61**(2): p. 395-404.
122. Wallengren, K., et al., *The A17L gene product of vaccinia virus is exposed on the surface of IMV.* Virology, 2001. **290**(1): p. 143-152.
123. Vazquez, M.I., et al., *The vaccinia virus 14-Kilodalton (A27L) fusion protein forms a triple coiled-coil structure and interacts with the 21-Kilodalton (A17L) virus membrane protein through a C-terminal a-helix.* Journal of Virology, 1998. **72**(12): p. 10126-10137.
124. Sodeik, B., et al., *Assembly of vaccinia virus: Incorporation of p14 and p32 into the membrane of the intracellular mature virus.* Journal of Virology, 1995. **69**(6): p. 3560-3574.
125. Grosenbach, D., D. Ulaeto, and D. Hruby, *Palmitylation of the vaccinia virus 37-kDa major envelope antigen.* The Journal of Biological Chemistry, 1997. **272**(3): p. 1956-1964.
126. Yang, G., et al., *An orally bioavailable antipoxvirus compound (ST-246) inhibits extracellular virus formation and protects mice from lethal orthopoxvirus Challenge.* J Virol, 2005. **79**(20): p. 13139-49.
127. Roper, R.L. and B. Moss, *Envelope formation is blocked by mutation of a sequence related to the HKD phospholipid metabolism motif in the vaccinia virus F13L protein.* J Virol, 1999. **73**(2): p. 1108-17.
128. Domi, A., A.S. Weisberg, and B. Moss, *Vaccinia virus E2L null mutants exhibit a major reduction in extracellular virion formation and virus spread.* J Virol, 2008. **82**(9): p. 4215-26.
129. Dodding, M.P., et al., *An E2-F12 complex is required for IEV morphogenesis during vaccinia infection.* Cell Microbiol, 2009.
130. Ward, B.M. and B. Moss, *Vaccinia virus intracellular movement is associated with microtubules and independent of actin tails.* J Virol, 2001. **75**(23): p. 11651-63.
131. Ward, B.M. and B. Moss, *Visualization of intracellular movement of vaccinia virus virions containing a green fluorescent protein-B5R membrane protein chimera.* J Virol, 2001. **75**(10): p. 4802-13.

132. van Eijl, H., et al., *The vaccinia virus F12L protein is associated with intracellular enveloped virus particles and is required for their egress to the cell surface.* J Gen Virol, 2002. **83**(Pt 1): p. 195-207.
133. Wolffe, E.J., A.S. Weisberg, and B. Moss, *The vaccinia virus A33R protein provides a chaperone function for viral membrane localization and tyrosine phosphorylation of the A36R protein.* J Virol, 2001. **75**(1): p. 303-10.
134. Ward, B.M. and B. Moss, *Vaccinia virus A36R membrane protein provides a direct link between intracellular enveloped virions and the microtubule motor kinesin.* J Virol, 2004. **78**(5): p. 2486-93.
135. Rietdorf, J., et al., *kinesin-dependent movement on microtubules precedes actin-based motility of vaccinia virus.* Nature Cell Biology, 2001. **3**: p. 992-1000.
136. Johnston, S.C. and B.M. Ward, *Vaccinia virus protein F12 associates with intracellular enveloped virions through an interaction with A36.* J Virol, 2009. **83**(4): p. 1708-17.
137. Morgan, G.W., et al., *Vaccinia protein F12 has structural similarity to kinesin light chain and contains a motor binding motif required for virion export.* PLoS Pathog. **6**(2): p. e1000785.
138. Newsome, T.P., N. Scaplehorn, and M. Way, *SRC mediates a switch from microtubule- to actin-based motility of vaccinia virus.* Science, 2004. **306**(5693): p. 124-9.
139. Arakawa, Y., et al., *The release of vaccinia virus from infected cells requires RhoA-mDia modulation of cortical actin.* Cell Host Microbe, 2007. **1**(3): p. 227-40.
140. Cudmore, S., et al., *Actin-based motility of vaccinia virus.* Nature, 1995. **378**(6557): p. 636-8.
141. Frischknecht, F., et al., *Actin-based motility of vaccinia virus mimics receptor tyrosine kinase signalling.* Nature, 1999. **401**(6756): p. 926-9.
142. Moreau, V., et al., *A complex of N-WASP and WIP integrates signalling cascades that lead to actin polymerization.* Nat Cell Biol, 2000. **2**(7): p. 441-8.
143. Perdiguero, B., M.M. Lorenzo, and R. Blasco, *Vaccinia virus A34 glycoprotein determines the protein composition of the extracellular virus envelope.* J Virol, 2008. **82**(5): p. 2150-60.
144. Payne, L.G., *Identification of the vaccinia hemagglutinin polypeptide from a cell system yielding large amounts of extracellular enveloped virus.* J Virol, 1979. **31**(1): p. 147-55.
145. Ulaeto, D., D. Grosenbach, and D.E. Hruby, *The vaccinia virus 4c and A-type inclusion proteins are specific markers for the intracellular mature virus particle.* J Virol, 1996. **70**(6): p. 3372-7.
146. Downie, A.W., *A study of the lesions produced experimentally by cowpox virus.* J Pathol Bacteriol, 1939. **48**: p. 361-379.
147. Marchal, J., *Infectious ectromelia. A hitherto undescribed virus disease of mice.* J Pathol Bacteriol, 1930. **33**: p. 713-728.
148. Knight, J.C., et al., *Further analyses of the orthopoxvirus volepox virus and raccoon poxvirus.* Virology, 1992. **190**: p. 423-433.

149. Randall, C.C., et al., *Composition of Fowlpox Virus and Inclusion Matrix.* J Bacteriol, 1964. **87**: p. 939-44.
150. Arif, B.M., *Isolation of an entomopoxvirus and characterization of its DNA.* Virology, 1976. **69**(2): p. 626-34.
151. Patel, D., D. Pickup, and W. Joklik, *Isolation of cowpox virus A-type inclusions and characterization of their major protein component.* Virology, 1986. **149**: p. 174-189.
152. Ichihashi, Y., S. Matsumoto, and S. Dales, *Biogenesis of poxviruses: role of A-type inclusions and host cell membranes in virus dissemination.* Virology, 1971. **46**(3): p. 507-32.
153. Ichihashi, Y. and S. Dales, *Biogenesis of poxviruses: relationship between a translation complex and formation of A-type inclusions.* Virology, 1973. **51**(2): p. 297-319.
154. Funahashi, S., T. Sato, and H. Shida, *Cloning and characterization of the gene encoding the major protein of the A-type inclusion body of cowpox virus.* Journal of General Virology, 1988. **69**: p. 35-47.
155. Patel, D.D., D.J. Pickup, and W.K. Joklik, *Isolation of cowpox virus A-type inclusions and characterization of their major protein component.* Virology, 1986. **149**: p. 174-189.
156. Amegadzie, B.Y., J.R. Sisler, and B. Moss, *Frame-shift mutations within the vaccinia virus A-type inclusion protein gene.* Virology, 1992. **186**: p. 777-782.
157. Ichihashi, Y. and S. Matsumoto, *Studies on the nature of marchal bodies (A-type inclusion) during ectromelia virus infection.* Virology, 1966. **29**: p. 264-275.
158. Sarov, I. and W.K. Joklik, *Studies on the nature and location of the capsid polypeptides of vaccinia virions.* Virology, 1972. **50**(2): p. 579-592.
159. Katz, E. and E. Margalith, *Location of vaccinia virus structural polypeptides on the surface of the virus particle.* Journal of General Virology, 1973. **18**: p. 381-384.
160. McKelvey, T.A., et al., *Identification of the orthopoxvirus p4c gene, which encodes a structural protein that directs intracellular mature virus particles into A-type inclusions.* Journal of Virology, 2002. **76**(22): p. 11216-11225.
161. Rohrmann, G.F., *Polyhedrin structure.* J Gen Virol, 1986. **67 (Pt 8)**: p. 1499-513.
162. Rohrmann, G.F., *Baculovirus molecular biology.* http://www.ncbi.nlm.nih.gov/bookshelf/br.fcgi?book=bacvir, 2008.
163. Gotz, P., A.M. Huger, and A. Krieg, *[A virus pathogenic for insects from the group of pox viruses].* Naturwissenschaften, 1969. **56**(3): p. 145.
164. Jehle, J.A., et al., *On the classification and nomenclature of baculoviruses: a proposal for revision.* Arch Virol, 2006. **151**(7): p. 1257-66.
165. Rohrmann, G.F., *Baculovirus structural proteins.* J Gen Virol, 1992. **73 (Pt 4)**: p. 749-61.
166. Hasnain, S.E., et al., *Involvement of host factors in transcription from baculovirus very late promoters -- a review.* Gene, 1997. **190**(1): p. 113-8.
167. Gross, C.H., R.L. Russell, and G.F. Rohrmann, *Orgyia pseudotsugata baculovirus p10 and polyhedron envelope protein genes: analysis of their*

relative expression levels and role in polyhedron structure. J Gen Virol, 1994. **75 (Pt 5)**: p. 1115-23.
168. Smith, G.E., M.J. Fraser, and M.D. Summers, *Molecular Engineering of the Autographa californica Nuclear Polyhedrosis Virus Genome: Deletion Mutations Within the Polyhedrin Gene.* J Virol, 1983. **46**(2): p. 584-93.
169. Xu, H.J., et al., *Bombyx mori nucleopolyhedrovirus ORF56 encodes an occlusion-derived virus protein and is not essential for budded virus production.* J Gen Virol, 2008. **89**(Pt 5): p. 1212-9.
170. Arif, B., *Recent advances in the molecular biology of entomopoxviruses.* Journal of General Virology, 1995. **76**: p. 1-13.
171. Dales, S. and B.G. Pogo, *Biology of poxviruses.* Virol Monogr, 1981. **18**: p. 1-109.
172. Miller, L.K. and L.A. Ball, *The insect viruses*. The viruses. 1998, New York: Plenum Press. xvii, 413 p.
173. Radek, R. and P. Fabel, *A new entomopoxvirus from a cockroach: light and electron microscopy.* J Invertebr Pathol, 2000. **75**(1): p. 19-27.
174. Hall, R.L. and R.W. Moyer, *Identification of an Amsacta spheroidin-like protein within the occlusion bodies of Choristoneura entomopoxviruses.* Virology, 1993. **192**(1): p. 179-87.
175. Banville, M., et al., *The predicted amino acid sequence of the spheroidin protein from Amsacta moorei entomopoxvirus: lack of homology between major occlusion body proteins of different poxviruses.* J Gen Virol, 1992. **73 (Pt 3)**: p. 559-66.
176. Palmer, C.P., et al., *Genetic modification of an entomopoxvirus: deletion of the spheroidin gene does not affect virus replication in vitro.* J Gen Virol, 1995. **76 (Pt 1)**: p. 15-23.
177. Mitsuhashi, W., et al., *Spindles of an entomopoxvirus facilitate its infection of the host insect by disrupting the peritrophic membrane.* J Virol, 2007. **81**(8): p. 4235-43.
178. Carpentier, D.C., C.M. Griffiths, and L.A. King, *The baculovirus P10 protein of Autographa californica nucleopolyhedrovirus forms two distinct cytoskeletal-like structures and associates with polyhedral occlusion bodies during infection.* Virology, 2008. **371**(2): p. 278-91.
179. Cheley, S., et al., *Phosphorylated baculovirus p10 is a heat-stable microtubule-associated protein associated with process formation in Sf9 cells.* J Cell Sci, 1992. **102 (Pt 4)**: p. 739-52.
180. Alaoui-Ismaili, M.H. and C.D. Richardson, *Insect virus proteins (FALPE and p10) self-associate to form filaments in infected cells.* J Virol, 1998. **72**(3): p. 2213-23.
181. Condit, R.C., N. Moussatche, and P. Traktman, *In a nutshell: structure and assembly of the vaccinia virion.* Adv. Virus Res., 2006. **66**: p. 31-124.
182. Tooze, J., et al., *Progeny vaccinia and human cytomegalovirus particles utilize early endosomal cisternae for their envelopes.* Eur. J. Cell Biol., 1993. **60**(1): p. 163-178.

183. Hiller, G. and K. Weber, *Golgi-derived membranes that contain an acylated viral polypeptide are used for vaccinia virus envelopment.* J. Virol., 1985. **55**: p. 651-659.
184. Schmelz, M., et al., *Assembly of vaccinia virus: the second wrapping cisterna is derived from the trans Golgi network.* J. Virol., 1994. **68**: p. 130-147.
185. Ward, B.M. and B. Moss, *Vaccinia virus intracellular movement is associated with microtubules and independent of actin tails.* J. Virol., 2001. **75**: p. 11651-11663.
186. Ward, B.M. and B. Moss, *Visualization of intracellular movement of vaccinia virus virions containing a green fluorescent protein-B5R membrane protein chimera.* J. Virol., 2001. **75**: p. 4802-4813.
187. Rietdorf, J., et al., *Kinesin dependent movement on microtubules precedes actin based motility of vaccinia virus.* Nature Cell Biol., 2001. **3**: p. 992-1000.
188. Hollinshead, M., et al., *Vaccinia virus utilizes microtubules for movement to the cell surface.* J. Cell Biol., 2001. **154**(2): p. 389-402.
189. Blasco, R. and B. Moss, *Role of cell-associated enveloped vaccinia virus in cell-to-cell spread.* J. Virol., 1992. **66**(7): p. 4170-4179.
190. Stokes, G.V., *High-voltage electron microscope study of the release of vaccinia virus from whole cells.* J. Virol., 1976. **18**: p. 636-643.
191. Kato, S., et al., *A study on the morphological and cyto-immunological relationship between the inclusions of variola, cowpox, rabbitpox, vaccinia (variola origin) and vaccinia IHD, and a consideration of the term "Guarnieri body".* Biken's J., 1959. **2**: p. 353-363.
192. Yoder, J.D., et al., *Pox proteomics: mass spectrometry analysis and identification of Vaccinia virion proteins.* Virol. J., 2006. **3**(1): p. 10.
193. Resch, W., et al., *Protein composition of the vaccinia virus mature virion.* Virology, 2006. **358**: p. 233-247.
194. Chung, C.S., et al., *Vaccinia virus proteome: Identification of proteins in vaccinia virus intracellular mature virion particles.* J. Virol., 2006. **80**(5): p. 2127-2140.
195. Ulaeto, D., D. Grosenbach, and D.E. Hruby, *The vaccinia virus 4c and A-type inclusion proteins are specific markers for the intracellular mature virus particle.* J. Virol., 1996. **70**: p. 3372-3375.
196. Patel, D.D. and D.J. Pickup, *Messenger RNAs of a strongly-expressed late gene of cowpox virus contains a 5'-terminal poly(A) leader.* EMBO J., 1987. **6**: p. 3787-3794.
197. McKelvey, T.A., et al., *Identification of the orthopoxvirus p4c gene, which encodes a structural protein that directs intracellular mature virus particles into A-type inclusions.* J. Virol., 2002. **76**(22): p. 11216-11225.
198. Chiu, W.L., et al., *Vaccinia virus 4c (A26L) protein on intracellular mature virus binds to the extracellular cellular matrix laminin.* J. Virol., 2007. **81**(5): p. 2149-2157.
199. Rodriguez, D., J.R. Rodriguez, and M. Esteban, *The vaccinia virus 14-kilodalton fusion protein forms a stable complex with the processed protein encoded by the vaccinia virus A17L gene.* J. Virol., 1993. **67**(6): p. 3435-3440.

200. Earl, P.L., et al., *Preparation of cell cultures and vaccinia virus stocks*, in *Current Protocols in Molecular Biology*, F.M. Ausubel, et al., Editors. 1998, John Wiley and Sons: New York. p. 16.16.1-16.16.3.
201. Fogg, C.N., et al., *Disparity between in vitro neutralization of vaccinia virus by antibody to the A27 protein and protection of mice to intranasal challenge.* J. Virol., 2008.
202. Wolffe, E.J., et al., *Vaccinia virus A17L open reading frame encodes an essential component of nascent viral membranes that is required to initiate morphogenesis.* J. Virol., 1996. **70**: p. 2797-2808.
203. Senkevich, T.G. and B. Moss, *Vaccinia virus H2 protein is an essential component of a complex involved in virus entry and cell-cell fusion.* J. Virol., 2005. **79**: p. 4744-4754.
204. Ward, B.M., *Visualization and characterization of the intracellular movement of vaccinia*
virus intracellular mature virions. J. Virol., 2005. **79**: p. 4755-4763.
205. Townsley, A.C., et al., *Vaccinia virus entry into cells via a low pH-dependent-endosomal pathway.* J. Virol., 2006. **80**: p. 8899-8908.
206. Davison, A.J. and B. Moss, *The structure of vaccinia virus late promoters.* J. Mol. Biol., 1989. **210**: p. 771-784.
207. Earl, P.L. and B. Moss, *Characterization of recombinant vaccinia viruses and their products*, in *Current Protocols in Molecular Biology*, F.M. Ausubel, et al., Editors. 1998, Greene Publishing Associates & Wiley Interscience: New York. p. 16.18.1-16.18.11.
208. Resch, W., et al., *Protein composition of the vaccinia virus mature virion.* Virology, 2007. **358**(1): p. 233-247.
209. Senkevich, T.G., et al., *A viral member of the ERV1/ALR protein family participates in a cytoplasmic pathway of disulfide bond formation.* Proc. Natl. Acad. Sci. USA, 2000. **97**: p. 12068-12073.
210. Sarov, I. and W.K. Joklik, *Studies on the nature and location of the capsid polypeptides of vaccinia virions.* Virology, 1972. **50**: p. 579-592.
211. Katz, E. and E. Margalith, *Location of vaccinia virus structural polypeptides on the surface of the virus particle.* J. Gen. Virol., 1973. **18**(3): p. 381-384.
212. Vazquez, M.I., et al., *The vaccinia virus 14-kilodalton (A27L) fusion protein forms a triple coiled-coil structure and interacts with the 21-kilodalton (A17L) virus membrane protein through a C-terminal alpha-helix.* J. Virol., 1998. **72**(12): p. 10126-10137.
213. Ichihashi, Y., *Unit complex of vaccinia polypeptides linked by disulfide bridges.* Virology, 1981. **113**: p. 277-284.
214. Ichihashi, Y. and S. Matsumoto, *Studies on the nature of Marchal bodies (A-type inclusion) during ectromelia virus infection.* Virology, 1966. **29**(2): p. 264-275.
215. Ichihashi, Y. and S. Matsumoto, *The relationship between poxvirus and A-type inclusion body during double infection.* Virology, 1968. **36**(2): p. 262-270.
216. Rodriguez, J.F. and G.L. Smith, *Inducible gene expression from vaccinia virus.* Virology, 1990. **177**: p. 239-250.

217. Chung, C.-S., et al., *A27L protein mediates vaccinia virus interaction with cell surface heparin sulfate.* J. Virol., 1998. **72**: p. 1577-1585.
218. Hsiao, J.C., C.S. Chung, and W. Chang, *Vaccinia virus envelope D8L protein binds to cell surface chondroitin sulfate and mediates the adsorption of intracellular mature virions to cells.* J. Virol., 1999. **73**(10): p. 8750-8761.
219. Howard, A.R., T.G. Senkevich, and B. Moss, *Vaccinia virus A26 and A27 proteins form a stable complex tethered to mature virions by association with the A17 transmembrane protein.* J Virol, 2008. **82**: p. 12384-12391.
220. Ching, Y.-C., et al., *Disulfide bond formation at the C-termini of vaccinia A26 and A27 proteins does not require viral redox enzymes and suppresses glycosaminoglycan-mediated cell fusion.* Journal of Virology, 2009. **83**(13): p. 6464-76.
221. Earl, P.L., et al., *Preparation of cell cultures and vaccinia virus stocks*, in *Current Protocols in Molecular Biology*, F.M. Ausubel, et al., Editors. 1998, John Wiley and Sons: New York. p. 16.16.1-16.16.3.
222. Ichihashi, Y. and S. Matsumoto, *The relationship between poxvirus and A-type inclusion body during double infection.* Virology, 1968. **36**: p. 262-270.
223. Nagaya, A., B.G. Pogo, and S. Dales, *Biogenesis of vaccinia: separation of early stages from maturation by means of rifampicin.* Virology, 1970. **40**(4): p. 1039-1051.
224. Moss, B., E. Katz, and E.N. Rosenblum, *Vaccinia virus directed RNA and protein synthesis in the presence of rifampicin.* Biochemical and Biophysical Research Communications, 1969. **36**(5): p. 858-865.
225. Shida, H., K. Tanabe, and S. Matsumoto, *Mechanism of virus occlusion into A-type inclusion during poxvirus infection.* Virology, 1977. **76**: p. 217-233.
226. Cairns, J., *The initiation of vaccinia infection.* Virology, 1960. **11**: p. 603-23.
227. Howard, A.R., A.S. Weisberg, and B. Moss, *Congregation of orthopoxvirus virions in cytoplasmic A-type inclusions is mediated by interactions of a bridging protein (A26p) with a matrix protein (ATIp) and a virion membrane-associated protein (A27p).* J Virol, 2010. **84**(15): p. 7592-602.
228. Moser, T.S., et al., *A kinome RNAi screen identified AMPK as promoting poxvirus entry through the control of actin dynamics.* PLoS Pathog. **6**(6): p. e1000954.
229. Ploubidou, A., et al., *Vaccinia virus infection disrupts microtubule organization and centrosome function.* EMBO J, 2000. **19**(15): p. 3932-44.
230. Rietdorf, J., et al., *Kinesin-dependent movement on microtubules precedes actin-based motility of vaccinia virus.* Nat Cell Biol, 2001. **3**(11): p. 992-1000.
231. De Carlos, A. and P. Eduardo, *Isolation and characterization of mutants of vaccinia virus with a modified 94-kDa inclusion protein.* Virology, 1991. **185**: p. 768-778.
232. Amegadzie, B.Y., J.R. Sisler, and B. Moss, *Frame-shift mutations within the vaccinia virus A-type inclusion protein gene.* Virology, 1992. **186**(2): p. 777-82.
233. Ichihashi, Y. and S. Dales, *Biogenesis of poxviruses: interrelationship between hemagglutinin production and polykaryocytosis.* Virology, 1971. **46**(3): p. 533-43.

234. Sonenberg, N., *eIF4E, the mRNA cap-binding protein: from basic discovery to translational research.* Biochem Cell Biol, 2008. **86**(2): p. 178-83.
235. Schmidt, E.K., et al., *SUnSET, a nonradioactive method to monitor protein synthesis.* Nat Methods, 2009. **6**(4): p. 275-7.
236. Nathans, D., *Puromycin Inhibition of Protein Synthesis: Incorporation of Puromycin into Peptide Chains.* Proc Natl Acad Sci U S A, 1964. **51**: p. 585-92.
237. Nathans, D. and A. Neidle, *Structural requirements for puromycin inhibition of protein synthesis.* Nature, 1963. **197**: p. 1076-7.
238. Grimley, P.M., et al., *Interruption by Rifampin of an early stage in vaccinia virus morphogenesis: accumulation of membranes which are precursors of virus envelopes.* J Virol, 1970. **6**(4): p. 519-33.
239. Holt, C.E. and S.L. Bullock, *Subcellular mRNA localization in animal cells and why it matters.* Science, 2009. **326**(5957): p. 1212-6.
240. Sanderson, C.M., M. Hollinshead, and G.L. Smith, *The vaccinia virus A27L protein is needed for the microtubule-dependent transport of intracellular mature virus particles.* J Gen Virol, 2000. **81**(Pt 1): p. 47-58.
241. Sood, C.L., J.M. Ward, and B. Moss, *Vaccinia virus encodes I5, a small hydrophobic virion membrane protein that enhances replication and virulence in mice.* J Virol, 2008. **82**(20): p. 10071-8.
242. Ching, Y.C., et al., *Disulfide bond formation at the C termini of vaccinia virus A26 and A27 proteins does not require viral redox enzymes and suppresses glycosaminoglycan-mediated cell fusion.* J Virol, 2009. **83**(13): p. 6464-76.
243. Chang, S.J., et al., *Vaccinia virus A25 and A26 proteins are fusion suppressors for mature virions and determine strain-specific virus entry pathways into HeLa, CHO-K1, and L cells.* J Virol. **84**(17): p. 8422-32.
244. Trcek, T. and R.H. Singer, *The cytoplasmic fate of an mRNP is determined cotranscriptionally: exception or rule?* Genes Dev. **24**(17): p. 1827-31.
245. Bassell, G. and R.H. Singer, *mRNA and cytoskeletal filaments.* Curr Opin Cell Biol, 1997. **9**(1): p. 109-15.
246. Wileman, T., *Aggresomes and pericentriolar sites of virus assembly: cellular defense or viral design?* Annu Rev Microbiol, 2007. **61**: p. 149-67.
247. Risco, C., et al., *Endoplasmic reticulum-Golgi intermediate compartment membranes and vimentin filaments participate in vaccinia virus assembly.* Journal of Virology, 2002. **76**(4): p. 1839-1855.
248. Rodriguez, J.F. and G.L. Smith, *Inducible gene expression from vaccinia virus vectors.* Virology, 1990. **177**(1): p. 239-50.
249. Rodger, G. and G.L. Smith, *Replacing the SCR domains of vaccinia virus protein B5R with EGFP causes a reduction in plaque size and actin tail formation but enveloped virions are still transported to the cell surface.* J Gen Virol, 2002. **83**(Pt 2): p. 323-32.